State Estimation for Enhanced Monitoring, Reliability, Restoration and Control of Smart Distribution Systems

by

Daniel Andrew Haughton

A Dissertation Presented in Partial Fulfillment
of the Requirements for the Degree
Doctor of Philosophy

Approved August 2012 by the
Graduate Supervisory Committee:

Gerald T. Heydt, Chair
Vijay Vittal
Rajapandian Ayyanar
Kory Hedman

ARIZONA STATE UNIVERSITY

December 2012

ABSTRACT

The Smart Grid initiative describes the collaborative effort to modernize the U.S. electric power infrastructure. Modernization efforts incorporate digital data and information technology to effectuate control, enhance reliability, encourage small customer sited distributed generation (DG), and better utilize assets. The Smart Grid environment is envisioned to include distributed generation, flexible and controllable loads, bidirectional communications using smart meters and other technologies. Sensory technology may be utilized as a tool that enhances operation including operation of the distribution system. Addressing this point, a distribution system state estimation algorithm is developed in this thesis.

The state estimation algorithm developed here utilizes distribution system modeling techniques to calculate a vector of state variables for a given set of measurements. Measurements include active and reactive power flows, voltage and current magnitudes, phasor voltages with magnitude and angle information. The state estimator is envisioned as a tool embedded in distribution substation computers as part of distribution management systems (DMS); the estimator acts as a supervisory layer for a number of applications including automation (DA), energy management, control and switching.

The distribution system state estimator is developed in full three-phase detail, and the effect of mutual coupling and single-phase laterals and loads on the solution is calculated. The network model comprises a full three-phase admittance matrix and a subset of equations that relates measurements to system states. Net-

work equations and variables are represented in rectangular form. Thus a linear calculation procedure may be employed. When initialized to the vector of measured quantities and approximated non-metered load values, the calculation procedure is non-iterative.

This dissertation presents background information used to develop the state estimation algorithm, considerations for distribution system modeling, and the formulation of the state estimator. Estimator performance for various power system test beds is investigated. Sample applications of the estimator to Smart Grid systems are presented. Applications include monitoring, enabling demand response (DR), voltage unbalance mitigation, and enhancing voltage control. Illustrations of these applications are shown. Also, examples of enhanced reliability and restoration using a sensory based automation infrastructure are shown.

DEDICATIONS

This dissertation is dedicated in part to my parents, Milton and Carol Haughton, who have provided much support, motivation and inspiration throughout my academic career; in part to Sasharie J. Haughton, whose continued understanding, patience and encouragement have also been a great motivating force; and to the memory of Professor Richard G. Farmer who is perhaps one of the kindest, most genuine and exceptional power engineers I will ever know.

ACKNOWLEDGEMENTS

I must acknowledge Dr. Gerald T. Heydt for his invaluable guidance, insights and continued encouragement throughout the writing of this dissertation. Thanks to the members of the committee, Dr. Vijay Vittal, Dr. Raja Ayyanar and Dr. Kory Hedman for their comments, feedback and time. Thanks also to Dr. Keith Holbert, for working with me and encouraging my participation in summer research programs for high-school scholars.

Acknowledgment is due to the Power Systems Engineering Research Center (PSerc), a Generation III Industry / University Cooperative Research Center, under grant NSF EEC-0001880 and EEC-0968993 and the Future Renewable Electric Energy Distribution and Management Center (FREEDM), an Engineering Research Center under grant NSF EEC-08212121 for mentorship and financial support. I would also like to acknowledge the IEEE power and energy society (PES) for their financial support in attending technical society conferences, and providing an arena for power systems researchers to grow.

TABLE OF CONTENTS

Page

CHAPTER Page

CHAPTER Page

CHAPTER Page

CHAPTER Page

CHAPTER Page

CHAPTER Page

APPENDIX Page

LIST OF TABLES

Table Page

Table Page

Table Page

Table Page

LIST OF FIGURES

Figure Page

Figure Page

Figure Page

Figure Page

Figure Page

Figure Page

Figure Page

NOMENCLATURE

A	Adjacency matrix
ACSR	Aluminum Conductor Steel Reinforced
AMI	Advanced metering infrastructure
ASAI	Average service availability index
AWG	American Wire Gauge
AWEA	American wind energy association
B	Binary connection matrix
CAIDI	Customer average interruption duration index
CT	Current transformer
DER	Distributed energy resources
DG	Distributed generation
DoE	Department of energy
DMS	Distribution management system
DR	Demand side response
DSM	Demand side management
DSSE	Distribution system state estimator
e	Error vector
E	Set of edges; Expectation of unserved energy (kWh/outage or kWh/y)
EISA	Energy independence and security act
FDIR	Fault detection, isolation and reconfiguration
FREEDM	Future renewable electric energy delivery and management

G	Gain matrix in state estimation
GMR	Geometric mean radius
GPS	Global positioning system
h, $h(x)$	Process matrix in state estimation calculation
h^+	Moore-Penrose pseudo-inverse
h_{LM}	Line measurement coefficient matrix
h_{meas}	h matrix subset relating measurement to state variables
I_{meas}	Injection current measurement vector (phasor)
I_{line}	Line current measurement (phasor)
IEEE	Institute of Electrical and Electronics Engineers
IPP	Independent power producer
ISO	Independent system operator
IT	Information technology
J	Incidence matrix
$J(x)$	Objective function of state estimation formulation
LSSS	Large Scale Simulation System Test Bed
m	Number of circuit breakers that are open
M_i	Mean of variable i
MLE	Maximum likelihood estimation
n	Number of elements in a vector or a row or column designator in a matrix
N	Set of nodes

N(0,1)	Standard normal distribution, zero mean, unit variance
n_b	Number of buses
n_{cb}	Number of circuit breakers
n_l	Number of lines
n_ph	Number of phases
N9, N9'	Number of nines in reliability
NSF	National Science Foundation
OMS	Outage management system
p	Order of a norm
PCC	Point of common coupling
PHEV	Plug-in hybrid electric vehicles
PMU	Phasor measurement unit
PSERC	Power Systems Engineering Research Center
PT	Potential transformer
Q	Reactive power
r	Residual vector in state estimation; repair time; expected outage duration in hours
r/x	Ratio of conductor resistance to reactance
R	Covariance matrix of measurement weights
RBTS	A test bed distribution system 'Roy Billinton Test System'
RES	Renewable energy standard
RPS	Renewable portfolio standard

RTO	Regional transmission organization
RYG	A test bed distribution system 'Red-Yellow-Green'
s_{max}	Maximum singular value
s_{min}	Minimum singular value
SAIDI	System average interruption duration index
SAIFI	System average interruption frequency index
SCADA	Supervisory control and data acquisition
SST	System status table
U	Annual unavailability (h/y); the identity matrix
V_n^{abc}	Three-phase voltage vector at bus n
V_{meas}	Voltage measurement vector (phasor)
Var_k	The variance of variable k
WLS	Weighted least squares
W	Weight matrix in state estimation
x	Solution vector of a linear system, a state vector
X	Reactance
Y, Y_{bus}	Bus admittance matrix
z	Measurement vector
Z_{aa}	Phase a conductor the self impedance in a three-phase network
Z_{ab}	Mutual impedance between phases a and b in a three-phase network
Z_{nm}^{abc}	Three-phase block impedance matrix, with self impedance and mutual impedance

Z_m	Mutual impedance between phases in a three-phase network
ΔASAI	Small increment in the ASAI index
ΔSAIDI	Small increment in the SAIDI index
ΔT	Time interval between measurement samples
δ	Bus voltage phase angle
η	A measurement noise vector
μ_{Ireal}	Expectation of the real part of the calculated current, I
μ_{Iimag}	Expectation of the imaginary part of the calculated current, I
κ	Condition number of a matrix
λ	Expected failure rate (failures/y)
σ, σ_k	Standard deviation, standard deviation of measurement k
φ	A phase in a three phase system, e.g., $\varphi = a, b, c$
$\hat{x}$	Estimated quantity
$(\cdot)^H$	Hermitian operation (complex conjugation followed by transposition)
$(\cdot)_r$, $(\cdot)_i$	Real and imaginary parts of a complex quantity
$\binom{n}{m}$	Combinatorial
$\|\|\cdot\|\|_p$	A p-norm of a vector
$(\cdot)^t$	Transposition
$\odot$	Boolean OR operation
$\otimes$	Boolean AND operation

1. The future electric distribution infrastructure

1.1 Scope of this dissertation

A distribution class state estimator is proposed as a feasible response to requirements for enhanced monitoring and control of a power distribution system in the Smart Grid environment. The Smart Grid initiative in the U.S. and similar initiatives globally are direct drivers of power grid modernization. Major weaknesses identified in contemporary distribution system architectures include the lack of feeder monitoring and visualization technology and a lack of control options.

As envisioned here, the estimator is a tool to facilitate: higher penetrations of distributed generation (DG); switching; distribution automation (DA); voltage scheduling; and optimized reactive power injections. Efficient operation, enhanced reliability and rapid restoration become possible. The estimator is designed to run in a distribution management system (DMS) supervisory application that utilizes measurements to calculate feasible solutions to solve near real-time operational issues, and alert operators to abnormal or problematic conditions.

This dissertation addresses the following as they relate to power distribution systems: the Smart Grid initiative; implications on future systems; theory of reliability and restoration; sensory based automation; characteristics of conventional versus smart systems; modeling assumptions used to build estimator algorithms; measurement infrastructure; historical context of state estimation; and formulation of a linear, non-iterative, three-phase distribution class state estimator.

Notable applications of the state estimation algorithm are illustrated. Applications include demand response (DR), voltage unbalance minimization, load estimation and enhanced voltage control. This dissertation attempts to analyze and obviate distribution level impacts of the Smart Grid initiative.

1.2 The Smart Grid initiative

The Smart Grid initiative may be summarized as the *modernization* of the U.S. electric energy infrastructure as discussed in the U.S. Department of Energy (DoE) Grid 2030 vision [1]-[6]. The salient points of Title XIII of the Energy Independence and Security Act (EISA) of 2007 [1] outline plans for a modern, reliable and secure electric infrastructure and are discussed in Table 1.1. Figure 1.1 is a graphic depiction of the Smart Grid concept.

Table 1.1 Salient Points of Title XIII of the EISA of 2007

1. Increased use of digital information and controls technology to improve reliability, security, and efficiency of the electric grid.
2. Dynamic optimization of grid operations, with full cyber-security.
3. Deployment and integration of distributed energy resources (DER) and distributed generation (DG), including renewable resources.
4. Development and incorporation of demand response (DR), demand-side management (DSM) resources, and energy-efficiency resources.
5. Deployment of 'smart' technologies for metering, communications concerning grid operations and status, and distribution automation.
6. Integration of 'smart' appliances and consumer devices.
7. Deployment and integration of advanced electricity storage and peak-shaving technologies, including plug-in electric and hybrid electric vehicles (PHEV), and thermal-storage air conditioning.
8. Provision to consumers of timely information and control options.
9. Development of standards for communication and interoperability of appliances and loads, including infrastructure serving the grid.
10. Identification and lowering of unreasonable or unnecessary barriers to adoption of Smart Grid technologies, practices, and services.

This research is part of a Power Systems Engineering Research Center (PSERC) project entitled "Implications of the Smart Grid Initiative on Distribution Engineering". The project statement identifies that 'Smart Grid initiatives' and similarly named efforts are targeting the modernization of the electricity grid. Noticing that efforts have largely focused on transmission system improvements, the project attempts to identify adaptations of the distribution system. This effort includes studying selective conversion to networked distribution, utilization of sensory signals at the local and hierarchically higher levels for both supervised and fully automated control, and the development of enabling strategies and interconnection configurations for renewable resources at the distribution system level.

This work is also supported in part by the National Science Foundation (NSF) under the Engineering Research Center program in a national ERC denominated FREEDM (Future Renewable Electric Energy Delivery and Management) center. The focus of FREEDM is the use of solid state devices for power system control. The use of solid state controllers considered here relate to the following roles:

- Rescheduling of power during restoration
- Control of DG – particularly renewable generation resources
- Control of selected loads to effectuate peak demand reduction.

Additionally, visualization is a key element of distribution system operation, and this too is part of the FREEDM portfolio; this is an important focus of state estimation in distribution systems. References [7], [8] relate to the FREEDM mission.

1.3 Industry changes and renewable portfolio standards

The deregulation and subsequent restructuring in many parts of the U.S. electric power industry assumes that a market based structure offers greater benefit to consumers as competing suppliers enter the market; this concept is elaborated in [9]-[15]. However, distribution businesses generally remain heavily regulated. Also, environmental concerns manifest themselves in regulations or incentives. An illustration of this point is the Renewable Portfolio Standard (RPS). RPSs are present in 34 U.S. states as of September, 2011; note that RPSs encourage renewable sources like solar and wind [16]-[18] and may provide penalties for utilities that fail to meet goals. Also, independent power producers (IPPs) become major participants in supplying electric power.

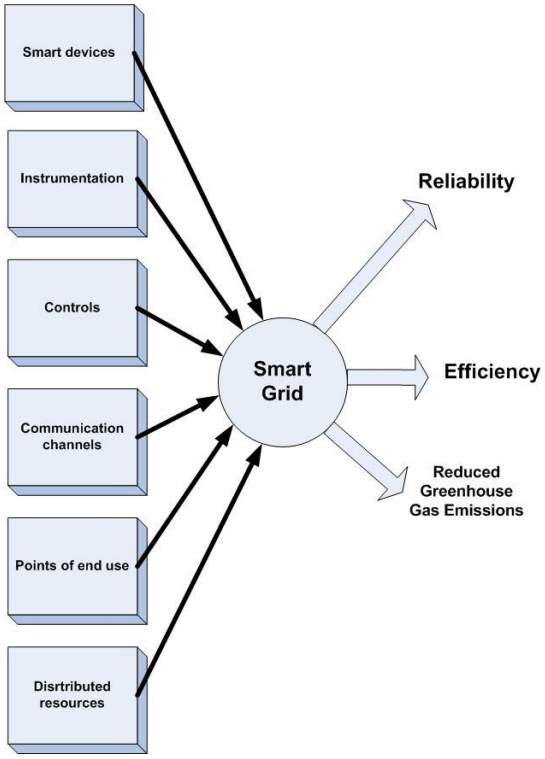

Figure 1.1 Depiction of the Smart Grid concept

1.4 Impacts of these changes on distribution systems

The impacts of deregulation and renewable incentives on distribution systems may be seen globally. In territories with aggressive RPS (or goals), small renewable electric generators are often connected at the distribution level. For example, California and Ireland target 33% and 40% of energy served must be supplied by renewables by 2020 [17], [21], [23]. Ireland expects 50% of new wind generators to be installed at distribution voltage. These events outline significant departure from conventional utility generation expansion. IPPs and small residential solar PV and wind farms are necessary to meet aggressive RPS targets.

The power system issues of monitoring, operation and control are likely to extend into the distribution level. Operators may seek to expand mitigation options to maintain system security and reliability. Table 1.2 identifies key attributes of the Smart Grid initiative and distribution level impacts. Challenges identified with certain items identified in Table 1.2 are elaborated. These are motivating factors behind the development of a distribution class state estimator.

1.5 Conventional distribution system design and operation

Designing, operating and measurement characteristics of distribution circuits are presented before state estimation and control may be introduced. Distribution systems interface most customer loads to the electricity supply. Unique characteristics prevent simple adaptation of transmission modeling and analysis methods for system studies, including state estimation. Literature on design, modeling assumptions and analysis methods includes [23], [25]-[28], [45] as a small sample.

Feeder reconfiguration, networking and automation are studied in [14], [23], [29]-[36], [45]. Distribution planning, operation and reliability are discussed in [23], [29]-[41].

Table 1.2 Distribution Level Requirements and Impacts of Smart Grid Initiative Items – Potential Applications Enhanced by Distribution State Estimation

Smart Grid Initiative Item	Distribution Level Requirements and Impacts									
	Monitoring	Control	Voltage regulation	Asset utilization	System protection and coordination	Sensory network	Advanced 2-way communications	Customer participation	Energy efficiency	Peak shaving
Digital controls	x	x			x	x	x			
Distributed generation	x	x	x	x	x	x	x	x		x
Distributed energy resources (DER)	x	x	x	x	x	x	x	x	x	x
Demand response (DR)	x	x	x	x	x	x	x	x	x	x
Demand side management (DSM)	x	x	x	x	x	x	x	x	x	x
Smart appliances			x	x			x	x	x	x
Smart metering	x	x		x		x	x	x		
Enhanced controls and communication	x	x	x	x	x	x	x	x	x	x
Price and control signals to consumers	x	x		x		x	x	x	x	x

† Distribution primary voltages range from about 7–15 kV

†† Distribution secondary or utilization voltages range from about 110–480 V

Conventional distribution system characteristics, sensory data, metering, DG, modeling and operation methods are discussed subsequently. Note that these differ significantly from transmission system operation. All design and operating

characteristics presented subsequently are critical aspects in the development of a practical state-estimation algorithm.

Network design

Networked design offers operational flexibility, redundant paths, and better service reliability [26], [29]-[40]. Distribution systems are designed as highly interconnected networked systems [23]-[28]. Figure 1.2 demonstrates a conventional distribution network design. Primary distribution feeders are generally constructed as networks but operated as radial feeders via normally-open tie switches.

Networked operation is preferred for dense loads requiring high reliability; for instance, many downtown/urban districts are operated as networks [23]-[28]. Even secondary distribution may be operated as networks [32]. Networked protection is often cited as a limitation; it is expensive and complicated to coordinate when compared to radial system protection [26]. High voltage transmission systems are often built and operated as highly interconnected networks as they demand high reliability.

Radial operation of conventional distribution systems

Radial operation is conventional in the U.S. Economics, simple overcurrent protection, operating flexibility and the nature of loads are often cited as reasons for radial operation [26]. Also, simplified modeling and simulation by voltage drop calculation [25]-[27] are achieved. Radial feeders are shown in Figure 1.2.

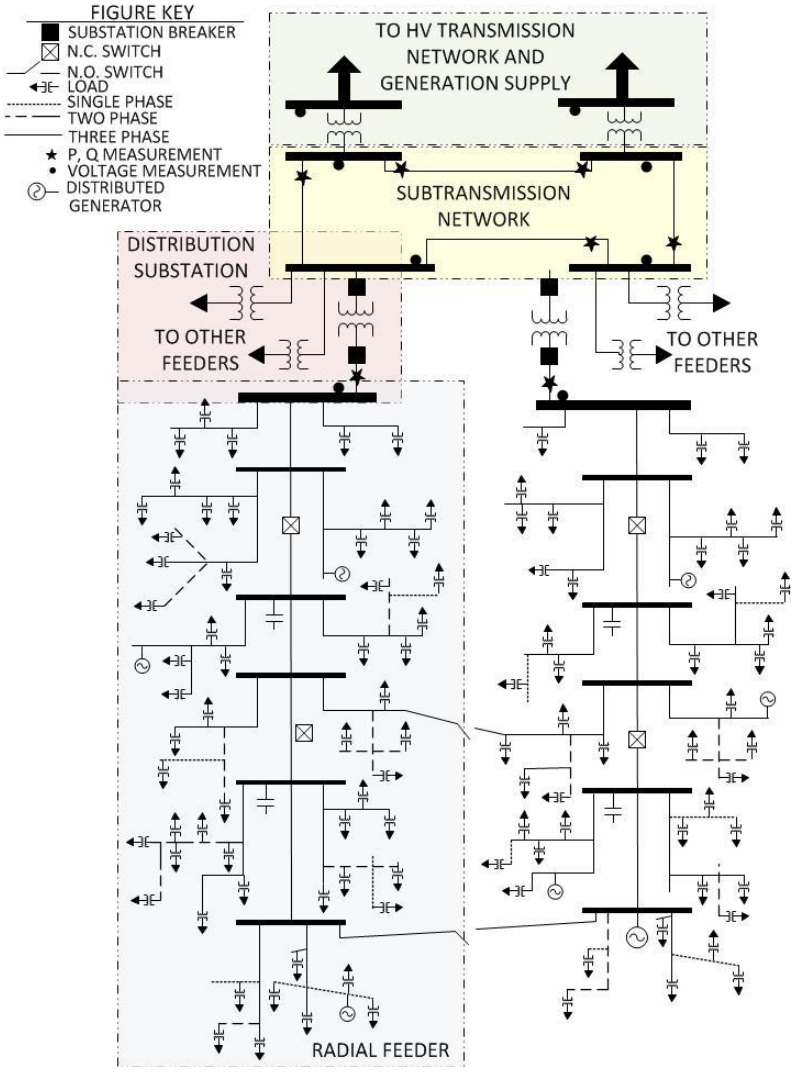

Figure 1.2 An example of conventional distribution system design

High r/x ratios

The literature often identifies high *r/x* ratios as characteristic of distribution systems. Significant impacts on modeling, simulation and analysis include: violation of assumptions used for fast decoupled power flows; documented instabilities when using Newton Raphson iterative algorithms; and inability to solve networks using DC approximations [25], [28], [42]-[45]. For example, assumptions that al-

low fast decoupled methods for power flow analysis are violated in networks with high *r/x* ratios (namely, the assumption that line *r* is much smaller than *x*). Figure 1.3 shows *r/x* ratios plotted for a range of ACSR conductor sizes (cross-sectional area in kcmils) for distribution and transmission lines; data is obtained from tables in [28][58]. In formulating a state estimator, the calculation procedure must work for networks with high *r/x* ratio conductors.

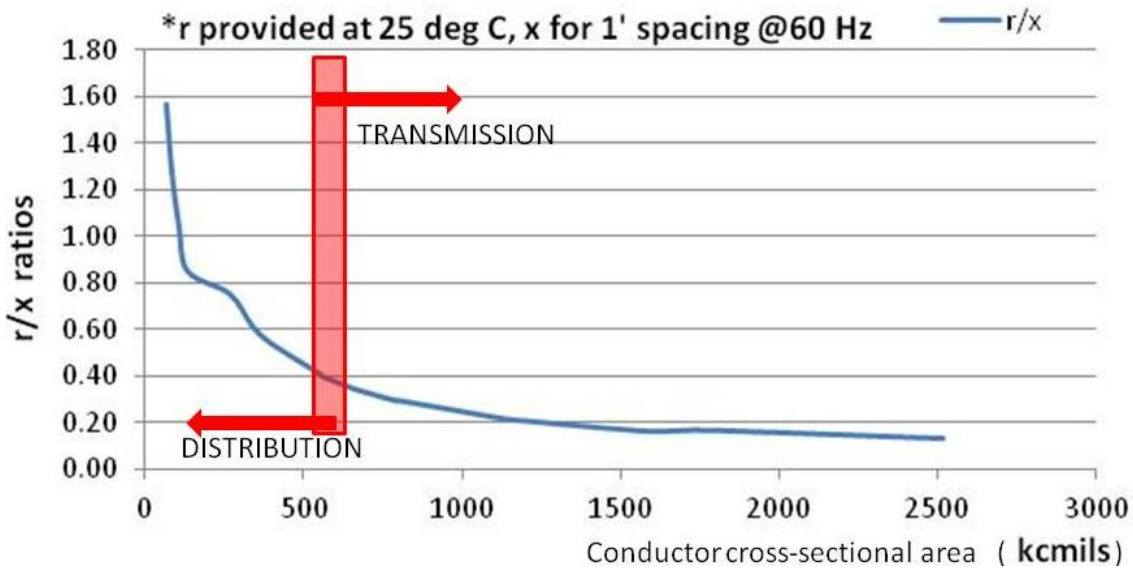

Figure 1.3 Typical *r/x* ratios for distribution and transmission ACSR conductors

Short run line segments serving distributed and unbalanced load

Distribution system design depends on a variety of factors including the environment, nature of loads to be served, economics, safety and others. Generally, most U.S. utilities use three-wire (delta, ungrounded) or four-wire (wye, multi-grounded) circuits with a common neutral. Advantages of four-wire multi-grounded systems include: high short-circuit currents for discrimination in over-current relaying; inexpensive single phase service; and lower surge arrester rat-

ings (multiple ground paths for surge impulse) [26]. A variety of transformer connections are also available. The interested reader is referred to [26].

Distribution circuits are characteristically populated by distributed loads separated by short physical distances [26], [27], [45]-[50]. Main feeders are generally three-phase. Laterals may be three-phase, single-phase, or consist of two-phase conductors and a neutral. Unbalanced loading and mutual coupling between phases result in unbalanced line flows and voltages during normal operation [25], [27]. In system modeling, distributed loads and short line segments increase complexity of system models. This is significant for both power flow and state estimation algorithms.

Unbalanced loads, laterals and voltage unbalance

The a priori planning method of balancing loads (MW/phase) does not entirely solve the unbalance issue. Individual loads vary widely with time (stochastic), but load types tend to follow similar patterns (correlation) [45]-[51]. The voltage unbalance issue is problematic for utilities. Operation of three-phase rotating equipment, effectiveness of protection systems, and protection coordination are affected [59]-[63]. Voltage unbalance is defined by IEEE as the ratio of negative to positive sequence voltages,

IEEE
$$V_{unbalance} = \frac{V^-}{V^+} * 100 \qquad (1.1)$$

Phase to sequence transformations can be found in the literature [25][28]. Voltage unbalance may be approximated from *magnitude-only* calculations. One such ap-

proximation for voltage unbalance uses phase to neutral voltage magnitudes to approximate, this results in higher % unbalances than obtained from Equation (1.1),

$$\%V_{unbalance}^{approximate} \cong \frac{max\left\{\left||V_{an}| - V_{avg}\right|, \left||V_{bn}| - V_{avg}\right|, \left||V_{cn}| - V_{avg}\right|\right\}}{V_{avg}} *100 \quad (1.2)$$

where,

$$V_{avg} = \frac{1}{3} * (|V_{an}|+|V_{bn}|+|V_{cn}|)$$

The National Electrical Manufacturers Association (NEMA) [63] definition for voltage unbalance uses line-line voltage magnitudes and approximates Equation (1.1) well for small percentage unbalance,

$$\%V_{unbalance}^{approximate} \cong \frac{max\left\{\left||V_{ab}| - V_{avg}\right|, \left||V_{bc}| - V_{avg}\right|, \left||V_{ac}| - V_{avg}\right|\right\}}{V_{avg}} *100 \quad (1.3)$$

where,

$$V_{avg} = \frac{1}{3} *(|V_{ab}|+|V_{bc}|+|V_{ac}|)$$

Literature suggests that the approximations given by Equation (1.2) and Equation (1.3) are valid for low values of unbalance but deviate appreciably as the percent unbalance increases [60]. Note that Equation (1.1) includes the effect of voltage phase angle which may be difficult to determine by direct measurement. Current unbalance is approximately 6-10 times the magnitude of percent voltage unbalance [59] [63]. More details are discussed in the state estimation formulation, and the effects of unbalance and load uncertainty are shown in illustrative examples.

Low penetration of installed DG

Conventional systems have low penetration of installed DG. Penetration level here is taken as installed capacity relative to installed feeder load. Conventional distribution feeders have no appreciable installed DG. RPSs and grid modernization efforts have started to change this characteristic. Monitoring, controlling and effectively utilizing DG may become necessary in smart distribution networks. The effective execution of microgrid strategies may depend on DG management [65]-[69]. Tools like the DMS based state estimator may become necessary in networks with high DG penetration.

Voltage regulation

Distribution circuit voltage regulation equipment may be sited on the feeder or at the substation [59]. Substation equipment comprises of utility DG, capacitors, or tap-changing (ULTC) transformers. Circuit regulators include shunt capacitors and step voltage regulators [24]-[26]. Regulators may control each phase voltage independently. Generally all phases of shunt capacitors are switched together.

Other options include raising primary feeder voltage, larger conductors, low impedance transformers, load balancing, converting line sections to three-phase, and transferring loads to other circuits [59]. A comprehensive voltage unbalance study with regulation options is provided in [59]. Note that in conventional distribution systems most DG cannot actively regulate bus voltage [45]. Distribution state estimation may enable DG-based voltage regulation in future systems.

Over-current protection

References [26][28] detail distribution system protection schemes, equipment and coordination. Overcurrent protection is employed on radial feeders. Feeder laterals are generally protected by a fuse, recloser or sectionalizer [26]. System protection is coordinated to ensure reliability while maintaining system security [26]. Protection and fault-isolation has direct implication on system reliability and related indices. Networked protection is more complex. The interested reader is referred to [26], [28], [96].

Conventional sensors and measurements in distribution systems

Various sensors are available in the distribution system. Transmission and distribution infrastructure has a variety of applications requiring sensing: relaying and protection, control, communication, condition monitoring, state monitoring and maintenance. Table 1.3 presents conventional transmission and distribution system measurements and units. Data reporting rates, communication protocols and communication technologies are beyond the scope of this dissertation.

Table 1.3 Conventional Transmission and Distribution System Measurements

Quantity being measured	Device	Units
Bus voltage magnitude	Potential transformer (PT)	V – kV
Line current magnitude	Current transformer (CT)	A
Real power injections or flows	PTs and CTs	W – MW
Reactive power injections or flows	PTs and CTs	VAr – MVAr
Revenue metering	Watt-hour meters	Wh - MWh

Transducer accuracy requirements depend on the application. For example, billing applications often utilize high-precision sensors. Lindsey presents a range of contemporary sensors (CTs and PTs), applications and device accuracies in [75]-[76]. Notable sensor accuracy ranges include PTs (0.3% - > 5%), [75], CTs (0.3% -5%). These are subset of available distribution system sensors; however, an exhaustive list may be obtained from [58], [75], [76].

In conventional distribution systems, only substation bus voltage, and line power/current flows are available. A few main feeder current or voltage measurements may also be provided. Sensor availability and placement are critical aspects in formulating a distribution state estimator.

Revenue metering and historical load data

Revenue metering of customer demands is done continuously. However, data has historically been analyzed for engineering/decision making only periodically. Customers may be charged for both energy consumed and peak usage. Previous approaches to distribution state estimation relied heavily on historical load data.

Distribution system modeling and simulation

The characteristics of distribution circuits justify the use of different analytical simulation tools from transmission system. The ladder iterative voltage drop method discussed in [25] is common for distribution system analysis. Analysis of feeders with weakly meshed networks may employ breakpoints to effectively rad-

icalize the system [54]. Abur in [57] developed a three-phase Newton-Raphson algorithm capable of solving distribution networks with DG and voltage regulators. Considerations include model detail / size, required solution accuracy, and the need to model down to individual customer loads / DG. These may be important factors in developing state estimation algorithms.

1.6 The smart distribution system and need for state estimation

Areas of focus in Smart Grid initiative adaptations include: improving delivery efficiency, maximizing asset utilization, creating flexible networks and enhancing communication and information exchange. References [6], [14], [23], [66], [86] present discussions of these issues. These evolving systems add sensors; two-way communications; DG; responsive loads; electronic controls and loads; and supervisory control and alarm systems for awareness [65]-[74]. Operating characteristics change as DG, switchable elements, and adequate communications permit self-sustaining microgrid islands [65]-[67]. Direct load control, responsive loads and local generation may interact to provide flexibility to operators and customers [65]-[69].

High penetration of distributed generation and storage

Residential and commercial PV systems and small wind farms connected to distribution voltages are DG examples [22], [23]. However, wind and solar DGs are characteristically variable. At higher penetration levels, DG variability and

power flow directions may become significant [85], [86]. Illustrations to this point are presented in later chapters.

Energy storage devices such as batteries are also likely in a smart distribution system [67], [72], [93]-[95]. The focus of this work is system control and reliability; therefore, storage devices are relegated to tools to accomplish control, and elements which allow increased operating flexibility. Monitoring, control and storage are likely limiting factors to effectively expanding DG interconnection.

Impact of solar and wind DG intermittency on distribution circuits

Distribution circuits with high DG penetration may be impacted by variability. One notable impact of intermittency is the effect on local system voltage, unbalance, and automatic voltage regulation equipment [23], [85]-[86]. Accommodating DG expansion is likely to be a major challenge for utilities. The distribution system state estimator is envisioned as a tool to assist control and optimization of DG and alerting operators to system issues.

Networked primary and secondary systems

References [30], [32]-[34], discuss both advantages and disadvantages of networked distribution systems and impacts on reliability and restoration. Networked operation provides superior redundancy, and therefore reliability [26], [29], [30]-[37]. High voltage transmission systems require high reliability; consequently, they are operated as interconnected networks.

Contemporary distribution systems are operated as radial feeders [25]-[27]. Normally open switches in Figure 1.2 shows how the primary voltage level may be networked by closing switches. In this case, adaptive protection systems are required. Cost of operating and protecting networked distribution has historically been a barrier, high except in dense urban networks or loads requiring high reliability [29]-[35]. Networked operation may facilitate higher DG penetration and maximize asset utilization. Estimation based monitoring and control in this case may be required.

Demand response and increased customer participation

Grid operators searching for an enhanced array of control options to help ensure system integrity and reliability may reach into distribution systems [14], [87]-[91]. Improved distribution level modeling, analysis, monitoring and control are essential to extending the opportunities for broad system control by power system operators. Demand response (DR) is one such mechanism being explored.

Electric demand is characterized as highly inelastic in power system economics [9]-[11]. DR and price transparency in distribution networks may increase demand elasticity [14], [87]-[89]. DR and conservation programs curtail loads during high (transmission) stress periods that generally correspond to high nodal prices [14], [87]-[91]. Direct load control, and DR options may characterize smart distribution systems [87]-[89], [91]. Aggregating small loads and DGs to achieve broader operational impact—also referred to as the virtual power plant—may be-

come viable given adequate monitoring and control. Reference [74] has identified 58,000 MW of demand response enabled load across the U.S. as of 2010.

Improved modeling of distribution networks

Better modeling of distribution systems will allow a greater degree of detail, control, and predictable system response. Therefore operators may push the distribution system closer to its operating limits and maximize asset utilization. References [23], [25], [68], [85]-[86] indicate that better modeling and analysis of the typically over-designed distribution system is necessary. An illustrative example in Appendix A demonstrates the difference in resulting bus voltage magnitudes comparing two different modeling assumptions.

Distribution automation

Distribution automation (DA) focuses on using technologies such as voltage regulators, tap changing transformers and others to regulate voltages. Automated functions at the substation level replace operator initiated action [14], [23], [68]-[72]. Simple reconfiguration or restoration actions may be automated from the distribution substation. The distribution state estimation application is proposed as a supervisory DMS application. The development and implementation of an information technology (IT) layer into distribution substation operations builds on lessons learned from transmission engineering. For instance, nascent DMSs per-

form functions analogous to energy management systems (EMS) prevalent in transmission systems [66]-[72].

Smart meters and the advanced metering infrastructure

State-of-the-art revenue meters (*smart meters*) collect and store power, energy consumption, and voltage magnitude data. Data may be reported directly to utility servers at common intervals (15-60 minutes) [73], [74]. Smart meters are an evolution of electricity metering; telecommunication and automation capability is added. Smart meters have increased penetration from 4.7 to 8.7% from 2008 to 2010 [74]. Some utilities have as high as 25% smart meter penetration. Smart meters are assumed to be a predominant sensor in the state estimator formulation developed here.

Phasor measurements in the power system

State-of-the-art power system sensors are capable of synchronously measuring voltages across the grid. The Global Positioning System (GPS) of satellites allows dispersed measurement devices to be synchronized to the same clock signal. In theory, 'time-stamped measurements' are compared to a single reference and angular information may be determined. Details are applications to power system are discussed in [97]-[105]. IEEE standard C37.118-2005 provides standards, definitions, device requirements, accepted sampling rates, data processing, measurement accuracy and message format [97]. Phasor measurement units (PMUs) are

expected to have a major impact on power system state estimation, grid visualization, adaptive protection systems and system operation [99]-[105]. PMUs compatible for distribution systems are utilized here to formulate the estimator.

Other considerations

Other technical issues surrounding the deployment of smart distribution systems relate to: energy storage; voltage and frequency regulation; different load types—e.g. plug-in hybrids and electric vehicles (PHEVs and EVs); energy management and optimization functions with DMS in substations; distribution automation and managing interactions of these subsystems to effectuate desired change at the bulk power system (i.e. demand response for peak shaving, energy storage and release for peak shaving) [23], [86], [92]-[95]. Strategies for optimizing the effectiveness of these technologies must be implemented [10], [12], [14].

Rethinking traditional distribution system operations and control may be required. For example, IEEE Standard 1547 prevents DGs from regulating system voltages, and requires disconnection of DGs (< 10 MVA) to disconnect from the grid during abnormal system operation [45]. Conventional operating practices, e.g. [31]-[45], may be shown to be suboptimal. Islanding into self-contained microgrids where local generation supplies local loads during a utility disturbance may become practicable [65]-[67].

1.7 Power system state estimation

State estimation for power systems was proposed by Schweppe [106] as a way of observing system state by fitting measurements to the assumed system model. The first commercially operational power system state estimator was implemented in AEPs system in the 1970s [100]. Today, state estimation is used extensively at the transmission level. The state estimate provides the best fit of measurements to the assumed system model [42], [105]-[107].

In transmission system state estimation, the state vector is taken as the positive sequence bus voltage magnitudes and angles [100]. Measurements include bus voltages magnitudes, injections, and line flows. The estimated topology is verified, and the static state vector is calculated. States at non-metered buses and all line flows may be calculated. Topology processing, observability analysis, estimation of states, bad data processing and parameter processing are typical functions of an estimator [105]. In transmission engineering, the estimator allows online assessment, real-time monitoring and other applications that give operators enhanced control.

Weighted least squares (WLS) estimation, maximum likelihood estimation (MLE) or minimum variance estimation are common solution methods for power system state estimation [42], [105]-[107]. The procedure assumes the network model is known. Topology error processing bad data detection are easily accommodated in most state estimator algorithms [42],[105],[107].

1.8 Distribution system state estimation

Previous approaches to the distribution state estimation formulation are discussed in [46]-[56]. In [46] a state estimation algorithm involves constraints on circuit quantities such as power factors, and real and reactive parts of substation transformer currents. In the classic reference, [47] weighted least squares (WLS) formulation for transmission systems is developed in three-phase for distribution systems. Use of branch current state vector was shown in [48]-[49]; decoupling of phases and increasing computational efficiency are shown. Note that bus voltages are calculated subsequent to a converged branch current estimation.

Authors of [50] discuss distribution system modeling using voltage-dependent load currents instead of conventional constant power loads; additionally, the authors introduce the synchrophasor measurement concept to distribution. Authors in [51] focus on modeling of loads, pseudo-loads and reliability of historical data; where already uncertain data is presented, added heuristic reliability factors are introduced. References [52]-[53] evaluate the choice of different estimator formulations on results and modeling of pseudo-measurements respectively. In [54] an estimation method based on the ladder iterative approach (e.g. [25]) is presented, along with criticisms of alternate formulations as being too complex and not easily adapted to existing distribution analysis methods. [55]-[56] present applications including topology error identification and observability analysis for distribution.

Common themes appearing in literature include real-time measurement paucity, dependence on historical load data, and large ratio of pseudo-measurements to

create observable scenarios [46]-[56]. An alternate distribution system state estimation formulation given communications and sensory advances is presented in Chapter 3.

1.9 Organization of this dissertation

In this research, applications utilizing distribution system state estimation are proposed for smart distribution systems. Applications include condition monitoring; reliability, reconfiguration and restoration functions; partial networking; DG and storage management; and automation. Smart metering, synchrophasors and bidirectional communications may be leveraged for control in the Smart Grid.

Chapter 2 contains an overview of power system reliability, restoration and networking theory. Algorithms intended to aid distribution system planners and operators are developed. Chapter 3 presents power system state estimation, distribution system modeling, and the formulation of a three-phase, linear distribution system state estimator. Illustrations of reliability and restoration in the Smart Grid are presented in Chapter 4. State estimation performance is shown in Chapter 5. Applications of the distribution system state estimator are shown in Chapter 6. Chapter 7 presents general remarks and concludes; appendices follow.

2. Distribution system reliability and restoration

2.1 Distribution system reliability

Distribution engineering is a complex science that involves striking a balance between multiple objectives that include: power quality, reliability, efficiency, voltage regulation, safety to the general public, environmental impacts, aesthetics and cost. Power quality refers to the nature of the delivery voltage waveform and minimizing harmonics and waveform distortion within the system [27], [31], [36], [96]. Reliability is a subset of power quality and entails the continuous supply of electrical power to the loads when needed [29]-[41].

Distribution system performance generally has the greatest effect on customer reliability. For example, [38] indicates that approximately 80% of interruptions to customers occur at the distribution level. Networking to provide redundant paths and adding DG and DER tend to increase reliability, but at a cost [14], [29]-[40].

2.2 Basic reliability indices

The system average interruption duration index, SAIDI, and the system average interruption frequency index, SAIFI, are perhaps the most eminent distribution system reliability indices,

$$SAIDI = \frac{Total\ duration\ of\ all\ interruptions}{Total\ number\ of\ points\ of\ delivery\ monitored} \tag{2.1}$$

$$SAIFI = \frac{Total\ number\ of\ interruptions}{Total\ number\ of\ points\ of\ delivery\ monitored} \tag{2.2}$$

SAIDI and SAIFI do not capture all information relating to system reliability. That is, they omit the magnitude of load lost during outages. These indices are also inconsistently calculated and factors that constitute omissions vary from one utility to another [41], [64]. Note, also, that SAIDI and SAIFI calculations exclude outages shorter than 5 minutes (and severe weather events). Exact calculations and exclusions may be found in [108].

Additional similar indices are the customer average interruption duration index (CAIDI) and the average service availability index (ASAI),

$$CAIDI = \frac{Sum\ of\ all\ \ customer\ interruptions\ duration}{Total\ number\ of\ customer\ interruptions} = \frac{SAIDI}{SAIFI} \tag{2.3}$$

$$ASAI = \frac{Customer\ hours\ service\ availability}{Customer\ hours\ service\ demanded} = \frac{8760 - SAIDI}{8760} \tag{2.4}$$

Note that the ASAI and similar indices may be expressed as a 'number of nines,' *N9*, where

$$N9 = -log10(1-ASAI). \tag{2.5}$$

Thus *N9* for ASAI = 0.9999 would be 4 as an example. Equation (2.5) may be approximated by the Taylor series expansion,

$$N_9' = N_9 + \frac{0.43429}{1-ASAI}(\Delta ASAI) \tag{2.6}$$

where a system upgraded from ASAI to ASAI + ΔASAI, results in a concomitant increase in reliability of N9 to N_9' ; note that approximation is most accurate

where ΔASAI is small. This concept is depicted in Figure 2.1 where small increases in ASAI, from $ASAI_1$ to $ASAI_2$, may be approximated by Equation (2.6).

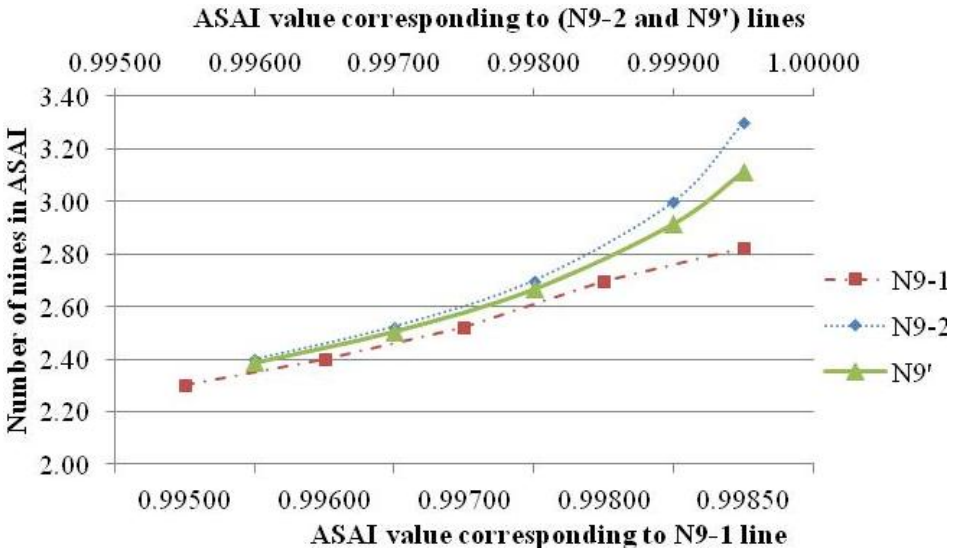

Figure 2.1 Approximating small increments in ASAI changes with Equation (2.6)

Similarly, for SAIDI change to SAIDI ± ΔSAIDI, where ΔSAIDI is small,

$$N_9' = N_9 - \frac{0.43429}{SAIDI}(\Delta SAIDI) \tag{2.7}$$

Since these indices are system averages, they may not give information on specific bus reliability. For specific bus reliability, load point indices are required. The reliability measures of distribution system components or individual buses, or load point indices [29],[30][38], can also be determined. These indices include the average failure rate, λ (expected number of failures/year); expected outage time, r (h); annual unavailability, U (h/y); and expectation of unserved energy, E (kWh/outage or kWh/y), that captures the energy demanded by system loads that cannot be delivered to those loads [38].

System failure rates, repair times and outage times depend on system configuration and series connected versus parallel connected components. Figure 2.2 shows a system of series connected components. Figure 2.3 shows a system of parallel connected components. System average failure rate, repair time and outage time are calculated in Equations (2.8)-(2.10).

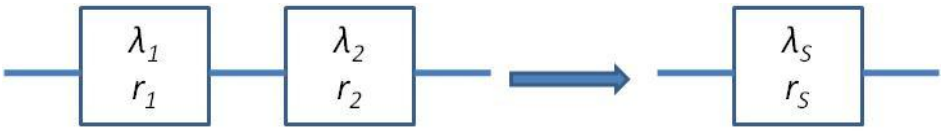

Figure 2.2 System representation of series connected components

System average failure rate	$\lambda_S = \Sigma(\lambda_i)$	outages/year	(2.8)
System average repair time	$r_S = (\Sigma \lambda_i r_i) / (\Sigma \lambda_i)$	hours/year	(2.9)
System average outage time	$U_S = \lambda_S r_s$	hours	(2.10)

Reliability calculations for parallel components are shown,

System average failure rate	$\lambda_P = \lambda_1 \lambda_2(r_1+r_2)$	outages/year	(2.11)
System average repair time	$r_P = (r_1 r_2)/(r_1+r_2)$	hours/year	(2.12)
System average outage time	$U_P = \lambda_P r_P$	hours	(2.13)

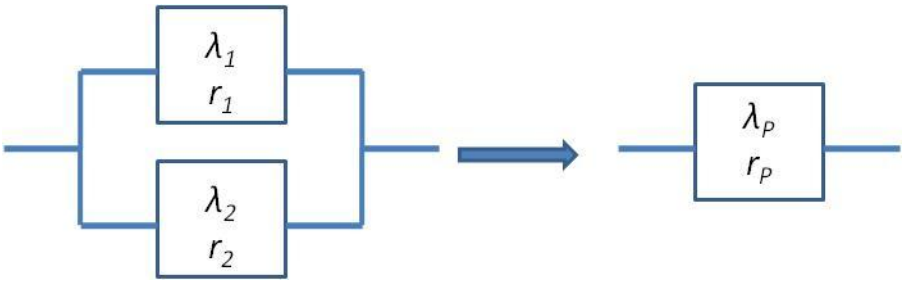

Figure 2.3 System representation of parallel connected components

Note that the probabilistic reliability data are based on manufacturer specifications and historical performance unique to the area of study. For example weather

effects, aged components and other factors affect life expectancy. Expected SAIDI and SAIFI indices may be calculated based on Equations (2.12) and (2.13) when the number of customers connected to each load point is known. Load point indices may be used to evaluate relative performance of alternative system designs, restoration plans or system topology changes. Reliability benchmarking in a repeatable and standardized environment is discussed in [41].

Background material developed here is used to develop illustrative examples of reliability analysis and improvement. Reliability improvement methods are presented subsequently. Illustrative examples are shown in Chapter 4. Examples include switching automation, reconfiguration for improved reliability and sensor based monitoring of the electric distribution infrastructure.

2.3 Improving distribution system reliability

High reliability and fault tolerance requires multiple redundant paths, and strategies for rapid fault detection, isolation and reconfiguration (FDIR). FDIR in contemporary distribution systems is limited to local protection schemes which typically do not communicate system wide activity. Thus, in order to selectively convert existing networked distribution systems into smart distribution systems, it is proposed to add FDIR mechanisms and automated control concepts; for example, embedded in DMS software. The methods used shall also replicate transmission system concepts that use system restoration logic to automatically restore the distribution system. Using circuit matrix concepts, the optimization of the relia-

bility at system buses shall be performed based on the reliability of individual components. Illustrative examples and discussion are provided in Chapter 4.

2.4 Distribution system restoration

Distribution system restoration is concerned with reenergizing feeders / loads that have experienced an outage. Transmission system restoration following a major outage is widely covered in the literature. However, references [108], [110]-[115] provide comprehensive coverage of distribution and transmission restoration. Transmission system restoration is critical following major grid disturbance. Expediency to allow load restoration; it is concerned with black-start generation, island synchronization then full system restoration. Many restoration functions rely on heuristics. Digitizing restoration functions is one aspect of distribution automation [24]. The foundation for developing a continuous running process to sensing when to restore is presented subsequently.

The size (e.g. MW) and duration of the outage are critical aspects to distribution system restoration; additionally, restoration time drastically affects expectation of unserved energy. Small, short duration outages are less problematic. However, if an entire distribution feeder has been de-energized for an hour, restoration includes cold-load pickup and inrush currents which become problematic for system protection; a more careful reenergization plan must be undertaken [26], [112]. Pre-outage loading, cold-load pickup effects, and available network topologies are critical aspects to distribution restoration. As a small example, consider a substation transformer serving 5 MVA on a radial feeder. A lateral serving 200

kVA experiences a fault and subsequent outage lasting 20 minutes: the reenergization plan may be simply to replace a blown fuse or switch to an alternate source to restore normal operation. This looks like a small positive step change in loading at the substation.

References [33], [36], [96], [109]-[116] identify challenges to distribution system restoration. Outage detection and restoration may be categorized: outage detection and location; data gathering via customer calls and SCADA systems; visual inspection for outage cause verification; take action to restore system from outage [116]. References [109]-[116], discuss distribution system restoration issues that include, but are not limited to, cold load pickup, transformer thermal behavior and optimizing restoration order. Discussions of restoration methods indicate that a combination of different techniques such as analytical, heuristic and knowledge-based systems are used to effect restoration.

Distribution system design should enable reconfiguration and restoration functions that improve reliability. Restoration may be objectively formulated, for example: reduction of SAIDI (duration index), minimization of expected unserved energy to loads, minimization of switching commands. A simple algorithm aimed at reliability monitoring and restoration assisting is provided in [117].

2.5 A network theoretic approach to distribution system reliability

An overview of graph theoretical concepts is presented in the next few paragraphs. The application of graph theory to the power distribution system is explained, and algorithms exploiting graph theoretical concepts are developed.

The physical layout of a power system may be represented by a set of nodes/buses, connected by a set of edges/branches/lines) [120]-[122]. From graph theory, a graph is an ordered pair consisting of a set of nodes, *n*, and a disjoint set of edges, *e*, that can be mathematically characterized by an incidence function – usually a matrix – that associates nodes with edges. Edges emanating from or arriving to a node are referred to as incident to a node. Branches may form loops, be parallel branches, or connect adjacent nodes.

Directed edges are specified as leaving one node and arriving at another; such a system is called a directed graph, or digraph. A symmetric digraph has bi-directional edges connecting nodes and may be treated as undirected [120]. Undirected graphs cannot have loops (a branch leaving and arriving at the same node). Figure 2.4 (a) and (b) show a digraph and undirected graph respectively. A power system can be represented as an undirected graph, where nodes / buses are connected by branches.

A *path* refers to a graph whose nodes are both linearly and sequentially connected, generally by a *directed walk* connecting *from-node* and *to-node*. In Figure 2.4 (a), the path {*a, b, c, d, a, a*} is connected by directed walk {1, 2, 3, 4, 5}. When all nodes are distinct a *directed path* exists, with length defined as the number of edges. Figure 2.4 (a) shows the set of directed walks M = {1, 2, 3, 4, 5} which is a 5-path digraph connecting the set of nodes {(a, b), (b, c), (c, d), (d, a), (a, a)}. Figure 2.4 (b) shows a 4-path undirected graph, where walks complete

path {*w, x, z, y, w*}. Both graphs are referred to as connected graphs since all nodes are simultaneously connected through edges. A *connected graph* contains at least one path between all distinct nodes. Power systems are generally represented by connected, undirected graphs (as in Figure 2.4 (b)). Subsequent discussions will refer to nodes as buses and edges as branches.

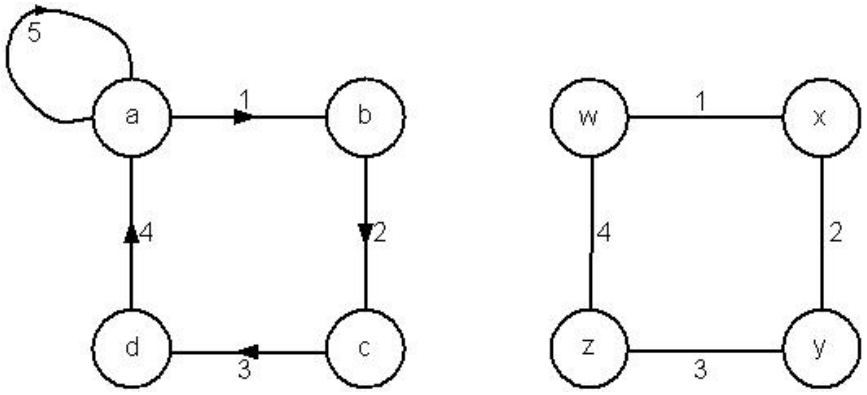

Figure 2.4 (a) A directed graph; (b) an undirected graph

If all buses in the graph are not connected, it is referred to as a disconnected graph or a component of the graph. In a power system, this corresponds to islanded systems. Matrix representation of graphs may be used for modeling and analysis [121]. Modeling the power system is accomplished through graph theoretical concepts such as incidence, *J*, and adjacency, *A*, matrices. The incidence matrix of a graph with *n* nodes, and *e* edges is of size *n* x *e* with entry *1* if a bus is connected to a branch and *0* otherwise. The adjacency matrix, *A*, is of size *n* x *n*, where entries are 1 if buses are connected, 0 otherwise. *J* and *A* for Figure 2.4 (b) are,

$$J=\begin{bmatrix}1 & 0 & 0 & 1\\ 1 & 1 & 0 & 0\\ 0 & 1 & 1 & 0\\ 0 & 0 & 1 & 0\end{bmatrix} \qquad A=\begin{bmatrix}0 & 1 & 0 & 0\\ 0 & 0 & 1 & 0\\ 0 & 0 & 0 & 1\\ 1 & 0 & 0 & 0\end{bmatrix}$$

J here is an unoriented incidence matrix since the graph is undirected.

As discussed, the distribution system may be represented as an undirected, connected graph, where matrices constitute bus and branch connectivity. Power system applications are particularly interested in how removal of a branch or bus impacts the system. Power system data comprise branch connectivity (from-to bus), branch impedance, and location of generators and loads. Power system models (*Y-bus*) are constructed via adjacency and incidence matrices. The subsequent discussion uses binary representation of graphs, and of the adjacency and incidence matrices, in power system applications.

2.6 The binary bus connection matrix

A binary connection matrix, *B*, is used to model the distribution system for connectivity for reconfiguration applications. Branches are modeled as ones when energized and zero otherwise,

$$B = \begin{cases} 1 \text{ for } i=j \\ 1 \text{ for bus } i \text{ connected to bus } j \\ 0 \text{ otherwise} \end{cases}$$

Connectivity for an *n* bus system entails raising *B* to higher powers; the matrix B^{n-1} will contain all *ones* except in positions *ij* where *i* and *j* are not connected to each other through any number of intervening buses. Thus a *zero* entry in B^{n-1} identifies buses that are not energized [44]. *B* is an *n* x *n* matrix containing binary entries. Powers of *B* are found using Boolean operations, e.g.,

$$\left[B^2\right]_{ij} = B_{i1} \otimes B_{1j} \odot B_{i2} \otimes B_{2j} \odot \ldots B_{in} \otimes B_{nj}$$

where $\odot$ and $\otimes$ are Boolean OR and AND operators respectively. Circuit breakers and switches are represented as *ones* when closed and *zeros* when open.

2.7 Application of *B* matrix to power system reliability and restoration

Powers of the *B* matrix (i.e. B^n) allow tracing network connectivity. Analysis of *proximity* (how close one bus is in relation to another via number of lines), degree of *connectivity* (how many lines connect two buses), and the calculation of intervening buses between two buses [44]. As discussed, in a system with *n* buses, B^{n-1} contains all *ones* for a fully connected system. Z*eros* in the matrix identify disconnected, and therefore, deenergized buses. Additionally, B^y for an *n* bus system contains *ones* only when buses are connected by *y* lines or less, for $y < (n-1)$. Evaluation of the calculation shows that there are $y-2$ intervening buses. Assessment of network connectivity may be used to evaluate reliability and build restoration algorithms. Chapter 4 presents illustrative examples of *B* matrix applications in reliability assessment.

Advantages of using the *B* matrix include the use of Boolean arithmetic to locate energized (or deenergized) buses. An example of distribution system application to reliability enhancement may be the minimization of unserved energy after a component failure and consequent reconfiguration. The *B* matrix allows energized loads, line segments and buses to be identified; consequently, near optimal network reconfiguration may be performed. Figure 2.5 outlines steps in which the *B* matrix is used in a distribution system reconfiguration / restoration algorithm. Application areas include *design* – to optimize placement of interrupt-

ing devices (breakers, reclosers, switches, electronic switches), or *operations* – as a method to automate circuit reconfiguration and restoration. Additional comments on this algorithm and elements of Smart Grid operation are shown in [118].

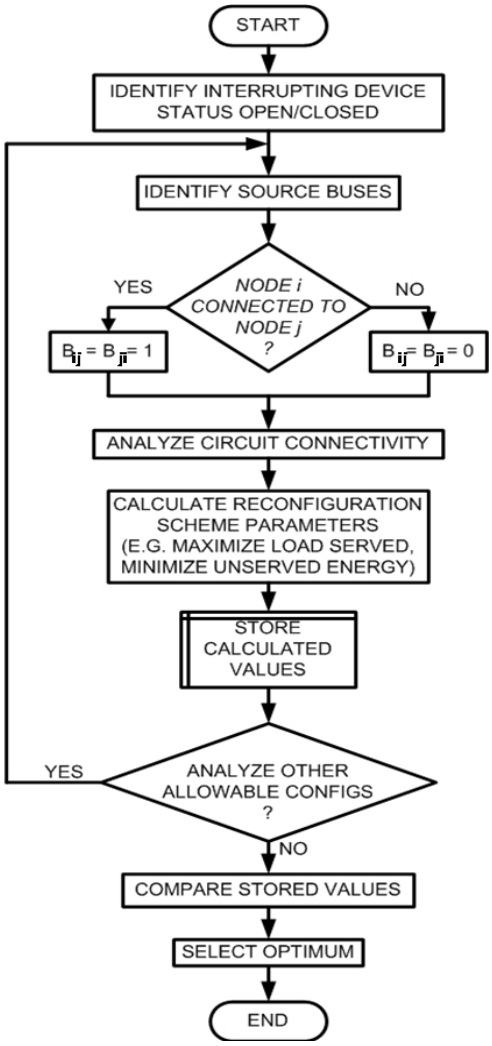

Figure 2.5 *B* matrix algorithm to be used in distribution system applications

The *B* matrix provides a foundation for the circuit connectivity analysis. Load diversity, daily load profile and seasonal load profile patterns require robust design and operation methodologies. The *B* matrix can be used in a running real-time control application that inputs sensory information about the system into an

algorithm that can enhance automated restoration and reconfiguration ability. For example, sensors in the distribution circuit can monitor real-time demand information and use these measurements to minimize the unserved energy in the event of an interruption. Figure 2.6 shows the elements of a potential application embedded in a DMS with the proposed concept of real time monitoring / sensing / reconfiguration / restoration calculation for distribution systems.

In circuit design applications, it is possible to compare alternative locations of interruption devices, switches, sensors, and circuit routing in order to achieve a given objective. In distribution design, the long list of objectives may include: loss mitigation, high reliability of service, voltage regulation, operation within component ratings, public acceptance, safety, compliance with standards, and satisfying cost constraints. In a subsequent example and discussion, Chapter 4 illustrates applications of an algorithm to 'seamlessly' reconfigure the system and restore service. In design and operation applications, possible objectives include:

- Reducing the SAIDI and SAIFI (reducing outages < 5 min.)
- Reducing expectation of unserved energy after a permanent fault
- Restoring maximum permissible load after a circuit disturbance.

Note that maximum permissible load may be connected MVA or pre-disturbance demand. Figure 2.8 presents a detailed flowchart comprising sensory information, operator alerts and automated reconfiguration / restoration of distribution systems.

In an algorithm utilizing the binary bus connection matrix, B, a system status table (SST) can be assembled as depicted in Figure 2.7 where n_{cb}, n_b, and n_{ℓ} de-

note the number of breakers, buses and lines respectively. This SST is constructed based on the physical system structure and binary representation of breaker states, bus states, load states and line availability.

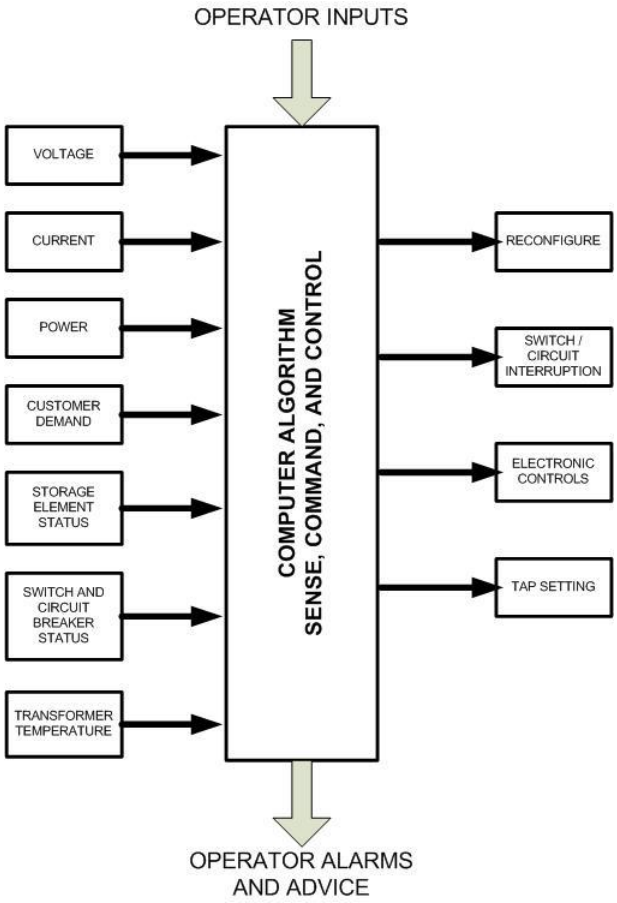

Figure 2.6 Sensing and real time monitoring of distribution system elements for computer assisted calculation and control

$$\begin{bmatrix} [2^{n_{cb}} \times n_{cb}] & [2^{n_{cb}} \times n_b] & [2^{n_{cb}} \times n_l] & [2^{n_{cb}} \times n_b] \\ \text{BREAKER} & \text{BUS} & \text{LINE} & \text{LOAD} \\ \text{STATUS} & \text{STATUS} & \text{STATUS} & \text{STATUS} \\ \text{TABLE} & \text{TABLE} & \text{TABLE} & \text{TABLE} \end{bmatrix}$$

Figure 2.7 System status table indicating status of breakers, buses, lines and loads

Breaker states, bus status, load status and line availability are represented by *zeros* and *ones*. That is, closed breakers / switches, energized lines, loads, and buses are represented by *ones*; conversely, open breakers, deenergized lines,

loads, buses are represented by *zeroes*. Note, however, that the number of rows in the table increases as the number of interrupting devices, n_{cb}, increases according to $2^{n_{cb}}$. In practical implementation, the number of automated interrupting devices within a distribution system remains low.

The restoration of a distribution system based on a table lookup method is discussed. The method is outlined as follows:

- First, communicate the status of all circuit breakers and availability of service at load buses every ΔT seconds.
- Next, the SST is updated as needed every ΔT seconds. Note that if a line was faulted or some distribution system device was unavailable, the corresponding row of the SST would be removed.
- Then, detected anomalies trigger examination of the remaining rows of the SST. The desired state lies inside the set of remaining rows. To select the desired target row, apply an optimal operating criterion; for example, as indicated in Table 2.1.
- The restoration algorithm of Figure 2.8 is repeated every ΔT seconds.

2.8 Sensors for reconfiguration and restoration

Note that ΔT depends on the sampled data and applications for which it is sampled. For example, ΔT of 5 minutes or less allows for switching that can significantly reduce reliability indices according to [123]. Also, recall that only interruptions lasting more than 5 minutes are considered when calculating SAIDI. The 5 minute sampling rate is well within contemporary technology, as SCADA

data are updated every 4 seconds and state estimation at the transmission level runs every 2-3 minutes [103].

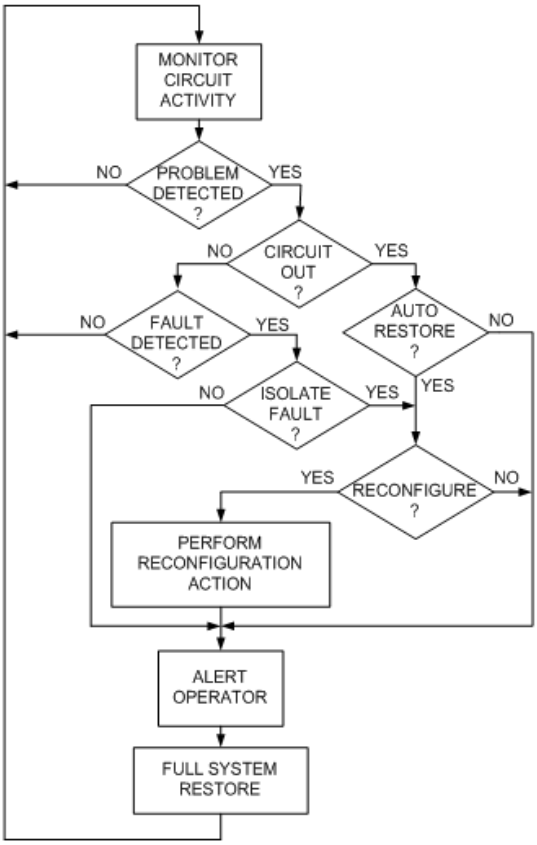

Figure 2.8 An automated restoration / reconfiguration algorithm

Table 2.1 Sample Optimal Operating Strategies for Restoration

Strategy	Objective
Minimum breaker operations	Minimize the number of switching operations, to accelerate the restoration
Maximize load restored	Restore large loads first, to minimize energy un-served (knowledge of load priorities may be needed)
Minimize unserved energy	Examine all permissible switching operations and choose those that minimize the unserved energy
Priority loads first	Restore priority loads first, regardless of load level

Under more stringent conditions, ΔT may be ½ cycle or 8.3 ms to stay within the Computer Business Equipment Manufacturers' Association (CBEMA) curve

requirements [36]. In this case, virtually no momentary interruption event contributes to SAIDI and SAIFI indices. Additional consideration is given to the sensory network required of the Smart Grid environment. Type of available measurements and application areas are presented in Table 2.2.

Table 2.2 Quantities Sensed for Distribution System Restoration

Sensed quantity	Purpose
Bus voltages	• On/off • Acceptable service delivered
Bus injection current	• On/off • Load level before disturbance • DG supply before disturbance
Line flows (real power, reactive power, current)	• Compare actual levels to equipment limits • Evaluate available paths
Breaker/switch status	• On/off • Available/unavailable
Generation set points (DG)	• Evaluate system supply to identify available paths • Identify available reactive support sources
Load operating point before disturbance or outage	• Important in understanding how much load needs restoring • Important for restoration involving cold-load pickup
Ambient / equipment temperatures	• Detect overloaded or overheated equipment • Find conductors that may be sagging excessively
Transformer temperature / pressure	• Detect overloaded or overheated transformers
Fuse status	• Reduce restoration and repair times by conclusively locating and addressing faulted components
Lightning arrester and protective device status	• Locate and repair protective equipment that failed while protecting the circuit

3. A distribution class state estimator

3.1 State estimation in the distribution system

Utilizing measurements to estimate the state of the power system has been used extensively at the transmission level as discussed in Chapter 1. Generally, the assumed system topology and SCADA data are combined with redundant measurements and reasonable assumptions based on previous operating points. Note that assumed data points may be derived from solved power flow solutions, historical data, and previously estimated solutions. Again, measurements include real and reactive power injections and flows, bus voltage magnitudes, and relative phase angles where phasor measurements are available. Solution of the estimation procedure provides state estimates where no measurement devices exist.

The state estimation process generally employs non-linear solution methods to iteratively find a least square approximation to an overdetermined problem [105]. Generally, the non-linear solution employed is the same as the Newton-Raphson technique used for power flow analysis, except for the measurement Jacobian describing the non-linear relation of the states to measurements. As discussed in Chapter 1, distribution systems have different characteristics that prevent simple transfer of modeling and analysis methods. Examples identified in Chapter 1 include high *r/x* ratios, radial configuration, two and single phase laterals, and unbalanced loading. Distribution power flow studies often utilize a robust ladder iterative technique [25] to find bus voltage profiles and current flows for radial sys-

tems. Considering the various requirements, a practical distribution system state estimator is developed subsequently.

3.2 Applications of a distribution class estimator

State estimation may be used to enable control functions in a number of scenarios. For example, comparing estimated flows and voltages to ratings or switching to prevent component overload. Applications of a distribution class state estimator enable smart distribution system initiatives. A list of potential benefits includes:

- Optimization and generation rescheduling based on forecasted state,
- Enhanced system wide voltage control capability,
- Single phase VAR control to facilitate voltage regulation and utilize DG,
- Enabling voltage regulation via local DG,
- Selective networking of primary and / or secondary systems for voltage control, loss minimization, or increased asset utilization,
- Facilitate real-time distribution level pricing based on congestion/flows,
- Energy storage management and optimization,
- DG location and control – i.e. to relieve congestion, manage prices,
- DMS that provide operators more effective distribution feeder interaction tools; i.e. monitor and visualize the grid like transmission systems, alarms and alerts of serious events,
- Enables control signals for demand-side-management of smart appliances, PHEVs and responsive loads,

- Enable demand response that truly impacts bulk grid operations, e.g. switch appliances to ‘reduced demand’ mode when directed,
- Fault detection (not protection), isolation, and reconfiguration for enhanced reliability,
- A validation tool– load and topology –for transmission system state estimators.

3.3 Synchronized phasor measurements in power system state estimation

Synchrophasors in state estimation is seen as revolutionary, since system states (bus voltage magnitude and angle) may be directly measured [77], [100], [102]-[104]. The application of synchrophasor measurements in distribution systems and distribution state estimation enables direct measurement of system states as well; however, direct measurement of three-phase unbalanced voltage magnitude and angle provides a significant amount of information to the distribution operator. This is particularly important, since most operators only have substation SCADA data to gauge feeder conditions [68]. Although wide deployment of measurement devices with synchrophasor technology is envisioned, even a few such measurements combined with smart meter data and other measurements may enhance the feasibility of distribution class estimators.

Additionally, the ability to visualize the grid enables more effective control and optimization strategies. For example, capacitor bank switching based on measured / estimated voltage profiles may become more effective than conventional time-of-day switching. Also, effectively utilizing available resources, i.e.

reformulating portions of the IEEE Standard 1547, to allow islanded / microgrid operation where available DG capacity can supply local loads. Knowledge of contemporary system conditions allows operators to push the distribution system closer to its operating limits.

3.4 Conventional state estimation formulation

The process of state estimation in transmission systems involves the use of measurements along with a mathematical system representation to obtain least squares fit of estimates to the assumed topology. General assumptions that allow the use of positive sequence equivalent circuit models to estimate the positive sequence states include:

- System topology is known (or processed to within an acceptable limit),
- Balanced three-phase loads,
- Fully transposed lines,
- Symmetrical series or shunt devices on all phases,

State estimation uses a large number of redundant measurements. Where an insufficient set of measurement data exists, historical data (i.e. pseudo-measurements) or virtual measurements (i.e. zero injections) may be substituted to obtain an observable / non-singular process matrix [42], [105]. States may be represented as polar or rectangular quantities. At a given operating point, the non-linear relationship of measurements to states is given by Equation (3.1),

$$h(x) = z' + \eta, \tag{3.1}$$

where z' and η are vectors of measurements and measurement errors respectively, x is the vector of system states (bus voltage magnitude and angle), and h is a non-linear vector valued function that relates system states to corresponding measurements. Typically the power system state estimation problem presents itself as an overdetermined system where redundant measurements outnumber states.

Weighted least squares estimation involves the minimization of the 2-norm of the residual vector denoted by r, $z = (z'+\eta)$ is the noisy measurement vector,

$$r = (z'+\eta) - h(x) = z - h(x) \tag{3.2}$$

Quite often, the 2-norm of the residual vector is taken as the objective function, given by the non-linear objective function, $J(x)$,

$$J(x)=\sum_{k=1}^{n}(z_k - h_k(x))^2=r^t r \quad , \tag{3.3}$$

where k is an arbitrary bus number and n is the number of measurements. Note that as the summation of the square of residuals of individual measurements, $J(x)$ is a scalar. The minimization of $J(x)$ entails equating the partial derivative of $J(x)$ with respect to the state vector, x, to zero,

$$\min J(x) = \frac{\partial J(x)}{\partial x} = \frac{\partial[\sum_{k=1}^{n}(z_k - h_k(x))^2]}{\partial x} = \frac{\partial r^t r}{\partial x} = 0 \; . \tag{3.4}$$

That is, the minimization of $J(x)$ simultaneously minimizes each measurement residual.

Power system state estimators utilize a large number of redundant measurements. Mathematically, state estimation becomes an overdetermined system of equations. Where data may be linearized around an operating point, Equation (3.1) becomes

$$hx = z. \tag{3.5}$$

Consequently, Equation (3.2) may be written as,

$$r = z - hx. \tag{3.6}$$

For an overdetermined system of equations, the *best-fit* estimated solution to Equation (3.4), linearized to produce Equation (3.5) – (3.6) is given by,

$$2h^t h\hat{x} - 2hz = 0$$

$$\hat{x} = [h^t h]^{-1} h^t z \tag{3.7}$$

Note that this result may also be found as,

$$\hat{x} = h{+}z, \tag{3.8}$$

where h^+ denotes the Moore-Penrose pseudo-inverse where h is of dimension n x m , $n > m$.

Note that in conventional transmission system state estimation, the state vector denoted $\hat{x}$ is a real valued vector with magnitude and phase information partitioned into sub vectors.

3.5 The gain matrix in power system state estimation

In the conventional power system state estimation formulation, there typically exists a gain matrix that provides weights for measurements. Measurement device accuracy and measurement type are common weighting attributes. Types of measurements include:

- Measured: low variance (high weight); corresponds to meter accuracy
- Virtual measurement: low variance (high weight) e.g. zero injections

- Pseudo-measurement: high variance (low weight), assumed values
- Critical measurement: pseudo, virtual or measured; to avoid singularity.

For example, the accuracy range for various PTs is presented in Chapter 1. Pseudo-measurements are assumed from historical data, thus, they are less reliable than metered node measurements. The gain matrix allows a solution procedure where reliable data dominate the solution subject to acceptable system condition.

The covariance matrix of the measurement vector is denoted by *R*. If the measurement variances are assumed to be independent, *R* is a diagonal matrix with entries corresponding to measurement variances; that is, when individual measurement variances are assumed to be independent, the off-diagonal terms are *zero*,

$$R = \begin{pmatrix} \sigma_1^2 & \cdots & 0 \\ \vdots & \ddots & \vdots \\ 0 & \cdots & \sigma_n^2 \end{pmatrix}$$

It is possible to weight the calculation of each measurement residual in *J(x)*. In this case, the matrix, *W*, is calculated as the inverse of the *R* matrix. A low variance corresponds to a high weight. Linearizing Equation (3.4) around the state vector by Taylor series expansion, one obtains correction terms to initial estimates. This enables an iterative solution to the non-linear set of measurements in conventional state estimation, similar to the calculation of the Jacobian in Newton Raphson power flow solutions. Incorporating *W* into the system of equations produces a gain matrix, *G*,

$$G = h_{meas}^{t} \, W \, h_{meas} . \tag{3.9}$$

h_{meas} represents the subset of the h matrix relating system measurements to the state variables. The solution to obtain the x vector in Equation (3.8) is then modified to produce,

$$\hat{x} = [G]^{-1} h^t W z \,. \tag{3.10}$$

References [42], [104]-[107] provide further discussion on weighted least squares estimation and the gain matrix.

3.6 A three-phase, linear distribution system state estimator using synchronized phasor measurements

The three-phase, untransposed distribution system requires a different set of tools capable of estimating all phase voltage information. The formulation developed utilizes complex synchronized phasor measurements and complex mathematical representation of state estimation equations. Note that in the case where synchronized phasor measurement devices are utilized, it is possible to obtain real and imaginary components of measured quantities. The foregoing formulation may be modified to accommodate complex measurements. For such measurements, the equations within the h matrix, measurements in the z and η vectors, and state vector are represented as complex quantities. Consequently,

$$h = h_r + j h_{im},$$

$$z = z_r + j\, z_{im},$$

$$x = x_r + j x_{im}.$$

Each matrix or vector can be partitioned into real and imaginary subsets denoted by the subscripts r and im respectively. To accomplish the minimization of equa-

tion (3.3) for a complex vector, $r = r_r + r_{im}$, the partial derivatives of the system of equations with respect to real and then imaginary variables must take place simultaneously. When the *n*, *x* and *z* vectors and *h* matrix are complex, the resultant *r* vector minimization given in Equation (3.4) requires complex conjugation followed by transposition for the equation to be minimized,

$$r^H r = (z_r - h_r x_r + h_{im} x_{im} + \eta_r)^2 + (z_{im} - h_{im} x_r - h_{im} x_{im} + \eta_{im})^2. \quad (3.11)$$

The Hermitian operation is transposition, followed by complex conjugation, and is denoted $(\bullet)^H$.

The expression of the minimization of the complex expression becomes,

$$\frac{\partial (r^H r)}{\partial x_r} = 0 \qquad \frac{\partial (r^H r)}{\partial x_{im}} = 0 \quad (3.12)$$

In commercially available software programs such as Matlab, the Moore-Penrose pseudo-inverse function correctly computes the pseudo-inverse of a matrix entered in complex form. The residual vector may be separated into its respective real and imaginary parts, the result is,

$$\begin{bmatrix} r_r \\ r_{im} \end{bmatrix} = \begin{bmatrix} (z_r - h_r x_r + h_{im} x_{im} + \eta_r) \\ (z_{im} - h_r x_{im} - h_{im} x_r + \eta_{im}) \end{bmatrix} \quad (3.13)$$

The solution for the estimation of state variables, $\hat{x}$, when variables are in rectangular form,

$$\begin{bmatrix} \hat{x}_r \\ \hat{x}_{im} \end{bmatrix} = \begin{bmatrix} h_r & -h_{im} \\ h_{im} & h_r \end{bmatrix}^+ \begin{bmatrix} z_r \\ z_{im} \end{bmatrix} + \begin{bmatrix} h_r & -h_{im} \\ h_{im} & h_r \end{bmatrix}^+ \begin{bmatrix} \eta_r \\ \eta_{im} \end{bmatrix} \quad (3.14)$$

Note that $\hat{x}_{\mathrm{r}}$ and $\hat{x}_{\mathrm{i_m}}$ are independent of each other. Estimation of sequence values follows the same formulation previously described. Phasor measurement de-

vices measure individual phase values, and calculate positive, negative, or zero sequence components.

Note that the 2-norm minimization of the complex quantities has real *r* vector, and that Equation (3.12) can be solved using Equation (3.8). Also, $h^H h$ is a square matrix and, provided it is not singular, may be used to solve the state estimation problem. Measurement weights may also be included. This point is discussed in a later subsection.

The preceding formulation may be developed for three-phase networks. Where synchronized phasor measurements are available, the real and reactive part of the measured quantity may be calculated (since magnitude and angle information are effectively measured). In conventional state estimation formulation, the process matrix and gain matrix grow by a factor of 3. Also, as in conventional power system state estimation, measurement weights of synchronized phasor measurements are generally higher than other measurements since these devices are generally assumed to have a higher degree of accuracy.

3.7 Three-phase radial distribution ladder iterative power flow

Three phase voltage profiles for radial distribution feeders are generally obtained via a ladder-iterative algorithm, also called the forward / backward sweep method. Algorithms detailing the forward sweep and backward sweep are presented in Appendix B. Calculating voltage and current at node *n* when values at node m are known may be accomplished for most distribution system components –lines, transformers, regulators– using a generic formulation,

$$\begin{bmatrix} V_n^{abc} \\ I_n^{abc} \end{bmatrix} = \begin{bmatrix} A & B \\ C & D \end{bmatrix} \begin{bmatrix} V_m^{abc} \\ I_m^{abc} \end{bmatrix} \quad (3.15)$$

This system may be solved when bus voltage and currents are known. Note that in conventional distribution systems only substation bus voltage magnitude and possibly line current magnitudes or power flows are measured. The *A*, *B*, *C*, *D* matrix in Equation (3.15) is inverted to solve for bus *m* quantities when bus *n* quantities are known. Note that for a given line topology, the unit quantities (e.g. Ω/mi.) remain constant; consequently, the inverse of A, B, C, D may be performed once for each line topology and stored. The forward iteration solves for bus voltages at successive downstream buses when an upstream bus voltage and branch currents are known. The backward stage solves for upstream voltages at successive buses when downstream bus voltages and line currents are known. Both forward and backward iterations assume current entering a branch is the same as current leaving a branch.

The untransposed line segments with high *r/x* ratio (e.g. three-wire or four-wire) are modeled with an *n_ph* square matrix where *n_ph* is the number of phases (typically 3). Four-wire segments are reduced to a 3 x 3 block matrix using Kron reduction by assuming neutral conductors are solidly grounded at every node [28]. For Figure 3.1, line segment impedance (effective line-ground after Kron reduction for 4-wire) matrix between buses *n* and *m* is,

$$Z_{nm}^{abc} = \begin{bmatrix} Z_{aa} & Z_{ab} & Z_{ac} \\ Z_{ba} & Z_{bb} & Z_{bc} \\ Z_{bc} & Z_{cb} & Z_{cc} \end{bmatrix}_{nm} \Omega$$

Where a single or two phase lateral is present, the row and column of the missing phase(s) are zeroed, and the corresponding voltage vector entries in V_{bus}^{abc} in Equation (3.14) are zero. Similarly, transformers are modeled by an *n_ph* x *n_ph* block impedance where diagonal elements represent phase self impedance; taps and delta-wye connections may also be modeled [25]. The modeling assumption for transposed transmission lines that allows use of the positive sequence impedance effectively averages off diagonal elements, $Z_m = {}^1\!/_3(Z_{ab} + Z_{ac} + Z_{bc})$.

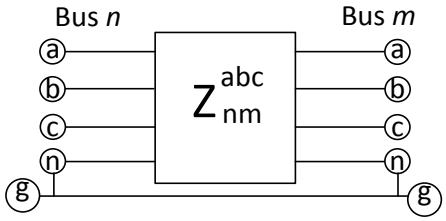

Figure 3.1 Line impedance between buses *n* and *m*

Quite often the same approach of averaging off-diagonal elements is used in the ladder iterative power flow but results in loss of solution accuracy. The stopping criteria for forward / backward sweep may be tolerance, *e*, around balanced substation voltages, $|V_{source}^{measured}| - |V_{source}^{calculated}| \leq e$, (as substation bus voltage magnitude may be the only measurement available).

The three-phase unbalanced distribution state estimator developed henceforth combines techniques from the ladder iterative algorithm to process measurements, and to find reasonable solutions for non-measured quantities. Also, reasonable estimator inputs may be obtained via measurements and supplementary calculated system quantities.

3.8 Three-phase unbalanced distribution state estimation

The general procedure for the pre-processing and state estimation algorithm is depicted in Figure 3.2. The two stages of the estimation procedure are a ladder iterative process followed by linear estimation. This is intended to provide a pre-processing method to obtain missing measurements in an environment where limited measurements may be available.

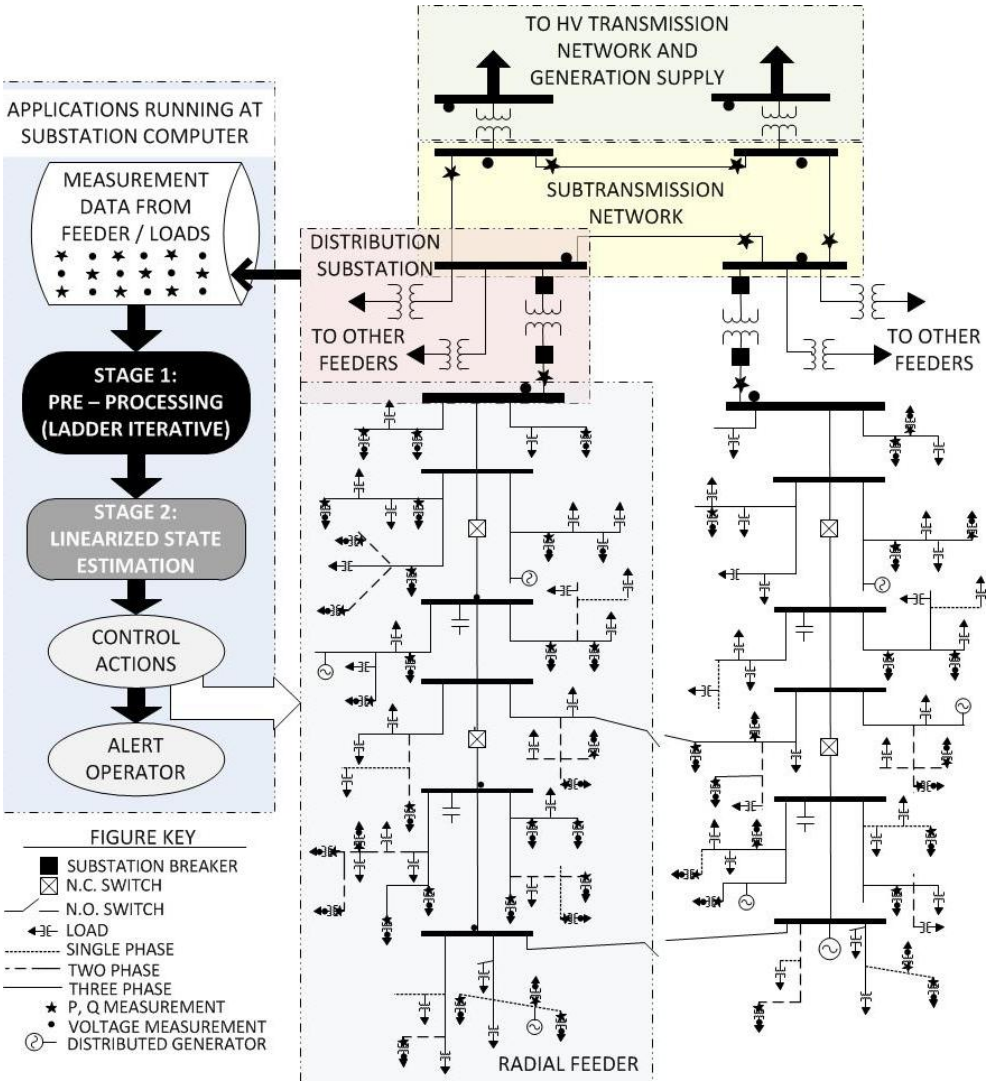

Figure 3.2 Three-phase unbalanced distribution state estimation overview

Where smart meters are available, real and reactive power consumption, as well as voltage and ampere magnitudes may be obtained at the customer load. When the clock on the smart meter is synchronized to some general reference, these quantities may prove coincident peak and near real-time voltage magnitude measurements. However, fully synchronized measurements that provide angle information are not likely to be available from the smart meter. Development of such devices to be included in next generation smart meters, protection systems and distributed generator protection and control may enhance distribution state estimation efforts. Additional discussion may be found in [134].

3.9 Condition number and state estimation

To assess the accuracy of solutions to the state estimation problem, certain concepts in linear system and matrix theory must be introduced. References [124]-[126] present matrix theory as applied to linear algebra and numerical analysis. Matrix theory applied to power system state estimation is discussed further in [105]-[107] and is discussed subsequently.

The vector *norm* is a scalar that measures the *length* or magnitude of distance between two vectors in the same fashion that absolute value measures the length of a line [124]-[128]. Norms must meet three criteria: positivity, homogeneity, and triangular inequality (as explicitly detailed in either reference). The most frequently cited vector norm is the Holder norm,

$$\|x\|_p = \left(\sum_{i=1}^{n} |x_i|_p\right)^{\frac{1}{p}}$$

$$n = \textit{number of elements in the vector}$$

$$x_i = \textit{the } i^{th} \textit{ element in the vector} \tag{3.15}$$

$$p = 1, 2, 3, \ldots \infty.$$

$||x||_p$ is referred to as the *p*-norm. Note that $p=2$ in Equation (3.15) is the Euclidian norm, or 2-norm, also utilized in the weighted least squares formulation.

Vector norms are often used to evaluate the difference between a calculated solution, $\hat{x}$, and the exact solution, x, which is rarely known. The error is given by $e = x - \hat{x}$. The basis of state estimation is the minimization of the norm of $Ax - b$. If for a given matrix, A, there exists a nonzero vector, x, for which $Ax = \lambda x$, then λ, is an eigenvalue of A, and x is an eigenvector of A associated with λ. The collection of all individual eigenvalues of A is known as the spectrum of A. The spectral radius of A is the maximum absolute value contained within the spectrum of A. Reference [124] identifies a disadvantage of using the spectral radius to measure the size of a matrix: i.e. when two matrices, A and B, have spectral radius $\sigma(A + B) \geq \sigma(A) + \sigma(B)$, as this condition violates the triangle inequality. Often used norms are calculated as,

2-norm or Euclidian length

$$\|A\|_2 = \sqrt{max\ singular\ value\ of\left(A^t A\right)} \tag{3.16}$$

Infinite norm

$$\|A\|_\infty = \max_{1 \leq i \leq n} \sum_{j=1}^{n} |a_{i,j}| \tag{3.17}$$

As summarized from [105][124]-[128] the condition number of a matrix provides a measure of how small perturbations in the right-hand-side of $Ax = b$ may

become magnified in the calculated solution of $\hat{x}$ to produce meaningless results. The condition number of a matrix is calculated via

$$\kappa(A) = ||A||\ ||A^{-1}|| \tag{3.18}$$

In conventional state estimation, A indicated above is $h^t h$. That is, the $h^t h$ matrix is nearly singular in some cases. Three situations cited for causing ill-conditioned power systems are identified as large weighting factors to certain measurements, short and long lines connected to the same bus, and a large number of bus-injection measurements [104][105]. In the state estimation formulation, it is expedient to examine the condition number of $h^t h$ which is obviously square and symmetric. The condition number of this formulation may also be calculated exactly by the ratio of the maximum to minimum singular values of $h^t h$,

$$\kappa\ (h^t h) = s_{max} / s_{min}\ . \tag{3.19}$$

Note that singular values are always non-negative real numbers. As identified in [105], the formulation of the conventional power system (transmission) state estimation problem is naturally ill-conditioned.

In power system state estimation, the condition number effectively gives the sensitivity of the solution to noise in the measurements. When the condition number is very large, there is a high sensitivity to noise. In traditional power engineering applications, literature cites condition numbers less than 10^{12} as normally encountered in practice [129].

The foregoing discussion of condition number in general, and in the traditional power engineering state estimator cases may be recast into the proposed distri-

bution state estimation solution given by Equation (3.8). The recast expression replaces *h* in Equation (3.19) by

$$\begin{bmatrix} h_r & -h_{im} \\ h_{im} & h_r \end{bmatrix}.$$

The condition number is then calculated as,

$$\kappa\left(\begin{bmatrix} h_r & -h_{im} \\ h_{im} & h_r \end{bmatrix}^t \begin{bmatrix} h_r & -h_{im} \\ h_{im} & h_r \end{bmatrix}\right). \tag{3.20}$$

Note that in Equation (3.20), all elements in the argument of the condition number calculation are real, and the argument is a square matrix.

The condition number for the distribution state estimator shall be revisited in connection with illustrative examples in Chapter 4. It provides a reasonable estimate of the sensitivity of the state estimation formulation to measurement noise and system model error. Further discussion of condition numbers and matrix concepts is provided in Appendix C.

3.10 Assignment of weights to calculated currents

As discussed in subsection 3.5, a weight assignment process biases calculation of states toward data identified as more reliable. In the distribution system state estimation algorithm developed here, load currents are linearized. The currents calculated are written in linear expressions in terms of the states, namely the bus voltages in rectangular notation. Substation active and reactive power flows may be expressed in terms of real and imaginary part of currents which are also linearly related to the states, particularly since substation bus voltage magnitude is

known. Measured values (i.e. from a smart meter) generally include active and reactive power, $S = P + jQ$, and voltage magnitude, $|V_m|$. Synchrophasors provide voltage magnitude and phase angle relative to a reference.

Assuming small change in nominal bus voltage phase angle obtained from the power flow solution, the current demanded by a load may be calculated. For example, a constant power load current may be represented as,

$$I_{re}^{\varphi} + jI_{im}^{\varphi} = \frac{P^{\varphi} - jQ^{\varphi}}{V_m^{\varphi} \angle (-\delta_v^{\varphi})} \tag{3.30}$$

$$I_{re} = \frac{[P\cos(\delta_v) + Q\sin(\delta_v)]}{V_m} \qquad I_{im} = \frac{[P\sin(\delta_v) - Q\cos(\delta_v)]}{V_m} \tag{3.31}$$

where φ denotes the phase (a, b, c) and voltage phase angle, δ_v, is assumed near nominal for that phase (i.e. 0^o, -120^o, 120^o respectively) when not measured directly via a synchrophasor. If measured via synchrophasor, the measured δ^{φ} may be used. Alternatively, phase angle information of nearby measured buses may be used as an initial estimate where no measurements / pseudo-measurements exist. Other load models may be employed. Note that constant impedance, constant current or composite load current may be calculated similarly [25], [46], [53], [57], [85]; additionally, models calculating current as a polynomial in terms of the voltage magnitude may also be included [59]. Field tuning of load models may be required for verification, especially for power flow study accuracy. At the operating point, the voltage and current relationship is simply $YV = I$.

The selection of weights for calculated, linearized currents may be approximated mathematically or determined heuristically. Measured P, Q, V_m and δ_v are random

variables each with an expected value and variance [132]. Approximate expressions for mean and variance of calculated currents from Equation (3.31), may be obtained when measurements are treated as independent random variables. The expected values of measured variables are $M_k = \{P, Q, V_m, \delta\}$, and their variances $Var_k = \{\sigma_P^2, \sigma_Q^2, \sigma_{V_m}^2, \sigma_{\delta_v}^2\}$ are chosen based on transducer expected accuracy. Transducer expected accuracies for typical power systems sensors are discussed in subsection 1.5 and of an example of a commercialized product is shown in [97]. Attention now turns to the approximation of variance of the calculated current.

The expectation of real and imaginary parts of I, are calculated in Equation (3.31). In statistics theory, these calculated values represent expectation of real and imaginary parts of current, $\mu_{I_{re}}, \mu_{I_{im}}$ respectively. The expectations are said to be approximated from the nonlinear functions in Equation (3.31). The variance of I_{re} and I_{im} are approximated from the Taylor series expansion, also commonly referred to as the 'delta method' [132], evaluated at M_i for each measurement (assuming independent measurement noise, $M_i = \{P, Q, V_m, \delta\}$),

$$Var_{I_{re}} \cong \sum_{k=1}^{n} \left[\left(\frac{\partial \mu_{I_{re}}}{\partial M_k} \right)^2 Var_k \right].$$
$$Var_{I_{re}} \cong \sum_{k=1}^{n} \left[\left(\frac{\partial \mu_{I_{im}}}{\partial M_k} \right)^2 Var_k \right]. \quad (3.32)$$

Alternatively, a heuristic approach may be taken: the variance of I_{re} and I_{im} may be approximated by choosing a value corresponding to the largest variance (normalized) of all random variables, i.e., truncate the sum in Equation (3.32) to

only the largest term(s). Note that calculated variance of the real and imaginary parts may differ significantly. Appendix D presents an illustrative example of approximating calculated current variance, as well as confirmation of the heuristic method described.

3.11 Bad data detection and the distribution system state estimator

Other applications of estimators for distribution systems include topology error identification, and a variety of operations dealing with bad data detection, identification, suppression, and correction. Baran et al. demonstrate the identification of incorrect modeling assumptions in [56]. Powalko et al. provide an analysis of the observability issue for a distribution network estimator in [55]. Abur's text [105] details algorithms for bad data detection. One illustration using chi-squares is explained briefly below.

Bad data detection and identification filters the measurement set for erroneous data. The bad measurement must not be a critical measurement (that makes the mathematical set of equations observable) [105]. Observability in this context means that the state estimation matrix h is such that $h^t h$ is nonsingular. Bad data detection and identification for the linear, three-phase distribution system state estimator formulation follow methods outlined in the literature for WLS estimators (e.g. [105]). An illustrative example is presented in Chapter 5. The individual measurement errors are assumed to follow a normal distribution, are independent and uncorrelated.

4. Illustrations of reliability enhancement in the Smart Grid

4.1 Reliability and the Smart Grid: test cases for reliability enhancement and restoration strategies

In this chapter, a key focus of the Smart Grid is presented – namely reliabilirty enhancement and distribution restoration. The objective is to use enhanced sensory information to improve reliability and to implement restoration. The approach taken is mathematical and illustrative (i.e., through the use of examples). The same sensory utilization approach will be the foundation of distribution system state estimation, the subject of the subsequent chapter.

Various test cases are used to illustrate the several algorithms that have been developed here. Standardized test beds provide a platform upon which comparative studies can be conducted, and where calculation results of different alternative methods or designs (i.e. to different reliability designs or switching strategies) can be obtained. Table 4.1 identifies the test beds used and related illustrations. Note that the names, number of examples / simulations, and more specific details are presented in each subsection.

Table 4.1 Examples Presented in Chapter 4

	RYG Test Bed	RBTS Test Bed (1-line)
Binary bus connection matrix	x	x
Restoration	x	
Reliability enhancement / automation		x

4.2 The RYG test system

Figure 4.1 presents the one line diagram for the RYG test system. Bus and line data for the RYG test system are available in Appendix E. The reconfiguration/ restoration algorithm and an interrupting device placement algorithm is demonstrated on this test bed; note that some results are presented in [117], [118]. These applications highlight two distinct areas of distribution engineering: operations and design. Operations applications include circuit switching strategies, reactive power dispatch and reconfiguration and restoration after a disturbance. Design applications include system expansion plans, upgrade of existing system assets to improve performance, and long term analysis of system reliability.

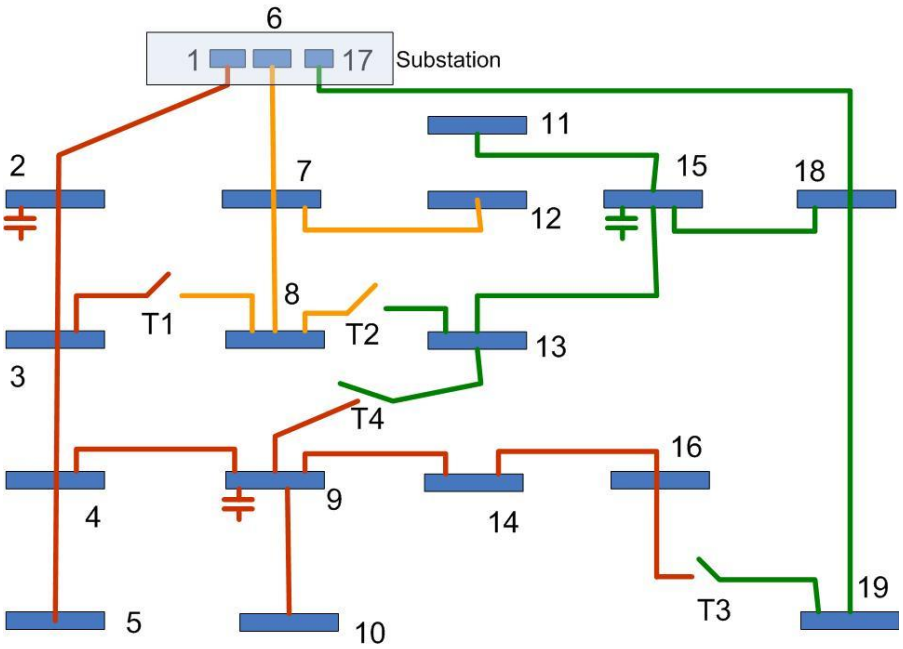

Figure 4.1 One line diagram of the RYG distribution system

4.3 The Roy Billinton test system-RBTS

As a standardized test bed, the RBTS has been used in calculating reliability indices, evaluating the performance of alternate designs and to demonstrate reliability improvements. The Roy Billinton Test System, or RBTS, was named for its developer and was presented in [37], [38] as a realistic power system test bed, complete with generation, transmission and distribution along with system reliability analysis and data. Details are presented in the identified references, and pertinent data related to examples shown here are presented in this chapter and in 0. The distribution network connected to Bus 3 of the RBTS network is redrawn and shown in Figure 4.2.

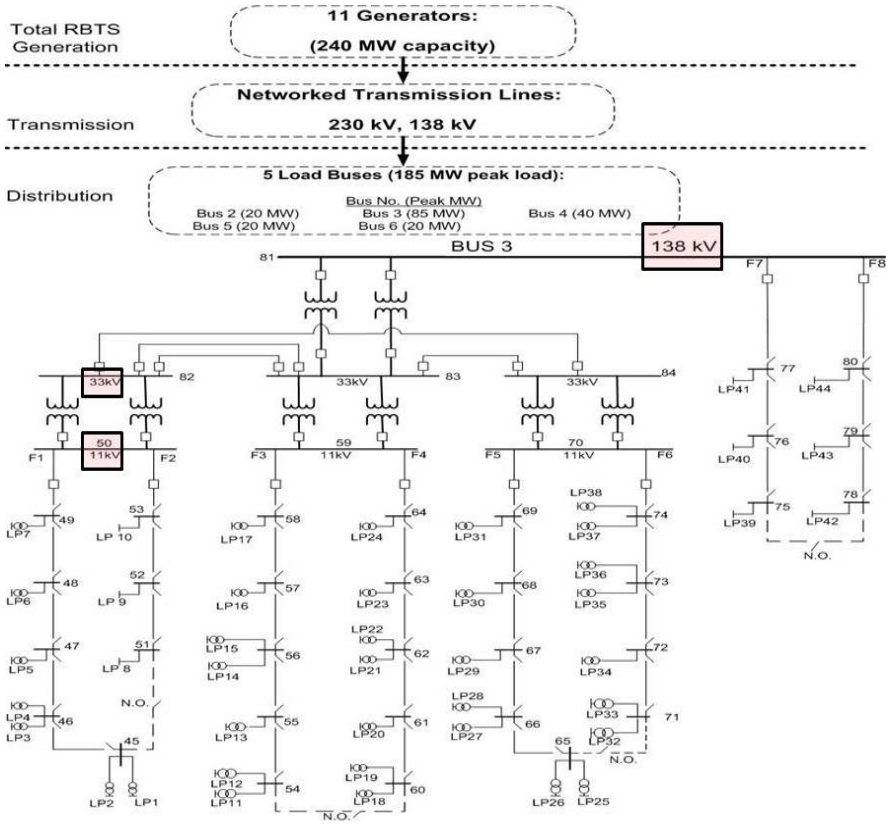

Figure 4.2 RBTS one-line diagram showing Bus 3 distribution network, recreated from [38]

4.4 The large scale simulation system (LSSS) test bed

The large scale simulation system (LSSS) test bed was developed in the FREEDM ERC to include more complex distribution feeder models together with a transmission, subtransmission and distribution networks. The RBTS is modified by including the IEEE 34 bus distribution test system [131] at feeder F5. Figure 4.3 presents the LSSS one-line diagram. Illustrative examples using the LSSS are presented in 6. Data used to build the LSSS may be found in [37], [38], [131] and 0. Sathyanarayanan [133] describes the LSSS in detail.

4.5 Illustration of Smart Grid planning, restoration and reconfiguration

The SST as discussed in subsection 2.9 may be constructed based on the physical system and binary representation of breaker states, bus states, load states and line availability. As discussed, breakers open / closed status is represented by *zeros / ones* respectively. Similarly bus and load status and line availability are represented by *ones* when energized / available; conversely, *zeros* when deenergized / unavailable. The number of rows in the SST increases as the number of interrupting devices, n_{cb}, increases according to the formula $2^{n_{cb}}$. Note than in typical distribution systems there are significant limitations on reconfiguration options (switching to alternate feeders / supplies) where this number may not become unmanageable.

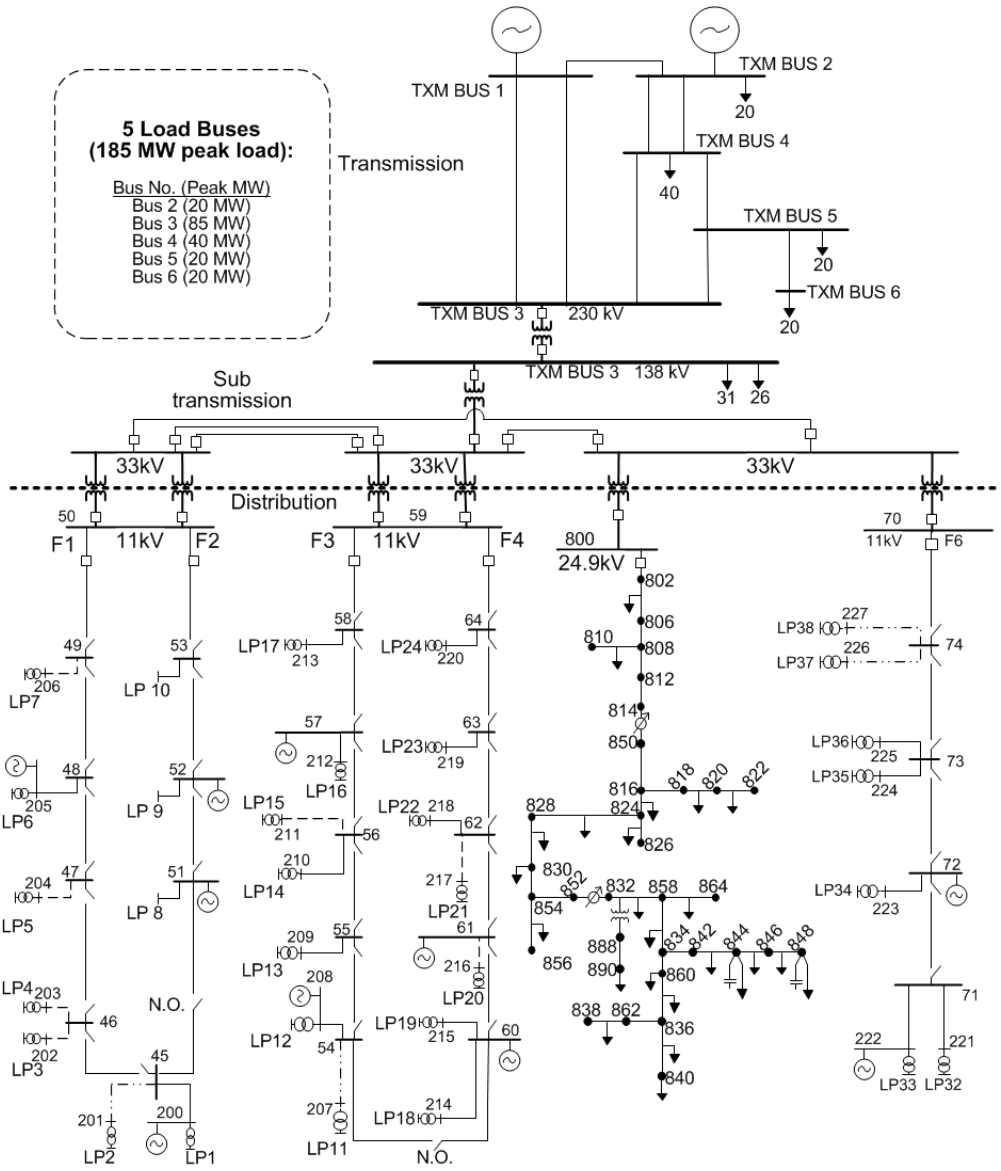

Figure 4.3 The Large Scale Simulation System test bed

Breakers here refer to any device capable of interrupting the circuit. In practice, they may be remotely controlled motor operated switches, solid state switches or other controllable switching devices. This SST allows operators insights into the present / switched operating state of the system. Also, visualization tools may incorporate this concept for near real-time system monitoring.

The following example uses the system presented in Figure 4.1 to illustrate an application in circuit design. The *B* matrix based algorithm may be used for real-time monitoring of the distribution system and to trace circuit connectivity as shown in Figure 2.5, Figure 2.6 and Figure 2.8 in Chapter 2. The objective of this specific study is to maximize the load restored, and minimize unserved energy following fault isolation. Practical implementations of this example may utilize a centralized controller that monitors the distribution system in real-time and optimizes automated circuit reconfiguration to meet preselected criteria.

4.6 Interrupting device location

To illustrate a circuit design application, tie switches in the RYG test bed of Figure 4.1 were assumed to have remote operation ability, like a solid state switch or breaker. Additional breakers (or switches) were added, one at a time, at various locations in the test system. Adding interrupting devices changes the structure of the *B* matrix. Assuming that the probability of a fault is directly correlated to the line length (i.e. longer lines are expected to experience faults more frequently), pseudorandom fault locations were simulated on the distribution feeders. This method is similar to the use of Monte Carlo simulation for evaluating power system reliability [39].

Circuit connectivity is assessed following the locating of this pseudo-random fault occurrence. Circuit reconfiguration and restoration options after isolating the faulted subsystem is assessed through the tracing of connectivity using the *B* matrix as identified in subsection 2.6 and using a system status table. The reduc-

tion in expectation of unserved energy after fault isolation is considered in adding each additional breaker. Starting with four interrupting devices, one additional breaker is added to the system. When the breaker location has been determined, another breaker is added to the system, until a total of eight interrupting devices are included.

The next interrupting device is added in the system on a line that does not already have an interrupting device (or switch) and the simulation is repeated as the distribution system is stressed by faults. An optimal interrupting device location allows isolation of faulted lines that have the greatest impact on expectation of unserved energy following reconfiguration after fault isolation. The result obtained is suboptimal for the following reasons: first, the bus loads are assumed to be fixed; power flow limitations are not considered; and the location of *n* circuit interrupting devices in *m* lines can occur according to the binomial coefficient equation as follows,

$$\binom{n}{m} = \frac{n!}{(n-m)!m!}.$$

According to this calculation, there are 1820 ways for which 4 interrupting devices may be placed in 16 lines on this system. Only a small subset of the entire solution set is simulated since for each interrupting device added to the system, a minimum expectation of unserved energy is obtained. That is, a sequential approach to locating a breaker then calculating expectation of unserved energy is used. Figure 4.4 shows how the expectation of unserved energy decreases as the number of interrupting devices increases. Table 4.2 shows the result of calculated

expected unserved energy after four interrupting devices have been placed. Unserved load refers to the average load that cannot be restored after 5000 pseudo-randomly simulated faults on the system are isolated by circuit reconfiguration.

Table 4.2 Results of the Breaker Placement Algorithm

Breaker placed in line	*E(U)* MWh
2, 3, 6, 17	1.2

4.7 Reconfiguration and restoration

For each available interrupting device combination, the B matrix algorithm is used to find the total load connected to the substation buses. Once the fault has been isolated, the status of interrupting devices is established. Note that there are $2^{n_{cb}-m}$ possible interrupting device configurations (where n_{cb} is the number of interrupting devices and *m* denotes interrupting devices that must remain open to isolate faulted sections) allowable; there are $2^{n_{cb}-m}$ remaining configuration states in the SST. An optimum solution selected as the resulting interrupting device combination that provides for the maximum load to be restored after the fault is isolated by circuit reconfiguration. This is the target 'optimum' operating state shown in Figure 2.5.

In an illustrative example, faults are once again pseudo-randomly located on the system of Figure 4.1 to test the performance of the algorithm. With every simulation, a feasible state is found, and at least one solution provides a maximum value for load served. Most often, there are multiple solutions (multiple rows in the SST) that correspond to the same value for maximum load restored; a prioriti-

zation method may be chosen so minimum switching operations are performed. For instance, a permanent fault occurring in line 17 requires opening of interrupting devices in lines 17, and 18. Note that there are $2^{8-2} = 64$ possible interrupting device configurations available since 2 of the 8 interrupting devices have been locked out. Only a small subset of these possible configurations, however, will allow the maximum load identified to remain energized. One possible interrupting device configuration (reconfiguration) that allows maximum load to be restored after this fault isolation is given by the following:

- close interrupting device T2
- open interrupting devices in lines 17 and 18 (T3).

Under the stated conditions, a total load of 8 + *j*3.9 MVA is restored. Only load connected to buses 18 and 19 (1 + *j*0.5 MVA) experiences an outage.

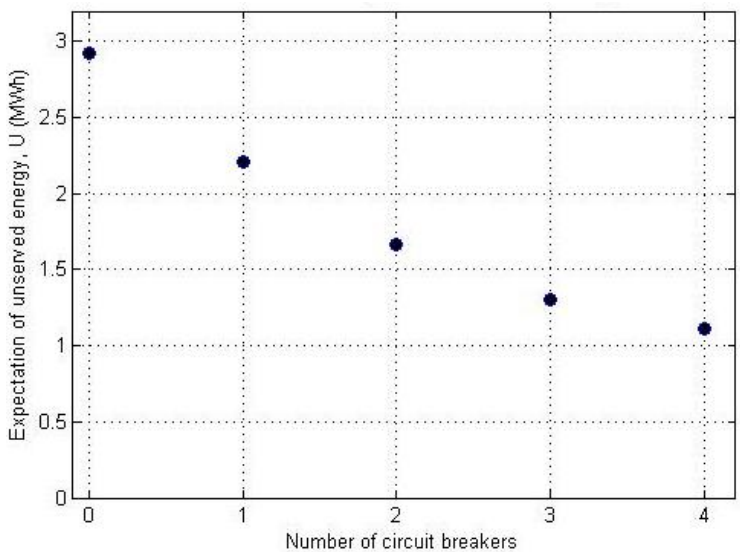

Figure 4.4 Expectation of unserved energy vs. no. of interruption devices RYG

4.8 Reliability enhancement and switching automation on the RBTS

For the application of the *B* matrix to the RBTS test bed, the previous approach of including interrupting devices one at a time was determined to be impractical for the demonstration of automated interrupting device location, since there are a large amount of switches. Note that this applies for a high number of automated isolation switches. Instead, cases were developed to assess the performance of contemporary design, with a source breaker and normally open tie switches, partial networking, and fully networked (parallel feeders only) distribution systems. Along with the placement of interrupting devices, manual switching versus automation is also studied. Seven cases were examined for the RBTS test bed. These seven cases are described in Table 4.3**.**

Table 4.3 Seven Cases for RBTS Reliability and Automation Illustrations

Case No.	Interrupting devices and location	Manual or Automated (M, A)
RBTS-1	Substation circuit breaker; normally open tie switch	M, A
RBTS-2	Add one switch per feeder, located at the midpoint	M
RBTS-3	Add one switch per feeder, located at the midpoint	A
RBTS-4	One switch per lateral bus, located at source side	M
RBTS-5	One switch per lateral bus, located at source side	A
RBTS-6	Two switches per bus serving a lateral	M
RBTS-7	Two switches on each bus serving a lateral	A

For each of the cases presented, note that there is a manual switching and automated switching comparison for each switching configuration (conventional, partial and fully networked). Note also that Case C6 data corresponds to the origi-

nal RBTS data as presented in [38]. The results are shown in Figures 4.4 and 4.5 with the reduction in expectation of unserved energy and the reduction in expected SAIDI on the circuit. Note that adding a few interrupting devices has the biggest immediate impact on reducing SAIDI. Furthermore, automation has the potential to increase reliability over manual (time-consuming) switching. Cost is generally a limiting factor in automation and control of the distribution infrastructure.

It is important in many automated systems that controls exist such that an operator may assume control of the distribution system. For example, maintenance work or construction may require that automated system reconfiguration or restoration be disengaged for the safety of utility personnel or construction workers.

The RBTS system of Figure 4.2 depicts the distribution network of bus 3 with 44 load buses, 77 line segments, switches and normally open points. In this illustration, examples compare the reliability enhancement of replacing manually operated isolation switches with remotely controlled switches in selected locations. This example assumes FDIR systems operate in an ideal manner and switching does not necessarily replace protection systems (i.e. protection systems clear faults, then reconfiguration may be undertaken post fault-clearing).

In this example, switching times are drastically reduced for automated restoration and system reconfiguration scenarios; that is, switching times in automated systems may be under 5 minutes so as to influence SAIDI and SAIFI indices. Failure probability and frequency of events are held constant for comparison pur-

poses. The results obtained show that average repair times, annual unavailability and expectation of unserved energy can be reduced.

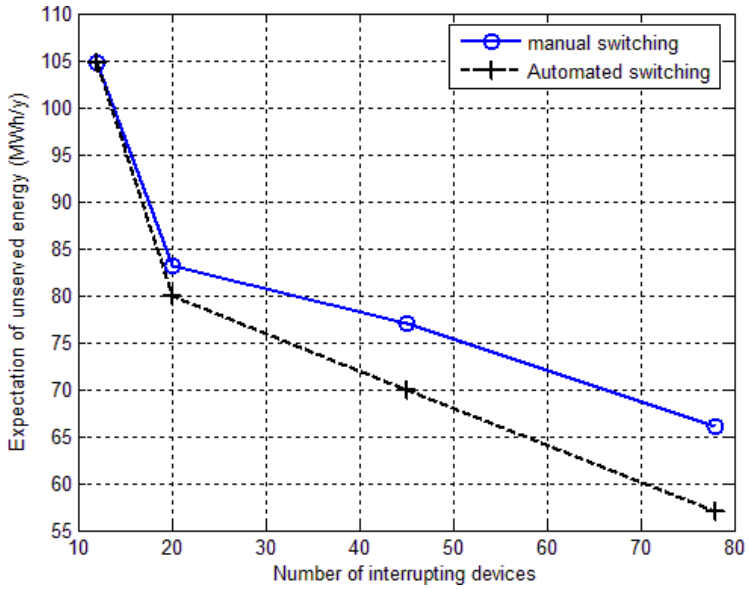

Figure 4.5 Expectation of unserved energy vs. no. of interruption devices RBTS

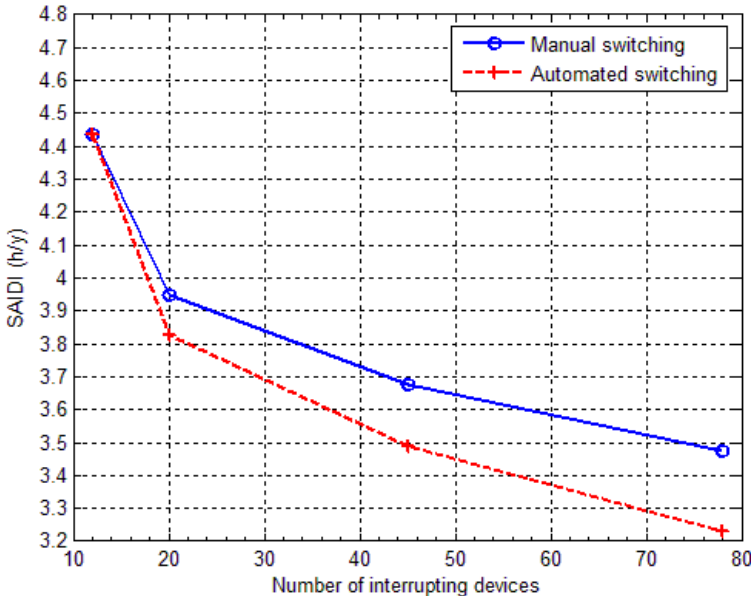

Figure 4.6 SAIDI versus number of interruption devices RBTS

Table 4.4 presents load point reliability indices of the base case situation presented in reference [38]. Table 4.5 presents results of an automated, 'smart' dis-

tribution system. As indicated, λ values for each load point are the same in each case, but all other indices are reduced with automation. Both tables 4.5 and 4.6 present failure rate (λ), repair time (r), annual unavailability (U) and expectation of unserved energy (E). Table 4.4 data is presented in reference [38] and serves as the benchmark by which 'upgrades' to the distribution system depicted in Figure 4.2 may be compared.

With the assumption that all switches in all feeders can be made remotely controllable and automated to switch within a 5 second time frame, the resulting reliability improvements to the system were calculated. These calculated improvements in load point (bus) reliability indices identified in [38] and system wide reliability indices are presented in Table 4.5. Note that SAIDI falls by almost 7.0%, while SAIFI remains the same. That is, with the same anticipated number of events, the duration of events can be drastically reduced by automated reconfiguration. Note also that the total expectation of unserved energy reduces by 14.3%.

Reference [117] goes on to estimate costs of reliability improvement by using historical price information and categorizing loads according to size and type. Note that all load size, classification and other pertinent data are provided in references [29]-[31], [37]-[40]. It should be noted here that further networking of the primary distribution system, and especially of the secondary distribution system, can produce far greater reductions in r, U, E, and SAIDI, as reliability increases when the number of redundant paths increase.

Table 4.4 Base Case Reliability Indices for Bus 3 of the RBTS System

Load Point	λ (f/y)	r (h)	U (h/y)	E (MWh/y)
1	0.3010	11.4352	3.4420	1.6122
3	0.3140	11.1688	3.5070	1.0121
8	0.2210	1.9412	0.4290	0.3634
27	0.3205	10.9626	3.5135	1.9957
41	0.1885	1.8276	0.3445	2.5319
44	0.2015	1.7742	0.3575	1.5689
Total†				66.68
SAIDI	3.4726			
SAIFI	0.3028			

* The data in the table are taken directly from [38] and they do not entail the use of any electronic switching devices. The notation *f/y* refers to failures per year.
† The total energy unserved is summed over all 44 load points

Table 4.5 Reliability Indices for Bus 3 of the RBTS with Electronic Switching

Load Point	λ (f/y)	r (h)	U (h/y)	E (MWh/y)
1	0.3010	10.6146	3.1950	1.4965
3	0.3140	10.3822	3.2600	0.9408
8	0.2210	1.1765	0.2600	0.2203
27	0.3205	10.1716	3.2600	1.8517
41	0.1885	1.0345	0.1950	1.4332
44	0.2015	0.9678	0.1950	0.8558
Total†				57.14
SAIDI	3.2322			
SAIFI	0.3028			

*The data in the table reflect system performance with electronic devices inserted in every branch. Note the improvement over data shown in [38] (Table 4.4).
† The total energy unserved is summed over all 44 load points

4.9 Discussion of reliability enhancement and restoration examples

The preceding examples demonstrated new algorithms, applications and control options for the smart distribution system. Examples of algorithms for use in distribution system reliability enhancement and restoration were presented. The effect of automation in switching and restoration functions was shown, and related distribution system reliability indices were used to quantify expected improvements in reliability.

On the RYG test bed, breakers were located such that expectation of unserved energy following disturbances in the distribution system is minimized. By adding four breakers to the system, expectation of unserved energy was reduced from 2.85 MWh/yr to approximately 1.15 MWh/yr.

Studies on the RBTS test bed showed reliability improvements via increasing the number of interrupting devices, and by automating restoration / switching in the distribution system. The results show that feeder automation and enhancement of network reconfiguration options may have a significant effect on improving expected reliability for similar expected failure rates. SAIDI was shown to reduce by 7 % by fully automating restoration. Expectation of unserved energy was shown to reduce by 14 % by fully automating switching and restoration. Limitations within examples shown include the omission of cost-benefit evaluation for practical implementation.

5. Illustrations of three-phase distribution system state estimation

5.1 Distribution system state estimation

All illustrations of the three-phase distribution system state estimation algorithm are shown for feeder F1 of the RBTS Bus 3 distribution sub-network, which has been developed in three-phase detail and is shown in Figure 5.1. Loading conditions for the illustrations are described in this subsection and additional data is provided in 0.

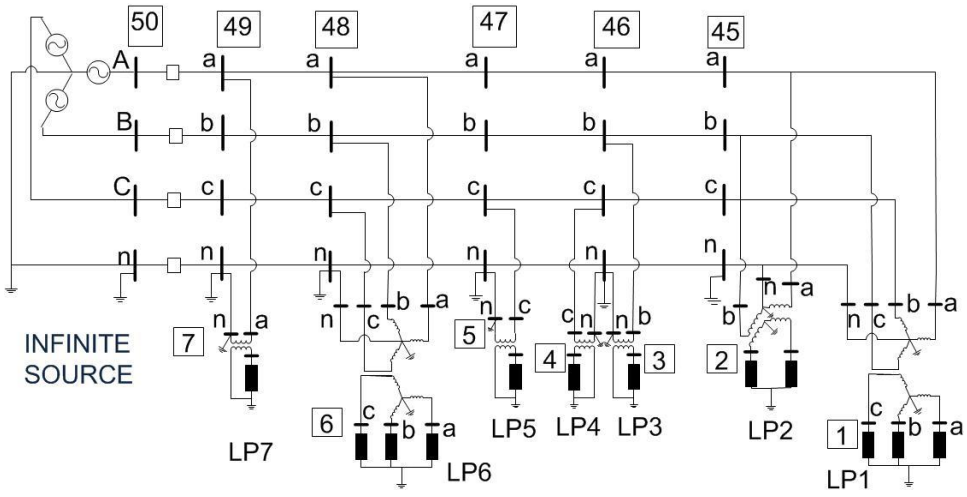

Figure 5.1 Three-phase detail of RBTS feeder F1

Table 5.1 Examples Presented in Chapter 5

	RBTS Feeder F1 (3ϕ) circuit	Examples
Distribution class state estimator	x	SE1, SE2, SE3
Weighted estimation	x	SE1, SE2, SE3
Bad data detection	x	SE2

As discussed in Chapters 1-4, the factors influencing the evolution of distribution systems also necessitate new tools for enhancing monitoring, operations and control. Distribution class state estimation has the potential to allow increased

levels of automation, control and to enhance operator interface. Of particular interest are those distribution networks with the following characteristics: high penetration of distributed generation; ability to selectively network to change power flows, voltage profiles and reduce losses; inclusion of new voltage regulation tools such as series and shunt capacitors and reactors.

To enable state estimation applications, sufficient measurement capabilities are needed. Measurements are envisioned with existing technology such as smart meters and conventional voltage magnitude, current magnitude and real and reactive power flow meters. Future generations of measurement devices are envisioned to have the capability to capture completely synchronized phasor quantities. Note that even conventional smart meters may be synchronized, but not to the level of detail to capture phasor quantities.

A key aspect of distribution system state estimation is the intended end-goal. It may be argued that the highly stochastic nature of distribution system loads (and renewable electric generation in distribution systems) makes fast response/control to rapid (seconds) changes impractical. However, enabling control as a response to 'slower' system changes (i.e. feeder loading / unloading and voltage unbalance over a day), or large fluctuations (i.e. sustained sudden shifts in power flows or voltage magnitudes) appears to be a feasible enhancement to distribution control. Examples of applications that are enabled through the use of state estimation include:

- As indicated in [85], DGs may be blocked from connecting to the grid if voltages exceed specified ranges. To maximize effective use of DG assets, utilities may need additional voltage regulation resources that increase operating flexibility in the distribution system.
- DG may potentially increase voltage unbalance between phases. Three-phase motors are sensitive to small voltage unbalance. Utilities may also require voltage balancing mechanisms beyond traditional regulators (that regulate each phase separately).
- Demand response and direct load control needs to be accomplished in a manner that does not exacerbate voltage unbalance or otherwise negatively impact system operations.
- Monitoring of line flows, transformer loading, and bus voltage magnitudes provide operators increased insights into the system. Operators may avert potential unsafe conditions with adequate visualization options and alerts to potential overloads.
- Knowledge of pre-outage loading may enhance restoration practice, especially for short duration outages.

The following illustration demonstrates the use of a distribution class estimator to calculate system states based on assumed system measurements. The true solution to the network is assumed to be the results of a power flow study based on a known load (i.e. ladder iterative or other). Those bus voltage magnitudes and angles obtained from the power flow solution are exact for the specific oper-

ating / loading conditions used in the study. However, in practice, all loads are not known simultaneously, and measured power flows, loads and voltage and current magnitudes are contaminated with measurement noise. The illustrations developed herein are summarized in Table 5.2. A graphic depiction of operating points are shown in Figure 5.2

Table 5.2 Description of Distribution State Estimation Illustrations

Example	Description
SE 1	'Measurement' data taken from a power flow study. All measurements exact. Bus voltages and line flows are estimated and compared to actual values.
SE 2	Operating conditions at heavy load (HE18† – Case C5) are estimated based on only a few real-time measurements and historical data from a power flow solution for light loading (HE3† – Case C6) with updated load approximations at unmetered buses. Bus voltages and line flows are calculated.
SE 3 (*SE3a*, *SE3b*)	Estimating bus voltages for load at (HE5†). First, the 'historical data' is taken from HE3† (Case C6) – this is denoted example *SE3a*. Estimation is repeated with data from 'historical data' taken from HE7† (Case C1) – this is denoted example *SE3b*. The results of estimates at HE5 based on two different starting assumptions are compared. Line flows are calculated.
†HE = hour-ending: see 0 for additional details	

Note that the process of state estimation assumes that loads are known and measurements around the network are available (error in load assumption may be identified in the final result). Also note that approximate component models may produce different results than exact component models as described in Chapter 3 and demonstrated in Appendix D. The state estimation developed here does not consider weighted measurements, although weights may be incorporated into the formulation.

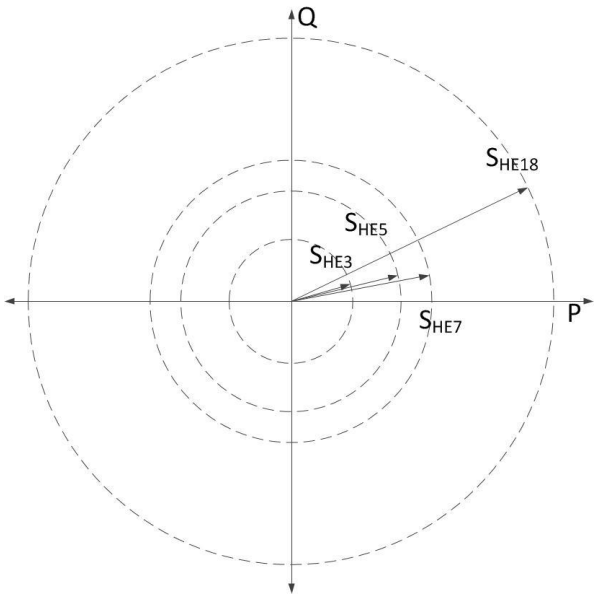

Figure 5.2 Graphic of operating points for HE3, HE5, HE7 and HE18.

The Cooper Power Systems software package, CYMDIST, was used to obtain solved power flow solutions for the RBTS network. A Matlab ladder iterative solver was also developed for this study. The resulting voltage profiles obtained from ladder iterative solutions in CYMDIST and Matlab agree exactly. Table 5.3 provides a summary of the 7 distinct cases studied, and Table 5.4 provides loading conditions as seen by the substation transformer.

Note that the seven cases are just a sampling of the 24 hour load profile as seen by the distribution substation transformer of feeder F1 shown in Figure 5.1. Each case corresponds to a different feeder loading condition as detailed explicitly in 0. The system base for all measurements and per-unit impedances is 100 $MVA_{3\phi}$.

Table 5.3 RBTS Feeder F1 Loading Conditions Considered for SE Examples

Load (Case)	Descrip-tion	Phase	Load served at bus (MVA)						
			LP1	LP 2	LP 3	LP 4	LP 5	LP 6	LP 7
C1	Base case (HE7)	A	0.2789	0.2583	-	-	-	0.2789	0.2789
		B	0.2789	0.2583	-	0.2789	-	0.2789	-
		C	0.2789	-	0.1741	-	0.2789	0.2789	-
HE5	Between C6 – C1	A	0.200 +*j*0.040	0.250 +*j*0.060	-	-	-	0.230 +*j*0.060	0.150 +*j*0.0450
		B	0.200 +*j*0.045	0.250 +*j*0.065	-	0.200 +*j*0.040	-	0.205 +*j*0.055	-
		C	0.200 +*j*0.040	-	0.155 +*j*0.030	-	0.2000 +*j*0.050	0.230 +*j*0.060	-
C2	Heavy load 1 (HE12)	A	0.2789 +*j*0.150	0.2583 +*j*0.140	-	-	-	0.2789 +*j*0.150	0.350 +*j*0.180
		B	0.2789 +*j*0.150	0.2583 +*j*0.140	-	0.2789 +*j*0.155	-	0.500 +*j*0.200	-
		C	0.2789 +*j*0.150	-	0.274 +*j*0.140	-	0.2789 +*j*0.150	0.2789 +*j*0.150	-
C3	Heavy load 2 (HE16)	A	0.3789 +*j*0.20	0.3583 +*j*0.195	-	-	-	0.3789 +*j*0.200	0.350 +*j*0.180
		B	0.3789 +*j*0.200	0.2583 +*j*0.140	-	0.3100 +*j*0.170	-	0.500 +*j*0.270	-
		C	0.3789 +*j*0.200	-	0.305 +*j*0.160	-	0.320 +*j*0.200	0.350 +*j*0.20	-
C4	Heavy load 2 with capacitor at bus 48. Loads are the same as Case C3 .								
C5	Heavy load 3 (HE18 peak)	A	0.470 +*j*0.220	0.470 +*j*0.230	-	-	-	0.450 +*j*0.240	0.4500 +*j*0.220
		B	0.450 +*j*0.200	0.490 +*j*0.250	-	0.450 +*j*0.218	-	0.510 +*j*0.250	-
		C	0.390 +*j*0.150	-	0.450 +*j*0.230	-	0.450 +*j*0.218	0.450 +*j*0.20	-
C6	Light Load (HE3)	A	0.0925 +*j*0.033	0.150 +*j*0.035	-	-	-	0.1175 +*j*0.036	0.1025 +*j*0.033
		B	0.1000 +*j*0.030	0.1625 +*j*0.038	-	0.0925 +*j*0.032	-	0.1275 +*j*0.038	-
		C	0.0975 +*j*0.023	-	0.100 +*j*0.035	-	0.125 +*j*0.037	0.1125 +*j*0.030	-

Figures showing main feeder and load point voltage magnitudes from power flow solutions are presented. Figure 5.3 - Figure 5.5 show bus voltage magnitudes along the three-phase main feeder (buses 45–50) and bus voltage magnitude at the load (buses 1–7). Data used to construct these figures are provided in tables in 0 and Appendix D.

Table 5.4 Feeder Load as Seen by the Substation Transformer for Each Case

Load Case	Load seen from the substation (MVA)			MW Total	MVAr Total	Substation Load (MVA)
	Phase A	Phase B	Phase C			
HE7 - C1	1.11	1.11	1.03	3.20	0.60	3.26
HE12 - C2	1.32	1.47	1.26	3.59	1.86	4.04
HE16 - C3	1.66	1.64	1.55	4.27	2.32	4.85
HE16 - C4	1.66	1.64	1.55	4.27	2.32	4.85
HE18 - C5	2.05	2.11	1.91	5.48	2.63	6.08
HE3 - C6	0.48	0.50	0.45	1.38	0.39	1.43
HE5	0.86	0.88	0.805	2.47	0.59	2.54

The process matrix, *h*, contains measurement data, pseudo-measurements and other pertinent topological data. Note that pseudo-measurements may be based on historical data, reasonable assumptions (i.e. voltage magnitudes of 1.0 p.u., angles in phases *a*, *b*, *c* of 0, 240, 120 degrees respectively) of unmeasured quantities and previously obtained network solutions.

Pseudo-measurements are also used in transmission system state estimation formulations. Pseudo-measurements are derived from the solution to a distribution power flow (i.e. ladder iterative or other procedure). The forward / backward sweep method incorporates load and topology assumptions and provides a feasible solution to the network. The linearized state estimation formulation incorporates real-time measured, pseudo-measurements and calculations / assumptions for unmeasured loads.

The flow chart of Figure 5.6 outlines this concept. The state vector is taken as the three-phase real and imaginary part of voltage. In the examples developed here, real and reactive power measurements are converted to equivalent currents to be incorporated into the state estimation,

$$\mathrm{h} = \begin{bmatrix} [Y_{\mathrm{BUS}}] \\ [U] \\ [h_{LM}] \end{bmatrix} \qquad \hat{x} = [\hat{V}] \qquad z = \begin{bmatrix} [I_{meas}] \\ [V_{meas}] \\ [I_{line}] \end{bmatrix} \tag{5.1}$$

U = identity matrix

h_{LM} = line measurement coefficient matrix

Y_{BUS} = system admittance model

V_{meas}, I_{meas}, I_{line} measurement vectors

I_{meas} contains measured and assumed injections / loads

Note that injection current '*measurements*' include those measurements from transducers as well as those pseudo-measurements obtained from historical (i.e. power flow solution). The corresponding line currents are calculated from the estimated voltages. Line current magnitudes on the main feeder are shown in Figure 5.9. Error in line current phase angle is shown in Figure 5.10. Note that line currents obtained from the estimator are nearly identical to power flow results (i.e. bus voltages are identical). In the subsequent examples, measurement devices (smart meters or synchronized phasor devices) are assumed to be located at load buses 2, 5, and 6, and on main feeder buses / transformer primary buses 11, 14, 45, 46 and 48 respectively.

Approximating non-measured load values

The smart distribution infrastructure is likely to have widely deployed smart metering. However, not every load point may be measured. Reasonable approximations of non-measured load values are made. Approximations are made based

on substation injection and measured loads. Bus voltage phase angles are determined as follows: available from synchrophasors, approximated from power flow data (pseudo), or assigned because the bus is close to a synchrophasor.

Bus voltage magnitude and aggregate load active and reactive power measurements are available at buses 2, 5, 6. Synchrophasor voltage measurements are assumed at buses 11, 14 distribution transformer primary, and main feeder buses 45, 46, and 48. At load points where no measurement devices are present (aggregate load unknown), an algorithm is used to apportion the unmeasured load based on historical loading and reasonable assumptions at the load point. Power flows measured at the substation,

$$P_{sub} = \sum_{i=1}^{n} P_i + P_{losses} \tag{5.2}$$

where n is the number of buses, and P_{losses} may be unknown or approximate. Measured bus loads total,

$$P_{meas} = \sum_{l=1}^{k} P_l \tag{5.3}$$

where k is the number of measured load points. When substation active power flow changes are observed,

$$\Delta P_{sub} = \sum_{i=1}^{n} \Delta P + \Delta P_{losses} \tag{5.4}$$

Aggregate unmeasured demands are approximated via,

$$P_{unmeas} + P_{losses} = P_{sub} - P_{meas} \tag{5.5}$$

Then, when substation power flow and measured loads change, the corresponding change in unmeasured aggregate load and subsequently unmeasured individual loads (historical or assumed) may be approximated,

$$\Delta P_{unmeas} = \Delta P_{sub} - \Delta P_{meas} \tag{5.6}$$

$$\Delta P_{i\_unmeas} = P_{i\_unmeas}\left(\frac{\Delta P_{unmeas}}{P_{unmeas}}\right) \tag{5.7}$$

Limitations and weights based on historical data or installed capacity may be imposed. However, care must be taken in limiting load estimation due to the highly stochastic nature of the individual instantaneous load. In the longer time horizon, load growth may need to be considered. Reactive power assumptions also follow (15)-(20), and total feeder power factor change can be used to check accuracy of assumptions.

Table 5.5 Demand at Each Bus Used in SE3a, SE3b, and SE2

	Demand at each bus (*P*/ *Q* in kW/ kVAr)						
	1†	2	3†	4†	5	6	7†
Power flow	600/ 125	500/ 125	155/ 30	200/ 40	200/ 50	665/ 175	150/ 45
SE3a, SE2	549/ 111	607/ 95	180/ 42	192/ 44	216/ 40	678/ 134	184/ 43
SE3b	594/ 116	347/ 125	136/ 39	200/ 40	219/ 39	594/ 162	175/ 45

† Pseudomeasurement – demand calculated based on measurements at other buses and the substation according to (15)-(20).
Metered (measured) values are shown in shaded columns.

Example SE1

Table 5.6 presents the true solution as obtained from a ladder iterative power flow study for the 20 (three-phase) buses in the RBTS feeder F1 network base case – Case C1. Table 5.7 presents the resulting branch currents for Case C1. The non-iterative, linear estimation utilizes 'measured' data at buses 2, 5, 6, 11, 14, 45, 46, 48.

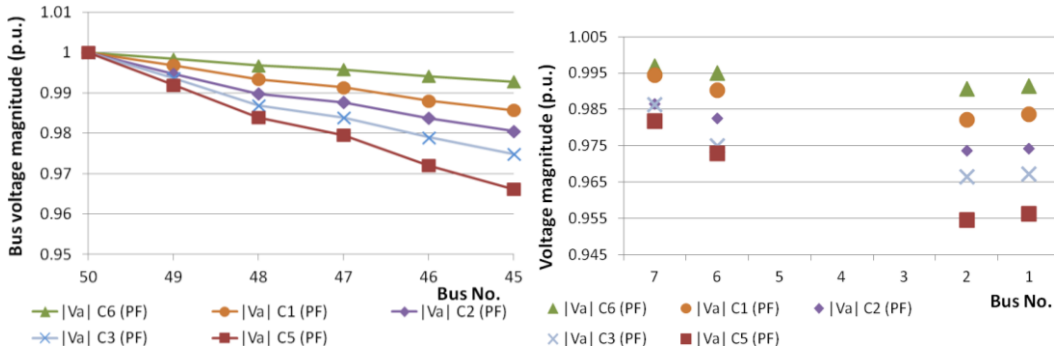

Figure 5.3 Phase *A* bus voltage magnitudes (a) along the main feeder and (b) at load buses, cases C1-C6

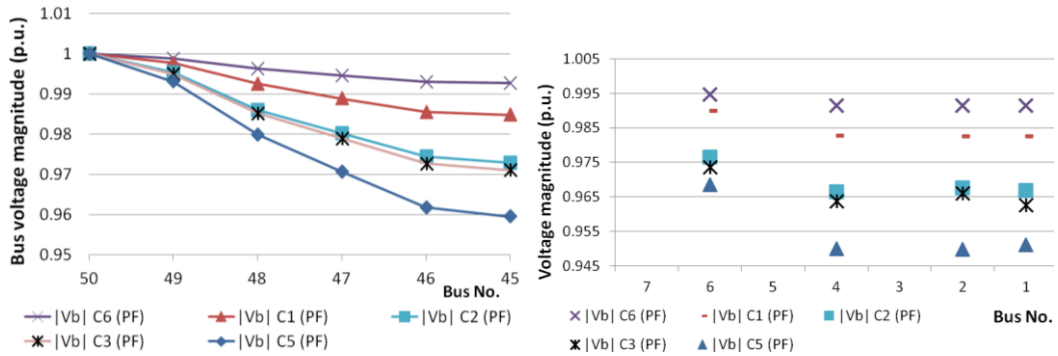

Figure 5.4 Phase *B* bus voltage magnitudes (a) along the main feeder and (b) at load buses, cases C1-C6

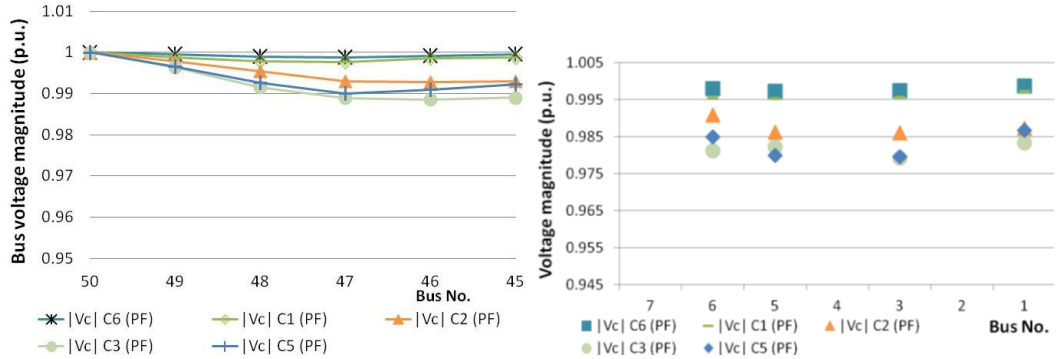

Figure 5.5 Phase *C* bus voltage magnitudes (a) along the main feeder and (b) at load buses, cases C1-C6

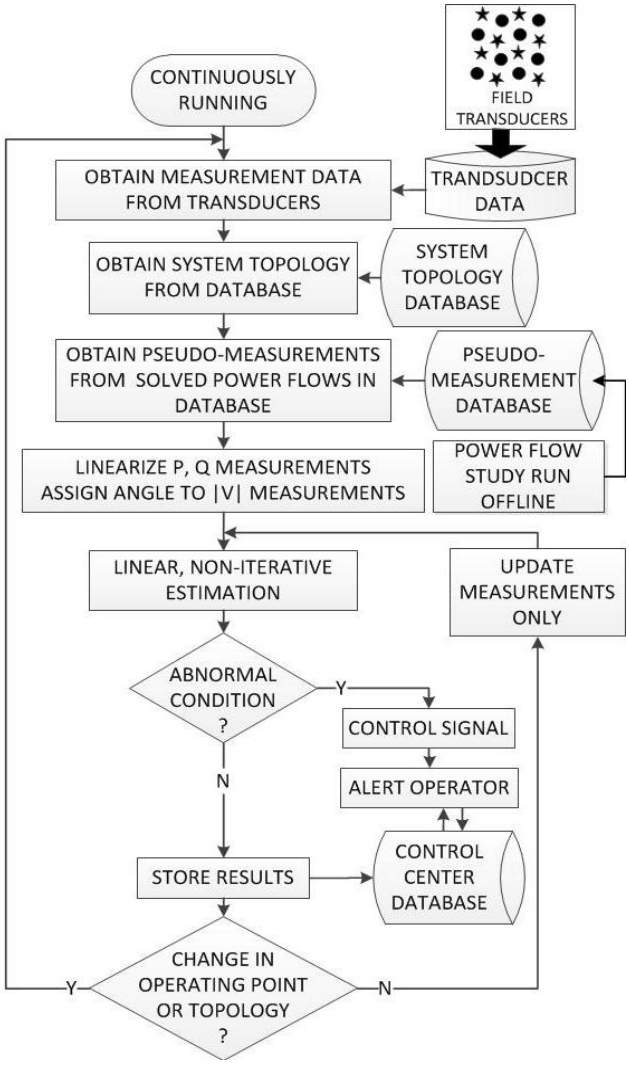

Figure 5.6 Flowchart of the distribution system state estimation algorithm

Table 5.6 Bus Voltages from a Power Flow Study for HE7 Loading Condition, Case C1, RBTS Feeder F1, Figure 5.1

Bus No.	$\|V_a\|$ (p.u.)	Angle V_a (deg.)	$\|V_b\|$ (p.u.)	Angle V_b (deg.)	$\|V_c\|$ (p.u.)	Angle V_c (deg.)
50	1.0000	0.00	1.0000	-120.00	1.0000	120.00
49	0.9968	-0.24	0.9977	-120.22	0.9988	119.80
48	0.9933	-0.44	0.9926	-120.57	0.9979	119.44
47	0.9913	-0.53	0.9888	-120.81	0.9977	119.19
46	0.9880	-0.64	0.9855	-121.15	0.9986	119.03
45	0.9857	-0.77	0.9848	-121.31	0.9989	119.01
14	0.9959	-0.36				
13	0.9923	-0.51	0.9918	-120.63	0.9975	119.37
12					0.9969	119.11
11			0.9842	-121.33		
10					0.9974	118.89
9	0.9841	-0.83	0.9848	-121.41		
8	0.9850	-0.84	0.9841	-121.37	0.9986	118.94
7	0.9944	-0.89				
6	0.9903	-1.01	0.9899	-121.13	0.9954	118.90
5					0.9952	118.73
4			0.9828	-121.87		
3					0.9957	118.41
2	0.9820	-1.34	0.9826	-121.92		
1	0.9836	-1.43	0.9825	-121.96	0.9972	118.37

Table 5.7 Line Currents from Power Flow Study for HE7 Loading Condition, Case C1, RBTS Feeder F1, Figure 5.1

From bus	To bus	$\|I_a\|$ (Amps)	Angle I_a (deg.)	$\|I_b\|$ (Amps)	Angle I_b (deg.)	$\|I_c\|$ (Amps)	Angle I_c (deg.)
49	50	177.64	-11.78	178.21	-132.33	161.42	107.29
48	49	133.54	-12.31	178.21	-132.33	161.42	107.29
47	48	91.14	-11.51	135.94	-132.10	120.78	107.92
46	47	91.14	-11.51	135.94	-132.10	88.24	109.11
45	46	91.14	-11.51	91.46	-133.05	47.79	110.78
14	49	44.13	-10.18				
13	48	42.43	-14.01	42.27	-133.08	40.67	105.40
12	47					32.62	104.69
11	46			44.52	-130.14		
10	46					40.49	107.15
9	45	42.78	-14.34	42.95	-135.95		
8	45	48.45	-9.02	48.61	-130.49	47.79	110.78

Results of example SE1

Table 5.8 presents the estimated bus voltages for the same system, assuming load data – at metered buses only – is known (i.e. identical to power flow solution). Also voltage phasor measurements are available at buses 11, 14, 45, 46, 48, and smart meter data (P, Q, |V|) at load buses 2, 5, 6 (angles assumed from the power flow study result). The difference between estimated and power flow study bus voltage magnitudes is shown in Figure 5.7. Bus voltage phase angle error (i.e. difference between power flow study and estimated) is shown in Figure 5.8. Estimated bus voltages and angles are exact.

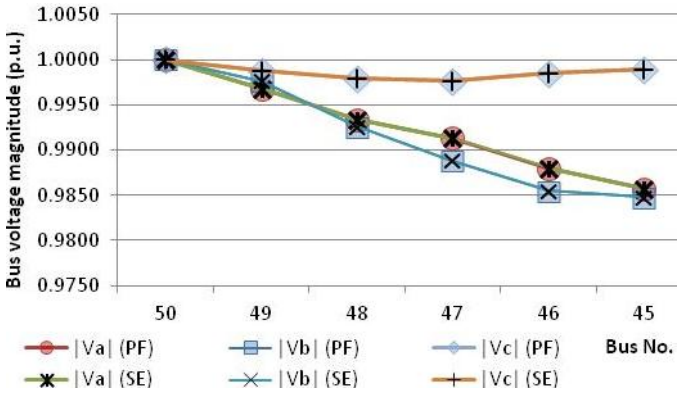

Figure 5.7 Main feeder bus voltage magnitudes for the power flow (PF) and estimated (SE) solutions for HE 7 loading condition, Case C1

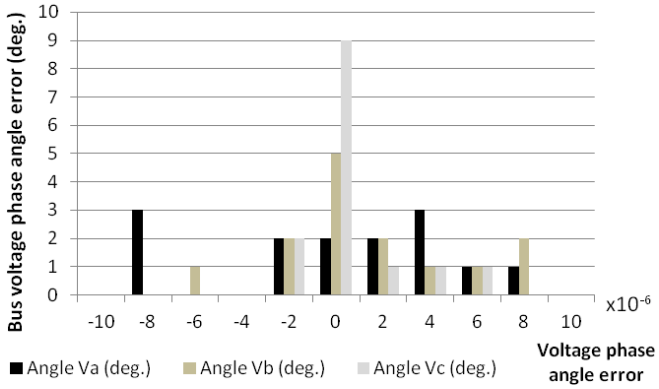

Figure 5.8 Bus voltage phase angle error (i.e. difference between power flow and estimated), for HE 7 loading condition, Case C1

Table 5.8 Estimated Bus Voltages, RBTS Feeder F1, Figure 5.1–Case C1

Case C1 - Base Case		Voltage measurements:		[2 5 6 11 14 45 46 48]		
Bus No.	$\|V_a\|$ (p.u.)	Angle V_a (deg.)	$\|V_b\|$ (p.u.)	Angle V_b (deg.)	$\|V_c\|$ (p.u.)	Angle V_c (deg.)
50	1.0000	0.00	1.0000	-120.00	1.0000	120.00
49	0.9968	-0.24	0.9977	-120.22	0.9988	119.80
48	0.9933	-0.44	0.9926	-120.57	0.9979	119.44
47	0.9913	-0.53	0.9888	-120.81	0.9977	119.19
46	0.9880	-0.64	0.9855	-121.15	0.9986	119.03
45	0.9857	-0.77	0.9848	-121.31	0.9989	119.01
14	0.9959	-0.36				
13	0.9923	-0.51	0.9918	-120.63	0.9975	119.37
12					0.9969	119.11
11			0.9842	-121.33		
10					0.9974	118.89
9	0.9841	-0.83	0.9848	-121.41		
8	0.9850	-0.84	0.9841	-121.37	0.9986	118.94
7	0.9944	-0.89				
6	0.9903	-1.01	0.9899	-121.13	0.9954	118.90
5					0.9952	118.73
4			0.9828	-121.87		
3					0.9957	118.41
2	0.9820	-1.34	0.9826	-121.92		
1	0.9836	-1.43	0.9825	-121.96	0.9972	118.37

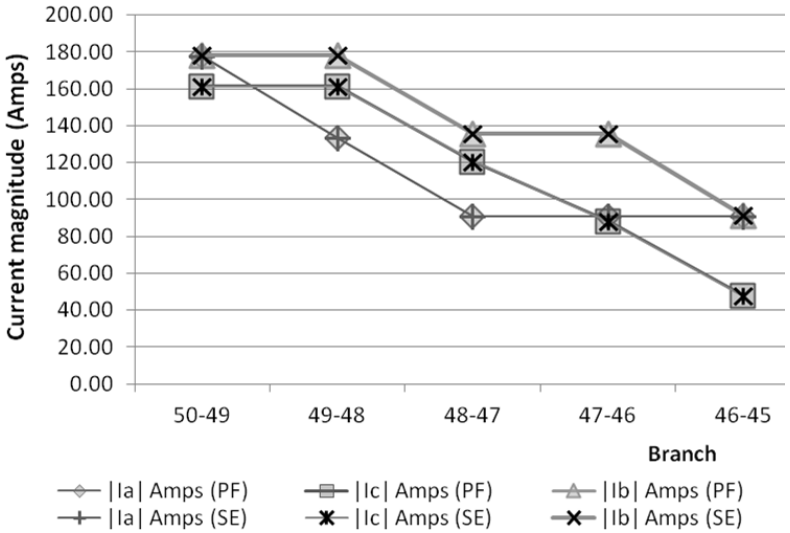

Figure 5.9 Main feeder line current magnitudes from power flow (PF) and estimated (SE), for HE7 loading condition, Case C1

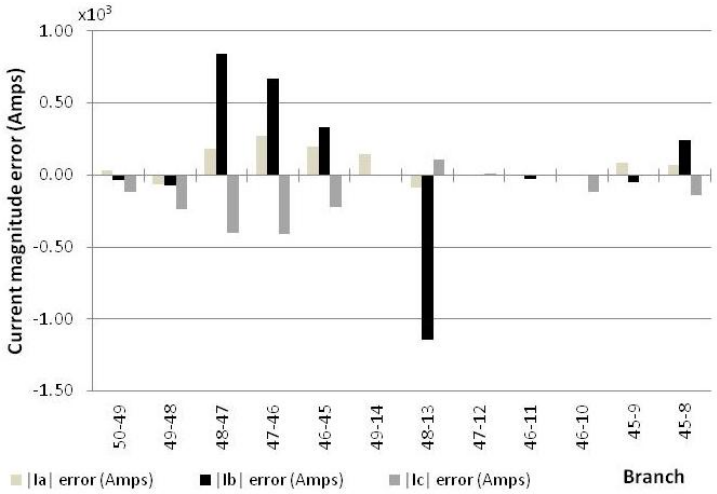

Figure 5.10 Difference between current magnitudes for the power flow and estimated solution corresponding to HE 7 loading condition, Case C1

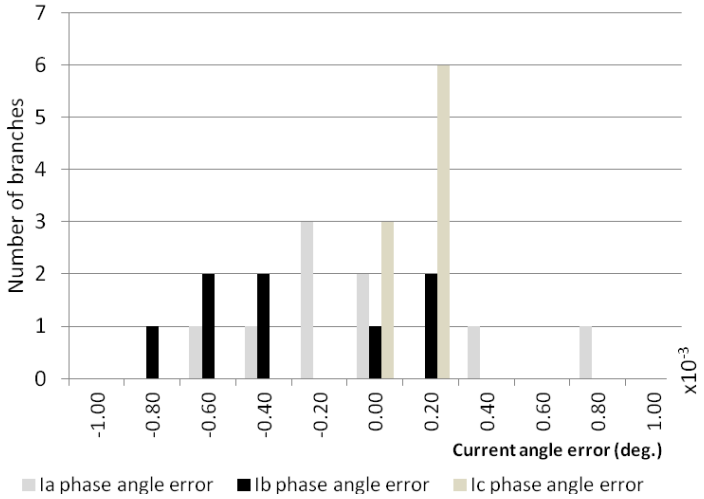

Figure 5.11 Current phase angle error histogram (i.e. difference between power flow and estimated solution), for HE7 loading condition, Case C1

Example SE2

Example SE2 estimates bus voltages at peak load (HE18 – Case C5). It is assumed that individual loads were known at a light load condition (HE3 – Case C6) for which a power flow study result is available. Note that at some instant in HE18, bus voltages are measured in full phasor detail at transformer primary bus-

es 11, 14 and at main feeder buses 45, 46 and 48. Bus voltage magnitudes at buses 2, 5, and 6 are also available. Power flowing into the circuit at the substation is measured. Loads at buses 2, 5 and 6 are also measured. The different states are depicted in Figure 5.2. The unknown load values are assumed (scaled based on known values at HE3 to match substation flow at HE18). The state vector at HE18 is then estimated.

Table 5.9 and Table 5.10 present bus voltages obtained from the power flow study of RBTS feeder F1 as depicted in Figure 5.1 for HE3 (Case C6) and HE18 (Case C5) respectively. Table 5.11 presents line currents on the main feeder and two laterals farthest from the substation for both cases (light load at HE3 and peak load at HE18).

Results of example SE2

The resulting state estimates are shown in the subsequent figures. Figure 5.12 shows main feeder bus voltage magnitudes for both the estimated and actual (power flow) solutions. Figure 5.13 presents the error histograms depicting number of bus within an error range (i.e. difference between the power flow study and estimated solutions). Figure 5.14 shows voltage phase angle error between power flow and estimated results.

Table 5.9 Bus Voltages from a Power Flow, RBTS Feeder F1, Figure 5.1–HE3, Case C6

Bus No.	$\|V_a\|$ (p.u.)	Angle V_a (deg.)	$\|V_b\|$ (p.u.)	Angle V_b (deg.)	$\|V_c\|$ (p.u.)	Angle V_c (deg.)
50	1.0000	0.00	1.0000	-120.00	1.0000	120.00
49	0.9984	-0.09	0.9988	-120.10	0.9995	119.91
48	0.9967	-0.17	0.9963	-120.25	0.9990	119.76
47	0.9958	-0.21	0.9945	-120.34	0.9987	119.65
46	0.9941	-0.25	0.9930	-120.49	0.9992	119.60
45	0.9928	-0.30	0.9927	-120.57	0.9995	119.61
14	0.9980	-0.13				
13	0.9962	-0.20	0.9958	-120.28	0.9989	119.73
12					0.9983	119.60
11			0.9924	-120.55		
10					0.9986	119.55
9	0.9918	-0.33	0.9927	-120.64		
8	0.9925	-0.32	0.9924	-120.59	0.9994	119.59
7	0.9969	-0.33				
6	0.9950	-0.42	0.9945	-120.53	0.9979	119.51
5					0.9972	119.38
4			0.9913	-120.72		
3					0.9974	119.36
2	0.9907	-0.62	0.9914	-120.95		
1	0.9914	-0.50	0.9914	-120.79	0.9987	119.41

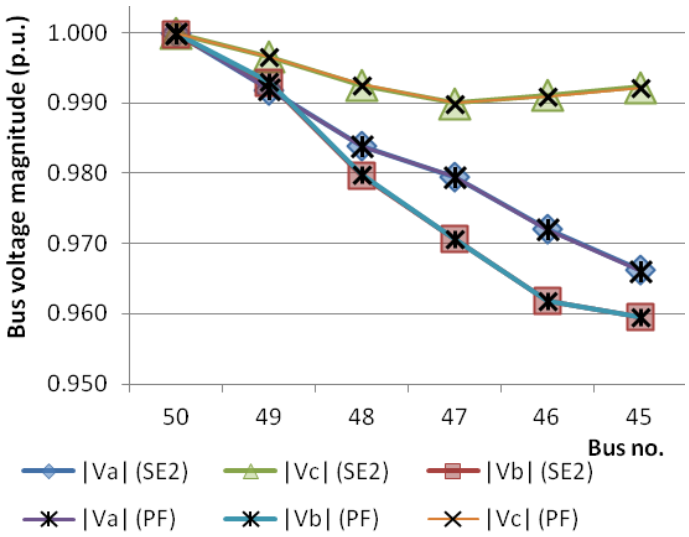

Figure 5.12 Bus voltage magnitudes along main feeder RBTS feeder F1, Figure 5.1, for HE18 loading condition, power flow and estimated solution

Table 5.10 Voltages from a Power Flow, RBTS Feeder F1, Figure 5.1, HE18, Case C5

Bus No.	$\|V_a\|$ (p.u.)	Angle V_a (deg.)	$\|V_b\|$ (p.u.)	Angle V_b (deg.)	$\|V_c\|$ (p.u.)	Angle V_c (deg.)
50	1.0000	0.00	1.0000	-120.00	1.0000	120.00
49	0.9919	-0.32	0.9931	-120.35	0.9966	119.65
48	0.9839	-0.54	0.9798	-120.87	0.9926	118.98
47	0.9795	-0.65	0.9707	-121.21	0.9900	118.52
46	0.9720	-0.75	0.9618	-121.76	0.9910	118.25
45	0.9662	-0.91	0.9595	-122.08	0.9922	118.26
14	0.9893	-0.49				
13	0.9811	-0.63	0.9772	-121.02	0.9918	118.86
12					0.9873	118.34
11			0.9577	-122.04		
10					0.9874	118.02
9	0.9625	-0.98	0.9585	-122.29		
8	0.9640	-1.00	0.9581	-122.18	0.9917	118.19
7	0.9818	-1.37				
6	0.9728	-1.52	0.9685	-122.03	0.9850	117.98
5					0.9799	117.46
4			0.9500	-122.97		
3					0.9795	117.14
2	0.9544	-1.95	0.9497	-123.30		
1	0.9562	-1.96	0.9511	-123.11	0.9866	117.44

Table 5.11 Line Currents from a Power Flow Solution, RBTS Feeder F1, Figure 5.1, Light Loading (HE3 – Case C6) and Peak Loading (HE18 – Case C5)

From bus	To bus	$\|I_a\|$ (Amps)	Angle I_a (deg.)	$\|I_b\|$ (Amps)	Angle I_b (deg.)	$\|I_c\|$ (Amps)	Angle I_c (deg.)
HE3 - Case C6							
49	50	76.45	-16.92	79.63	-136.69	70.44	103.86
48	49	59.45	-16.56	79.63	-136.69	70.44	103.86
47	48	40.00	-16.13	58.59	-136.60	52.07	103.60
46	47	40.00	-16.13	58.59	-136.60	32.43	103.28
45	46	40.00	-16.13	43.05	-135.31	15.78	106.41
9	45	24.46	-13.58	26.49	-133.94		
8	45	15.60	-20.13	16.58	-137.49	15.78	106.41
HE18 - Case C5							
49	50	334.61	-28.02	347.88	-148.63	306.74	92.86
48	49	254.28	-28.20	347.88	-148.63	306.74	92.86
47	48	171.77	-27.54	255.54	-148.80	228.04	92.46
46	47	171.77	-27.54	255.54	-148.80	147.70	92.92
45	46	171.77	-27.54	172.66	-148.80	66.69	96.40
9	45	86.33	-28.02	91.20	-150.33		
8	45	85.45	-27.05	81.53	-147.08	66.69	96.40

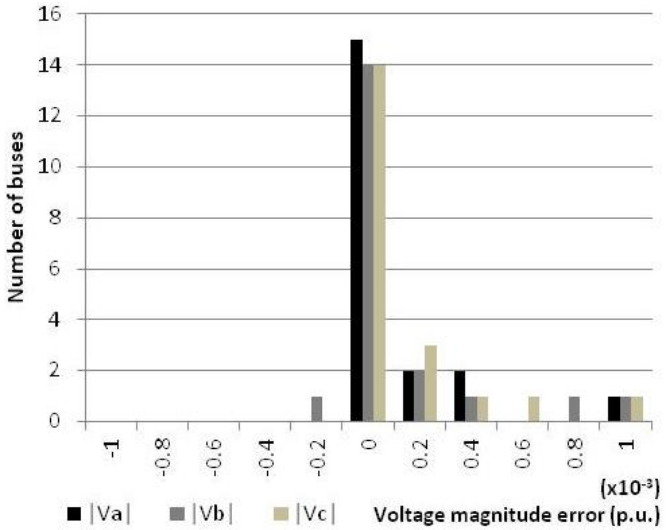

Figure 5.13 Voltage magnitude error histogram (i.e. difference between power flow and estimated solution), example SE2

Figure 5.15 shows line current magnitudes along the main feeder for both the power flow (true) and estimated solutions. Figure 5.16 and Figure 5.17 show error histograms for branch current magnitude and phase angle errors respectively.

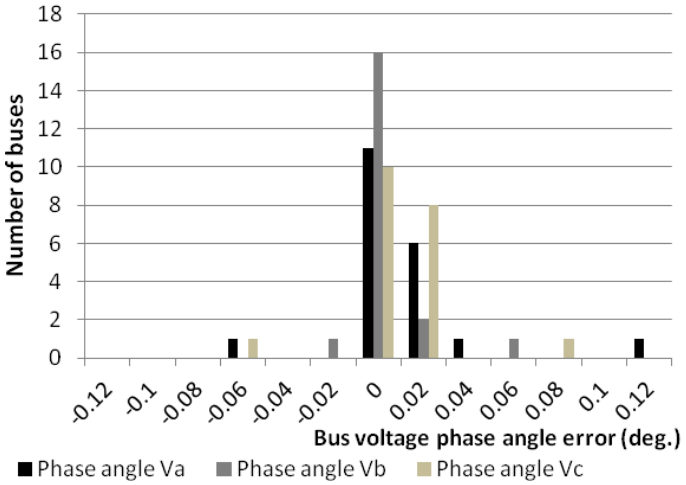

Figure 5.14 Bus voltage phase angle error histogram (i.e. difference between power flow study and estimated), example SE2

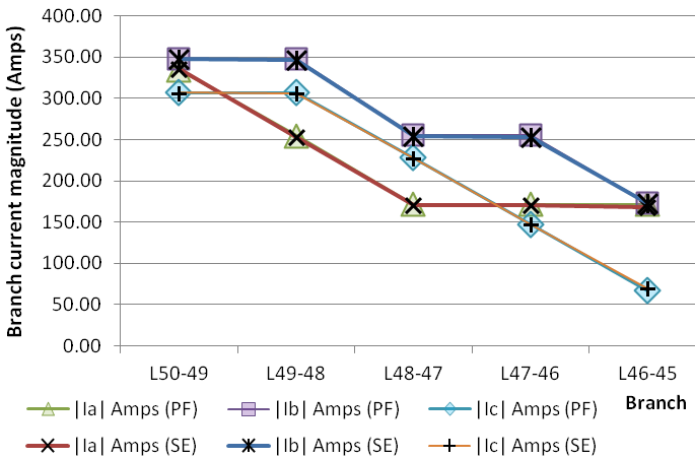

Figure 5.15 Line current magnitudes along the main feeder for RBTS feeder F1, power flow and estimated

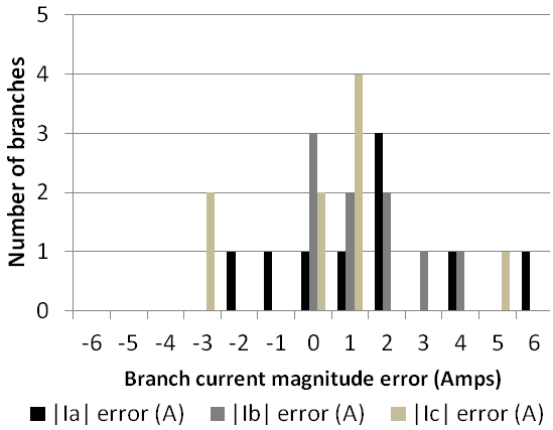

Figure 5.16 Branch current magnitude error (Amps), RBTS feeder F1, SE2

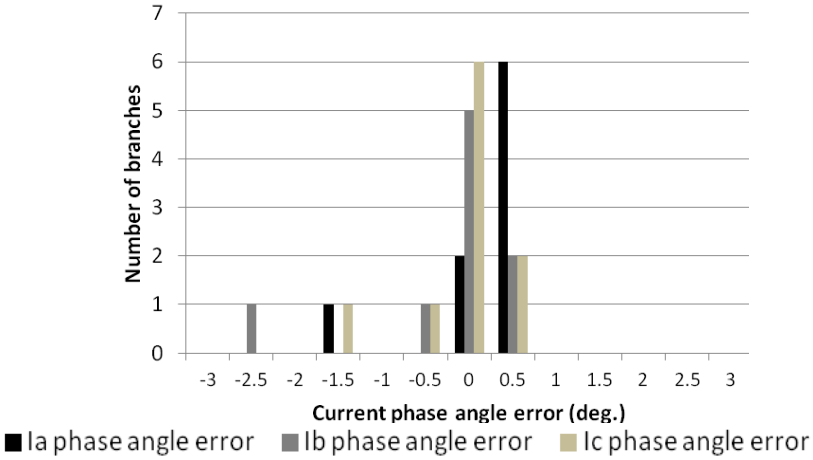

Figure 5.17 Branch current phase angle error (deg.), RBTS feeder F1, SE2

Example SE3

Example SE3 evaluates the estimator algorithm performance under a different set of circumstances. The test bed RBTS feeder F1, in full three-phase detail, as shown in Figure 5.1 is used. The system state under the loading conditions at hour ending (HE) 5:00 is estimated from two different starting assumptions, denoted here as *SE3a* and *SE3b*. Loading condition at HE 5:00 is estimated, first using the known (power flow) loads at HE3 (Case C6) – *SE3a*. The process is repeated for the known loads at HE7 (Case C1). Loading conditions for the three cases are as follows (details are shown graphically in Figure 5.2):

- HE 3:00, Case C6, substation serves load of 1.43 MVA
- HE 5:00, substation serves load of 2.54 MVA
- HE 7:00, Case C1, substation serves load of 3.26 MVA.

Table 5.12 Values of Non-Metered (Pseudo-Measurement) Loads Obtained from Equations (5.2) – (5.7) at HE5

Non-metered load at HE 5	Actual		Based on HE 3		Based on HE 7	
	P (kW)	Q (kVAr)	P (kW)	Q (kVAr)	P (kW)	Q (kVAr)
LP 1	600	125	549	111	594	116
LP 3	155	30	180	42	136	39
LP 4	200	40	192	44	200	40
LP 7	150	45	184	43	175	45

Bus voltage magnitudes during HE3 (Case C6) and HE7 (Case C1) have already been shown in Table 5.9 and Table 5.6 respectively. Line current magnitudes for both loading conditions have also been presented in Table 5.7 and Table 5.11. Voltage magnitudes from the power flow study results for HE5 loading is shown in Table 5.13. Line currents for HE5 solution is shown in Table 5.14. The

specific loads at HE5 are largely unknown to the estimator (only measured bus values are known).

Note that bus voltages at buses 2, 5, 6, 11, 14, 45, 46, and 48 are measured, and are updated in the state estimation stage of the algorithm. Also, bus voltage and power flowing into the circuit from the substation is known. Estimating states under HE 5 (05:00) loading conditions is first performed based on the power flow results of HE 3 (03:00). The estimation process is repeated, however, the 'most recent' power flow study results of HE 7 (7:00) are used to supplement non-measured data.

Table 5.13 Bus Voltages from a Power Flow Study, RBTS Feeder F1 for Loading Condition HE5

Bus No.	$\|V_a\|$ (p.u.)	Angle V_a (deg.)	$\|V_b\|$ (p.u.)	Angle V_b (deg.)	$\|V_c\|$ (p.u.)	Angle V_c (deg.)
50	1.0000	0.00	1.0000	-120.00	1.0000	120.00
49	0.9974	-0.17	0.9979	-120.17	0.9991	119.84
48	0.9944	-0.34	0.9938	-120.44	0.9983	119.56
47	0.9925	-0.41	0.9909	-120.63	0.9981	119.38
46	0.9895	-0.50	0.9884	-120.91	0.9991	119.30
45	0.9874	-0.61	0.9878	-121.04	0.9995	119.30
14	0.9967	-0.23				
13	0.9936	-0.41	0.9931	-120.48	0.9976	119.49
12					0.9973	119.30
11			0.9873	-121.03		
10					0.9984	119.21
9	0.9858	-0.66	0.9878	-121.14		
8	0.9868	-0.65	0.9873	-121.08	0.9992	119.26
7	0.9952	-0.52				
6	0.9915	-0.85	0.9913	-120.87	0.9956	119.05
5					0.9956	118.92
4			0.9859	-121.42		
3					0.9974	118.92
2	0.9838	-1.15	0.9856	-121.62		
1	0.9855	-1.04	0.9858	-121.47	0.9979	118.88

Table 5.14 Line Currents Obtained from a Power Flow Study, RBTS Feeder F1, Figure 5.1, HE 5

From bus	To bus	$\|I_a\|$ (Amps)	Angle I_a (deg.)	$\|I_b\|$ (Amps)	Angle I_b (deg.)	$\|I_c\|$ (Amps)	Angle I_c (deg.)
49	50	136.21	-14.79	140.26	-134.84	127.26	106.03
48	49	111.46	-14.25	140.26	-134.84	127.26	106.03
47	48	73.72	-13.63	106.55	-134.51	89.68	106.70
46	47	73.72	-13.63	106.55	-134.51	57.11	107.74
45	46	73.72	-13.63	74.00	-135.29	32.18	107.57
14	49	24.78	-17.22				
13	48	37.75	-15.47	33.71	-135.89	37.59	104.43
12	47					32.60	104.88
11	46			32.57	-132.73		
10	46					24.92	107.96
9	45	41.15	-14.65	41.27	-136.20		
8	45	32.59	-12.35	32.74	-134.15	32.18	107.57

Results of example SE3

The results of this illustration are shown in the subsequent figures. Figure 5.18 presents bus voltage magnitudes along the main feeder for the power flow, *SE3a* and *SE3b* results. Figure 5.19 presents the histograms for the voltage magnitude error for both *SE3a* and *SE3b* for all buses of the RBTS feeder F1 as seen in Figure 5.1.

Figure 5.21 shows the line current magnitudes along the main feeder for the power flow study, *SE3a* and *SE3b* estimated results. Figure 5.22 and Figure 5.23 present the line current magnitude error histogram and line current phase angle error histograms respectively.

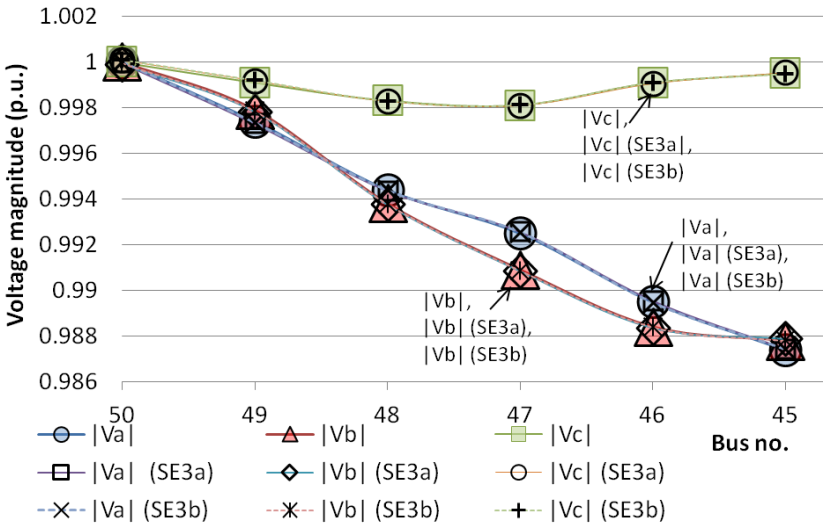

Figure 5.18 Bus voltage magnitudes along the main feeder for HE5 loading condition based on *'historical data'* from HE3 (*SE3a*), then from HE7 (*SE3b*)

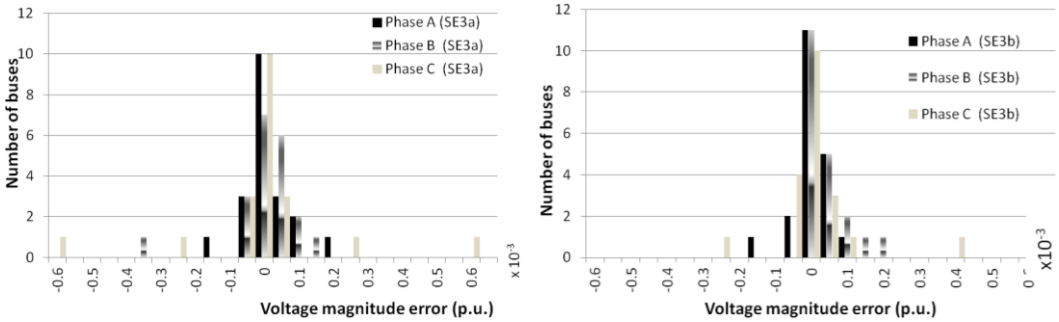

Figure 5.19 Voltage magnitude error histograms (i.e. difference between power flow study and estimated), examples *SE3a*, *SE3b*

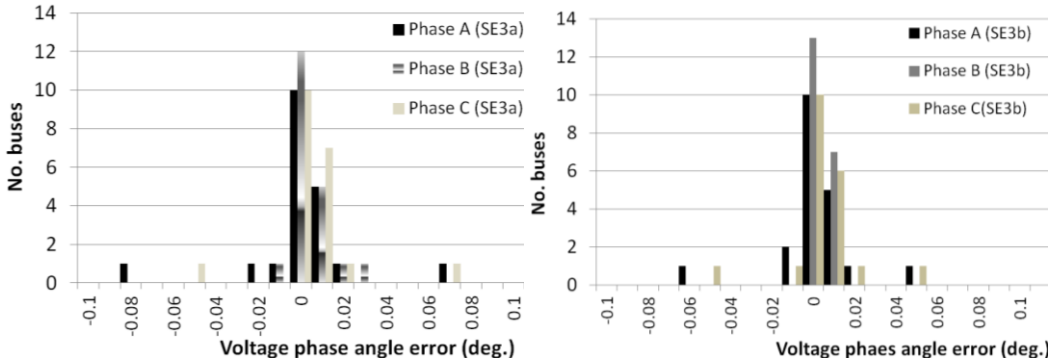

Figure 5.20 Voltage phase angle error histograms (i.e. difference between power flow study and estimated), examples *SE3a*, *SE3b*

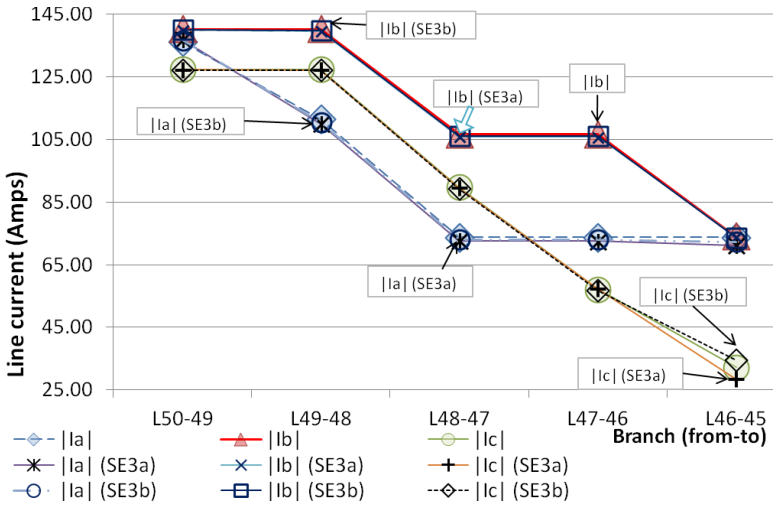

Figure 5.21 Line current magnitudes along the main feeder for HE5 loading condition based on *'historical data'* from HE3 (*SE3a*), then from HE7 (*SE3b*)

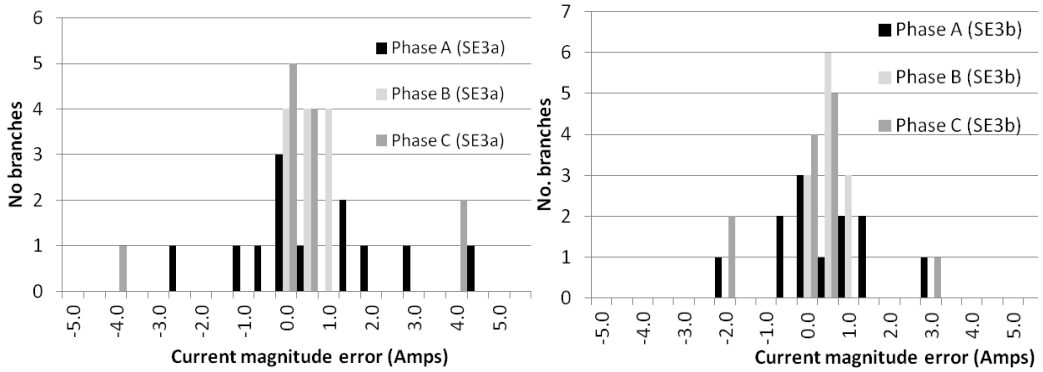

Figure 5.22 Line current magnitude error histograms (i.e. difference between power flow study and estimated), examples *SE3a*, *SE3b*

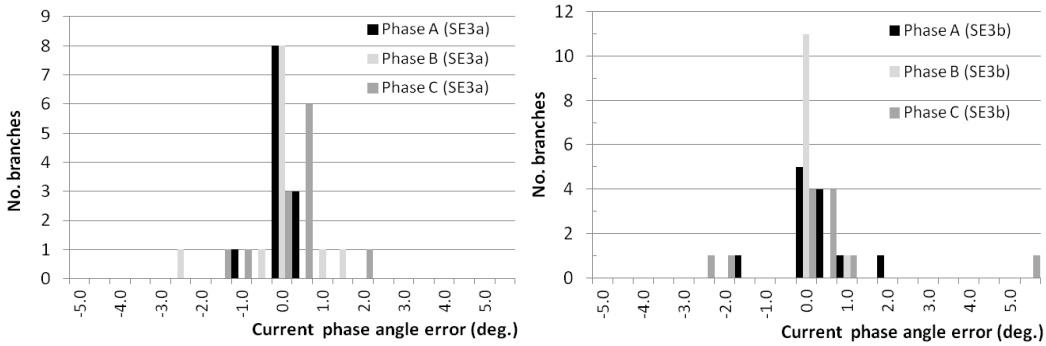

Figure 5.23 Line current phase angle error histograms (i.e. difference between power flow study and estimated), examples *SE3a*, *SE3b*

The results show that bus voltage magnitudes are estimated reasonably accurately for this system considering the uncertain loading, assumed measurement configuration and estimator formulation. The uncertainty in assumed loads (i.e. unmetered loads assumed based on apportioned measured substation flow less measured load) is seen in calculated branch current magnitudes of Figure 5.21. Details are discussed at the end of this chapter.

5.2 Biased measurements for improved estimation

The assignment of a biased weighting factor to a measurement function is accomplished by introducing the weight matrix, *W*, as in Equation (3.10). If *W* is the inverse of the covariance matrix of the measurement noise, and the measurement noise is multivariate normally distributed, the solution obtained is the maximum likelihood solution [42]. If the measurement noise among the several measurements is independent, the covariance matrix of the noise is diagonal and therefore the weight matrix is also diagonal.

High variance is generally assigned to pseudo-measurements due to the uncertainty created by using historical data to approximate near real-time operating conditions. The gain matrix, *G*, contains the biasing factors to perform WLS estimation (see Equation (3.9)).

As described in subsection 5.1, measurements vary by type and location. Assigned weight varies by measurement type. Representative values used in this illustration are shown in Table 5.15. The three cases, SE1, SE2 and SE3 are re-

peated with biased measurement functions to illustrate the impact of the weights. Error histograms for the results of biased estimation are presented and discussed subsequently.

Table 5.15 Measurement Type, Standard Deviation and Weights

Measurement type	Standard Deviation, σ (% of measured value)	Weight $\left(\frac{1}{\sigma^2}\right)$
Pseudo measurement (Non metered demands only)	50.0	4
Bus voltage magnitude	5.0	400
Power flow	5.0	400
Smart meters	3.0	1111
Phasor bus voltage	1.0	10000
Virtual measurement	0.5	40000

Results of biased estimation - example SE2

Based on the examples studied, the results show that biased estimation produces superior accuracy to unbiased estimation. This remark is possible because in these examples, the *exact* solution is known (the examples are 'synthetic'). Error histograms of voltage magnitudes and phase angles for example SE2 are shown in Figure 5.24. Note that both sets of error histograms are plotted on a common scale for comparison.

Results of biased estimation - example SE3

Error histograms of voltage magnitudes and phase angles for illustration SE3a and SE3b are presented in Figure 5.25 and Figure 5.27. Similarly, error histograms of current magnitudes and phase angles for examples SE3a and SE3b are presented in Figure 5.26 and Figure 5.28. When plotted on a common scale (bins on the *x-axis*), the error histograms show that biased estimation as discussed

above have significantly reduced error. This is the same observation as obtained in the conventional, positive sequence state estimation formulation [42], [105].

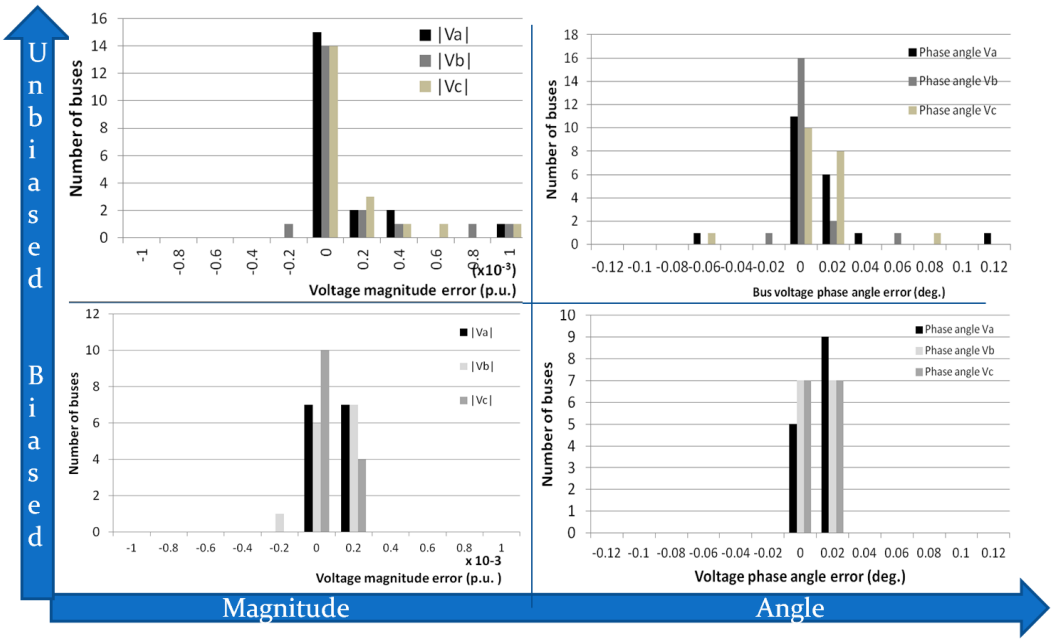

Figure 5.24 Comparison of unbiased versus biased voltage magnitude and angle estimates for example SE2

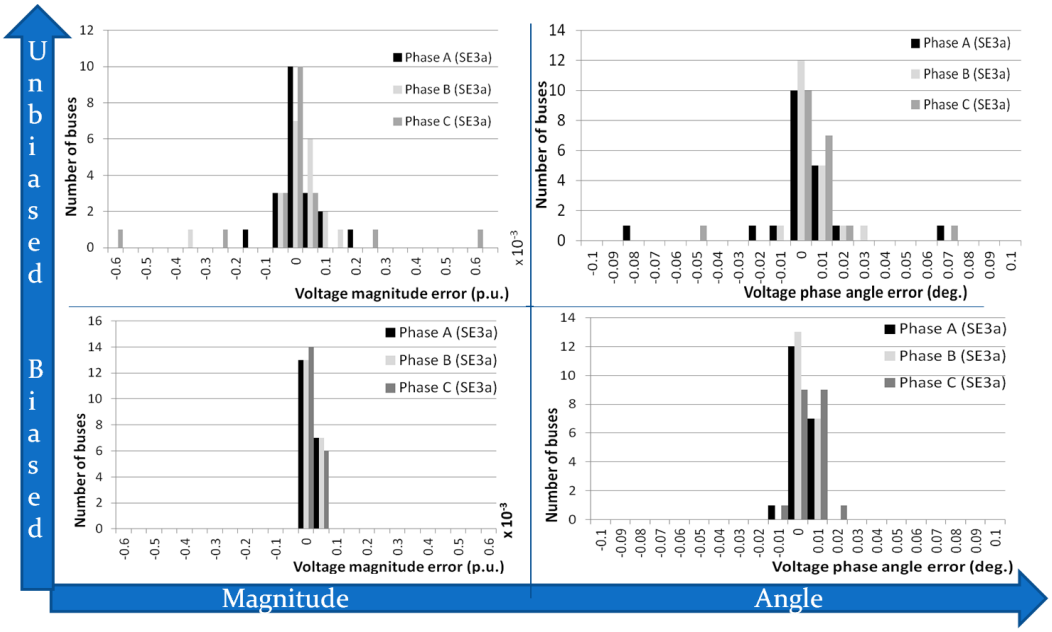

Figure 5.25 Comparison of voltage magnitude and phase angle error histograms for unbiased and biased estimates corresponding to example SE3a

Comparison of maximum voltage magnitude and phase angle errors show approximately 85% improvement accuracy (in range) when biased measurements are used. Calculation of line currents and errors shows 80% improvement in calculation accuracy when biased estimates are employed. Current magnitude calculation of SE3a was found to be 16% in error (approximately 5.5 Amperes) for the unbiased case; however, the biased formulation improved accuracy to 4% error (1.8 Amperes from true / power flow solution).

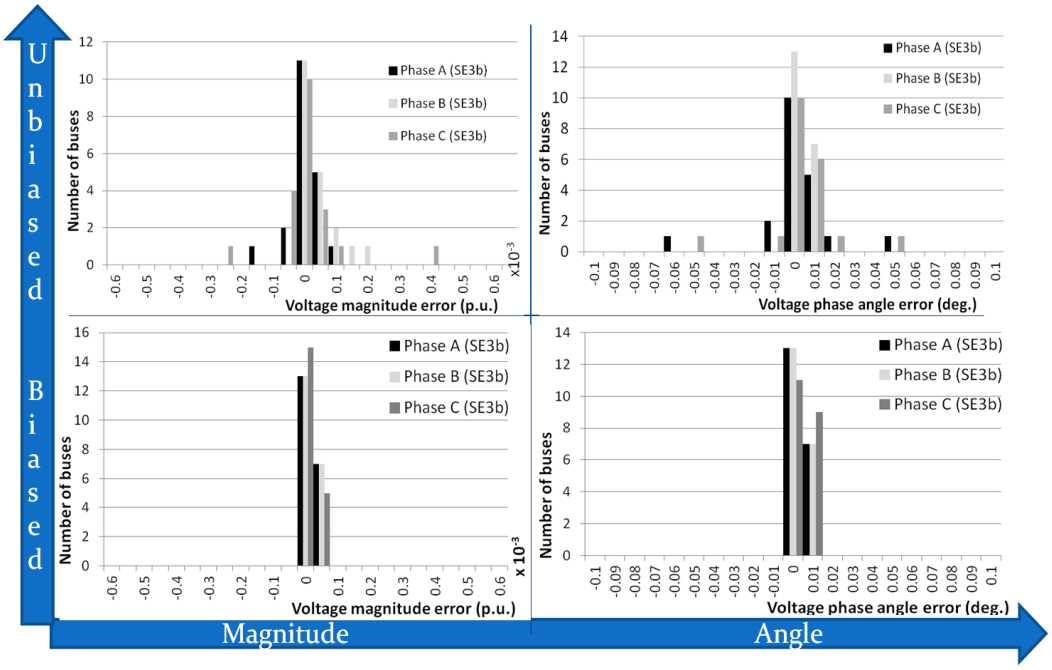

Figure 5.26 Comparison of current magnitude and phase angle error histograms for unbiased and biased estimates corresponding to example SE3a

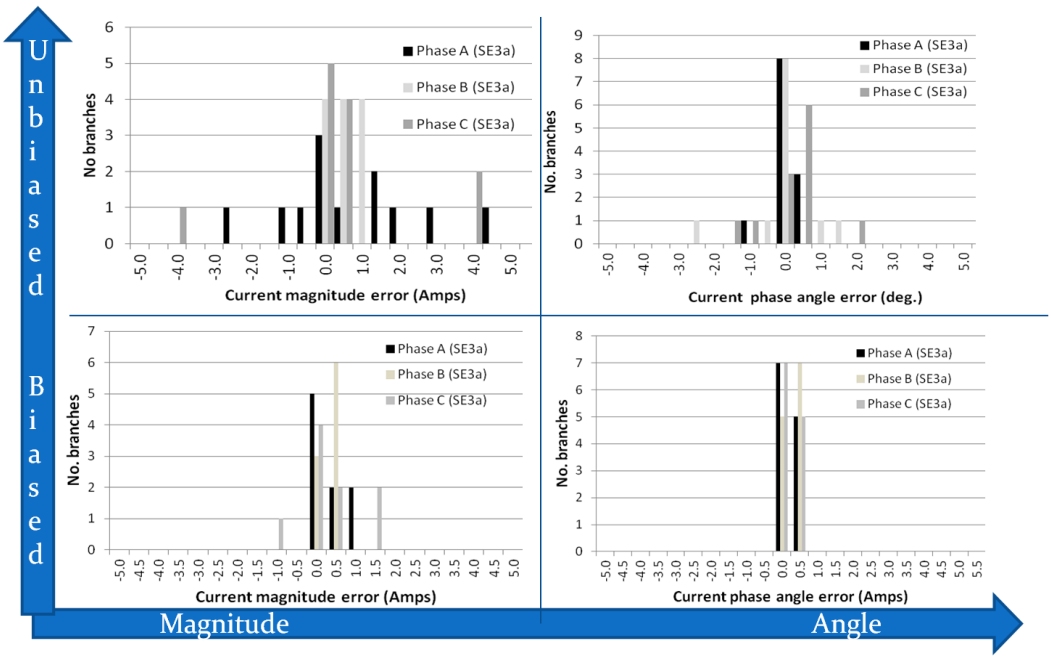

Figure 5.27 Comparison of voltage magnitude and phase angle error histograms for unbiased and biased estimates corresponding to example SE3b

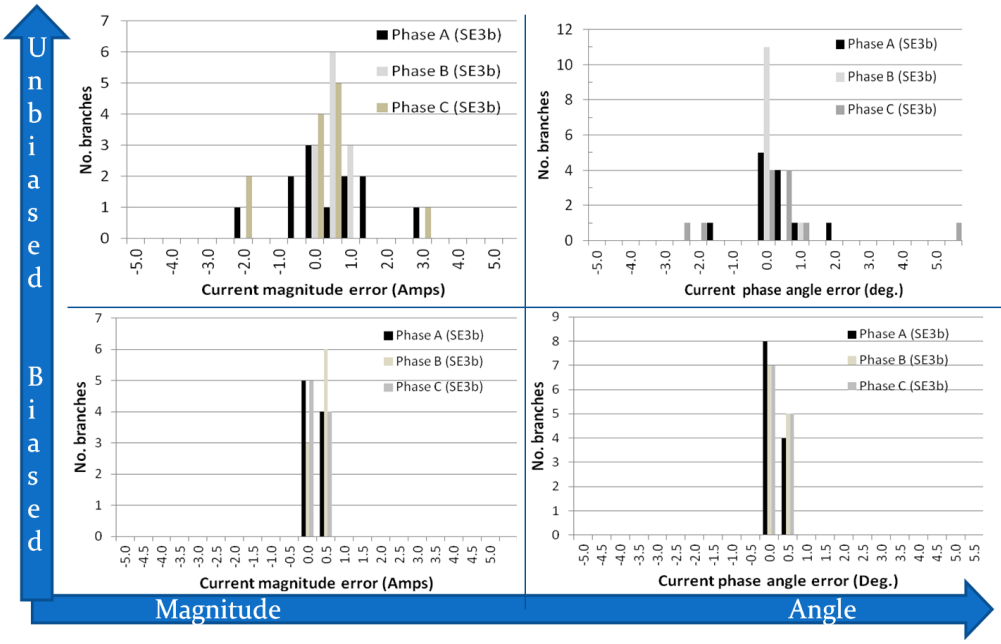

Figure 5.28 Comparison of current magnitude and phase angle error histograms for unbiased and biased estimates corresponding to example SE3b

5.3 Illustration of bad data detection

Bad data detection is investigated here using the well known chi-squares test. The chi-squares test is applied to the examples shown previously. The measurement set comprises all types of measurements used. A confidence level (e.g., 95%) is selected, and degrees of freedom is set equal to the difference between number of measurements and states. Sample results are presented for example SE2 with load on phase *A* at bus 2 measured erroneously as 50% of its true value. Results are shown in Table 5.16.

Table 5.16 Sample Bad Data Detection Results on Example SE2

Example	$J(x)$	Detection threshold $\chi^2_{0.95,24}$	Bad data suspected
EX2 (unbiased)	$9.95*10^{-4}$	36.42	No
EX2 (biased)	19.41	36.42	No
EX2 (bad data)	81.42	36.42	Yes

5.4 Discussion of results

Discussion of unbiased distribution system state estimation results

The development of a three-phase distribution system state estimator that runs in a substation computer is presented. Examples illustrate the estimator performance for feeder loading conditions ranging from light load to peak load. The algorithm uses an assumed system topology, measured quantities, and assumed (unmeasured) loads values. The algorithm performs a linear, non-iterative least squares estimation to obtain the best estimate of the system state.

Example SE1 illustrates the performance of the estimation algorithm with no errors. Estimated bus voltage magnitudes and line currents are identical to theoret-

ical power flow study values for a given feeder topology. The estimator formulation provides good performance in the absence of measurement error and load uncertainty. Subsequent examples include measurement error and load uncertainty.

Example SE2 illustrates estimator performance under uncertain load assumption. That is, a power flow study for the system at low load (HE3, Case C6), and exact values for loads at this time interval are given. A power flow study at heavy load (HE18, Case C5) is assumed to be unavailable (i.e., values are not available to the estimator algorithm). Likely values of non-measured loads are provided to the estimator. The resulting state estimate obtained is close to the actual state vector. Maximum bus voltage magnitude estimate error is 0.1%, or 0.001 p.u. Maximum voltage phase angle estimate error is 0.12^{o}. Maximum branch current error is calculated at approximately 5.97 Amperes at the non-metered (transformer primary, bus 8) load bus (bus 1) furthest from the substation. Along branch 45-8, the actual phase *a* current magnitude should be 85.45 Amperes, corresponding to a 6.95% error. The worst case branch current phase angle error of 2.9^{o} is located on phase *b* of the same branch.

Example SE3 demonstrates the effects of load uncertainty and *'historical data'* in obtaining a state estimate. An estimate of system bus voltages (at HE5) is sought from two separate starting assumptions (load at HE3 and load at HE7). That is, the exact loads at HE5 are unknown; however, the exact loads at HE3 are known, and are used to approximate HE5 load then system state (*SE3a*). The load approximation and state estimation is repeated when HE7 loads are known

(*SE3b*). Results show that both starting assumptions provide fairly accurate bus voltage magnitude estimates for this system, (i.e. to within 0.0006 p.u. for the worst case error at two of the 20 buses).

Bus voltage phase angles in all cases are estimated to within 0.09^{o}. Greater accuracy observed for example *SE3b* estimates is explained by examination of load assumptions. Note that each load's active and reactive consumption at HE7 more closely matches loading conditions of HE5. Therefore, adjusting HE7 loads based on substation measurements provides good approximation of HE5 loading. By contrast, the estimated voltages and line current magnitudes for *SE3a* is less accurate. *SE3a* worst case line current magnitude error is 4.5 Amperes compared to 3.0 Amperes for *SE3b*. The largest percentage errors for *SE3a* and *SE3b* line current magnitude are found to be 16.0% and 10.1% respectively, for phase *c* branch 46-10 (LP 3 on Figure 5.1). The percentage errors are calculated using,

$$\% I_{error} = \frac{I_{est}-I_{actual}}{I_{actual}}.$$

Discussion of biased distribution system state estimation results

Performance of the three-phase distribution system state estimation algorithm is improved when biased measurement functions are used. Comparison of unbiased bus voltage magnitude estimates for example SE2 to biased estimates show significant improvement for the biased case. The maximum error magnitudes (largest difference in power flow solution and estimated solution) for bus voltage magnitudes are approximately $1*10^{-3}$ and $2*10^{-4}$ per unit for the unbiased and biased cases respectively. Similarly, maximum bus voltage phase angles error

magnitudes are approximately 0.12 and 0.02 degrees for the unbiased and biased cases respectively.

Comparison of maximum error magnitudes for the results of unbiased and biased cases for examples SE3a and SE3b are summarized in Table 5.17. Note that in all cases, the biased estimates have greater accuracy than the unbiased estimates.

Table 5.17 Comparison of Maximum Error Magnitudes for Unbiased and Biased Estimates of Voltage and Current for SE3a and SE3b

Quantity	SE3a		SE3b	
	Unbiased	Biased	Unbiased	Biased
Voltage magnitude (p.u.)	$0.6*10^{-3}$	$1*10^{-4}$	$4*10^{-4}$	$5*10^{-5}$
Voltage phase angle (deg.)	0.08	0.02	0.06	0.01
Current Magnitude (A)	4.5	1.6	3.0	0.5
Current phase angle (deg.)	2.5	0.5	5.5	0.5

Discussion of bad data detection

Bad data detection is illustrated (Example SE2 – bad data, see Table 5.16). The load current in phase A is measured in error at 50% of its true value. The error is detected using the chi-squares test. In practice, bad data detection depends on the measurement configuration, network topology and algorithms used. In the illustration presented here, the chi-squares test was used to detect bad data for the WLS estimation algorithm.

6. Illustrations of applications of a non-linear, three-phase distribution system state estimator

6.1 Voltage unbalance

Voltage unbalance has potentially negative impacts on distribution system operation. For example, derating of motors or induction machines may be required [59]-[63] because of excessive heat generated in machine windings. The percentage temperature rise in the machine increases as approximately twice the square of the percent voltage unbalance; therefore, a 2% unbalance leads to about an 8% temperature increases [59]-[63]. DG may be impacted in Smart Grid networks that experience voltage unbalance [59]. An estimator may obviate voltage unbalance issues.

Voltage unbalance also impacts protection coordination, pre-loading of fuses and loss of sensitivity of ground fault relaying [59] when higher neutral currents occur since voltages are unbalanced. The ability to detect and mitigate voltage unbalance may be an important application of the distribution state estimator.

6.2 Voltage control

Voltage control examples demonstrate the effect of voltage unbalance and problems with conventional methods of voltage control in distribution systems. Note that future distribution systems may experience exacerbated voltage regulation problems when compared with conventional ones. This may become especially apparent where high penetration of intermittent renewable DG is present. Conventional methods of voltage regulation include two classes of equipment,

that is, equipment installed at substations or installed out on the circuit / feeder [59]. Substation regulation equipment comprises utility connected DG, capacitors, or under-load tap-changing (ULTC) transformers. The circuit may have shunt capacitors and voltage regulators [24]-[26]. Regulators may independently control each phase voltage. Generally all phases of shunt capacitors switch together.

Where the preceding options fail to deliver adequate voltage regulation, long-term response also includes: using higher primary distribution voltage, upgrading to larger conductor sizes, replacing transformers to provide lower impedance, load balancing, converting line sections to three-phase, and transferring loads to other circuits [59]. Also note that most DG is barred from regulating bus voltages in present systems [45].

For the RBTS feeder, F1 as shown in Figure 5.1, unbalanced voltages occur at the system peak (Case C5). The unbalanced bus voltage magnitudes may be observed in Table 6.1 and Figure 5.3 - Figure 5.5. Note that unbalance in Table 6.1 is calculated according to Equation 1.2, which may be much larger than if calculated by the IEEE unbalance factor, Equation (1.2), or its general approximation, Equation (1.3), given line voltages.

The effect of reactive power support via capacitor banks in distribution systems is well understood. For example, a capacitor on bus 47 may avoid a low voltage condition at remote load buses 1 and 2. However, conventional operation attempts to simultaneously switch in three phases of a capacitor bank (that is, provided there are no blown fuses or defective capacitors).

Note that in this case the voltage unbalance condition may persist. As discussed, large three phase motors and induction generators may need to be derated or risk thermal damage due to overheating. Protection systems may also be negatively affected; for example, pre-loading fuses on laterals degrades effectiveness of existing protection coordination. It can be seen from results in Table 6.1 that the unbalance is well outside desirable ranges cited in the literature [59]-[63].

Table 6.1 Bus Voltage Magnitudes and Unbalance for Case C5

Bus No.	V_{avg} (p.u.)	$\|V_a\|$-V_{avg} (p.u.)	$\|V_b\|$-V_{avg} (p.u.)	$\|V_c\|$-V_{avg} (p.u.)	% V_u
1	0.9732	-0.0221	-0.0122	0.0343	3.53
2	0.9558	-0.0051	0.0051		0.54
6	0.9780	-0.0076	-0.0060	0.0136	1.39
8	0.9779	-0.0197	-0.0099	0.0296	3.03
9	0.9630	-0.0049	0.0049		0.51
13	0.9860	-0.0070	-0.0054	0.0124	1.25
45	0.9787	-0.0174	-0.0102	0.0275	2.81
46	0.9803	-0.0126	-0.0105	0.0231	2.36
47	0.9840	-0.0078	-0.0076	0.0154	1.57
48	0.9881	-0.0063	-0.0047	0.0109	1.11
49	0.9950	-0.0037	-0.0006	0.0043	0.43
50	1.0000	0.0000	0.0000	0.0000	0.00
Lowest load-bus voltage magnitude = 0.9539 p.u.					
†Highlighted cells have excessive voltage unbalance.					

The following examples are generated to demonstrate mitigation strategies to severe voltage unbalance in the Smart Grid environment. The cases are titled *voltage unbalance (VU)* cases, and are conducted as follows:

- VU 1: Three-phase capacitor bank, 900 kVAr (300 / phase) on bus 47,
- VU 2: Three-phase capacitor bank, 1.8 MVAr (600 / phase) on bus 47,
- VU 3: Capacitor bank, 300 kVAr/phase, independent phase control

- VU 4: Capacitors on phases *A*, *B*; reactor on *C*, each 200 kVAr / phase,
- VU 5: Reactor of 300 kVAr on phase *C* only,
- VU 6: Capacitors on *A*, *B*, 500 kVAr/phase; reactor on *C*, 200 kVAr.

Note that for all cases, capacitors or reactors are added at bus 47 which is about halfway down the feeder as shown in Figure 5.1.

The results are presented in Table 6.2, along with the minimum bus voltage magnitude on the feeder. Graphs showing voltage drop along the feeder for *VU*1 and *VU*2 resemble results shown in Figure 5.3 - Figure 5.5 (a); that is, the unbalance remains the same, but voltage magnitudes along the main feeder increase. Figure 6.1 shows results for the *VU*3 – switch in only phases *A* and *B* of a capacitor bank. Figure 6.2 shows results *VU*4, switch in 2 phases of capacitors in *A* and *B*, and a reactor in phase *C*. Figure 6.3 presents resulting voltages along the main feeder for *VU*5, switching in a 300 kVAr reactor into phase *C*.

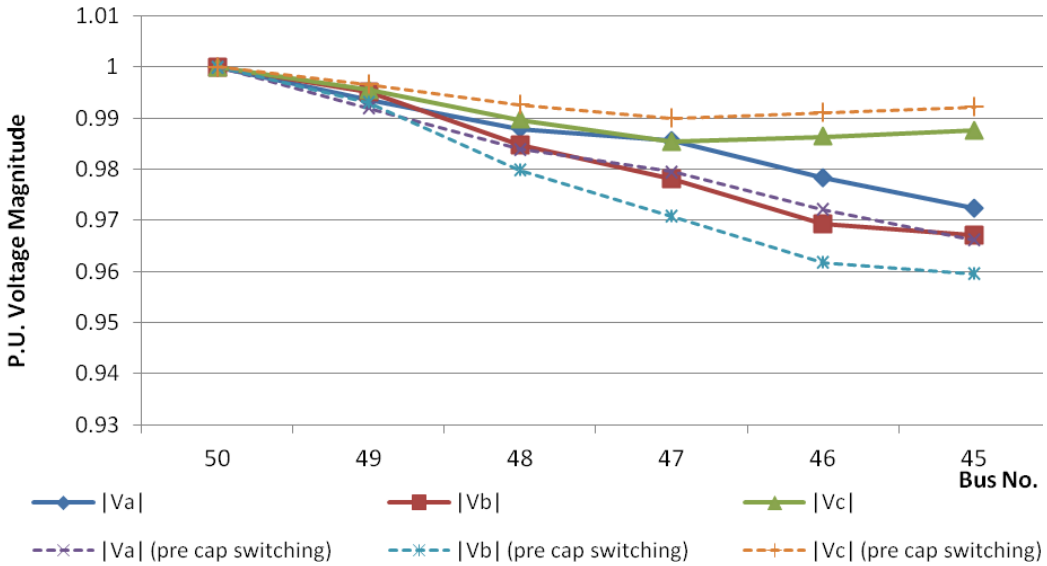

Figure 6.1 *VU* 3: Bus voltage magnitudes along the main feeder of RBTS feeder F1, Figure 5.1, after switching 300 kVAr capacitors into phase *A* and *B* only

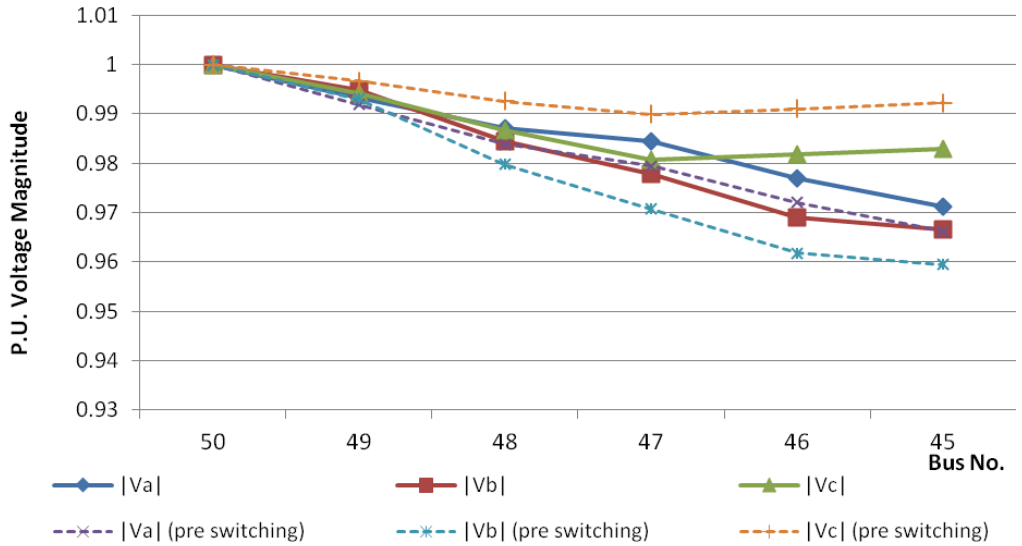

Figure 6.2 *VU* 4: Bus voltage magnitudes along the main feeder of RBTS feeder F1, Figure 5.1, after switching capacitors into phases *A*, *B*, and switching a reactor into phase *C*

Table 6.2 Results of Controlling Voltage Unbalance on RBTS feeder F1, as Shown in Figure 5.1, with Capacitors and Reactors

Case	*VU* 1†	*VU* 2†	*VU* 3	*VU* 4	*VU* 5	*VU* 6
Cap/phase (kVAr)	300	600	300	200		500
Reactor/phase (kVAr)				200	300	200
Switching order	3ph	3ph	1ph	1ph	1ph	1ph
Bus no.	% Vu	% Vu	% Vu	% Vu	% Vu	% Vu
1	2.26	2.24	1.47	1.21	1.48	0.40
2	0.28	0.32	0.18	0.13	0.14	0.07
6	0.97	0.97	0.46	0.29	0.46	0.22
8	2.09	2.07	1.31	1.05	1.31	0.25
9	0.24	0.28	0.14	0.09	0.10	0.03
13	0.85	0.85	0.35	0.22	0.35	0.32
45	2.00	1.98	1.22	0.96	1.23	0.25
46	1.63	1.62	0.89	0.71	0.86	0.44
47	1.01	1.01	0.50	0.35	0.47	0.79
48	0.72	0.72	0.28	0.16	0.25	0.44
49	0.28	0.27	0.11	0.09	0.12	0.20
50	0.00	0.00	0.00	0.00	0.00	0.00
Lowest |*V*| p.u.	0.9540	0.9584	0.9573	0.9570	0.9530	0.9645
†Highlighted cells have excessive voltage unbalance.						

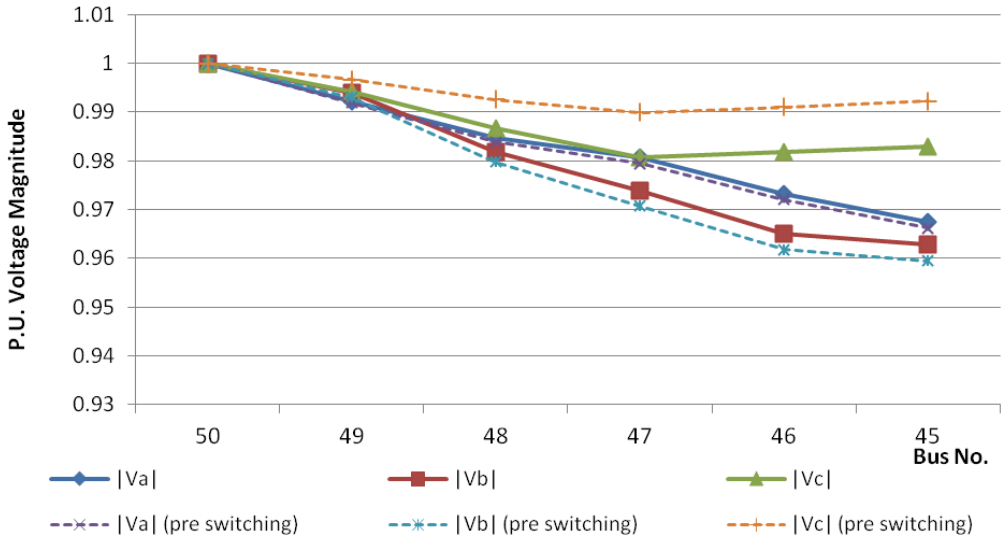

Figure 6.3 *VU* 5: Bus voltage magnitudes along the main feeder of RBTS feeder F1, Figure 5.1, after switching in a 300 kVAr reactor on phase *C*

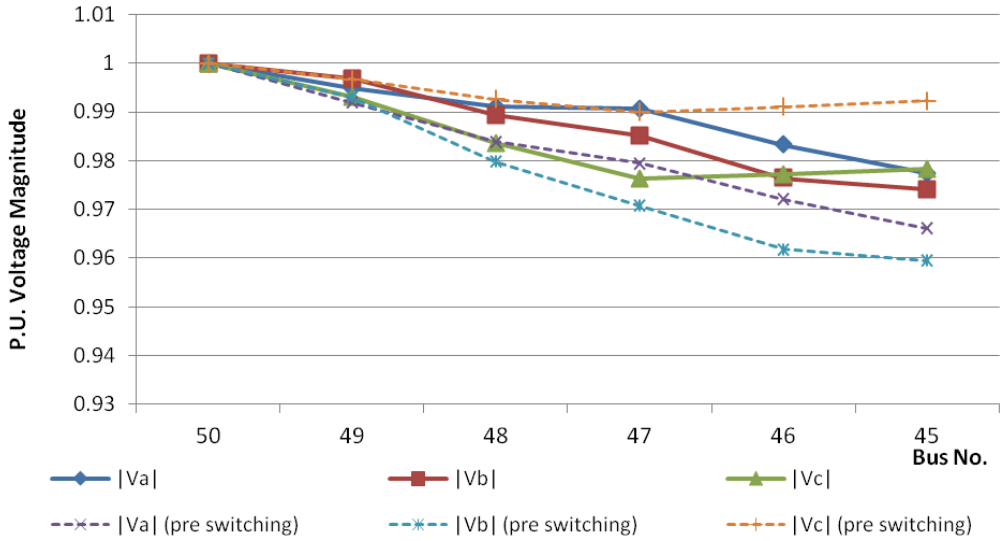

Figure 6.4 *VU* 6: Bus voltage magnitudes along the main feeder of RBTS feeder F1, Figure 5.1, after switching 500 kVAr/ph caps into phase *A* and *B*, and a 200 kVAr reactor into phase *C*

6.3 Distributed generation

As indicated in the literature on DG in distribution systems and in subsection 1.6 of this dissertation, voltage regulation issues and the possibility of bidirectional power flows exist [82]-[86]. Contemporary research in DG has seen efforts re-

lated to power injections in distribution systems. The literature focuses on renewable DG and local storage for voltage control, peak shaving and other control options [92]-[94], [96].

The illustrations developed here explore implications of DG in the estimation of three-phase, possibly unbalanced distribution networks. In the three-phase unbalanced circuit of the RBTS for feeder F1, shown in Figure 5.1, two wind generators are placed at buses 8 and 13. These buses are at the primary of a three-phase distribution transformer at the high side rated 11 kV. Each DG unit is assumed to inject approximately 1.0 MW peak output (nameplate value) following the profile shown in Appendix G. In practice, this may be an aggregated capacity of DG. Note that present standards for interconnecting DG [45] strictly state that no active voltage regulation is allowed for non-utility controlled installations at less than 10 MW. To this point, reactive power injections for this illustration are assumed to be zero. The presence of DG in distribution systems is illustrated in examples DG1, DG2, and DG3 as shown in Table 6.3.

Table 6.3 Examples Illustrating the Presence of DG in Distribution Systems

Example	Description
DG1	Example illustrates bidirectional power flows in the distribution system. Power flows in different directions in each phase for some line segments. Power also flows into the transmission system.
DG2	This example illustrates the possible voltage rise on the distribution feeder. Based on estimator calculations, DG reactive output is altered to mitigate voltage rise.
DG3	In this illustration, energy storage (batteries) and DG are used to perform energy management and peak shaving.

Bidirectional flows with DG (Example DG1)

The illustration commences with 1.0 MW of wind DG being injected into the circuit of RBTS feeder F1 in the early morning hours (HE3). Note that at this time, DG injection is at a maximum value and load is near a minimum value (see Appendix G). As anticipated, DG injection is larger than the load so power flows into the substation node and into the distribution primary and subtransmission network.

Perhaps more interesting is the direction of power flows on branches 48-47 and 47-46 where the direction of power flowing on phases is different for each phase. Also note that at bus 47, phase *C* power flows into this bus from both buses 48 and 46 (see Fig. 6.5). The three-phase network model is needed to observe this result since positive sequence analysis may fail to explicitly display the power flow direction in individual phases.

The main feeder bus voltage profile corresponding to the loading and power flow condition as indicated in Figure 6.5 is shown in Figure 6.6. Note that there is voltage rise on all three phases at the end of the feeder (DG located at the last node on the system) and that *phase-C* voltage rises above the source voltage. If the substation voltage was 1.05 p.u. (not uncommon), safe operating voltage would be violated according to ANSI C84.1 'Range A'.

This bidirectional flow phenomenon impacts coordination of protective devices [26], regulation of voltages using step-type line voltage regulators [25], [96] and system operation with uncertain loading. Investigations where net-load seen

by the substation transformer is positive yielded expected power flow and voltage profile results; therefore, additional results are not shown here. Similarly, characteristic solar generation that ramps up during daytime hours along with load yielded conventional power flow and voltage profile results and, therefore, are not elaborated here. Note that in practice, it is also possible to have net injection at a substation when solar injections exceed loads.

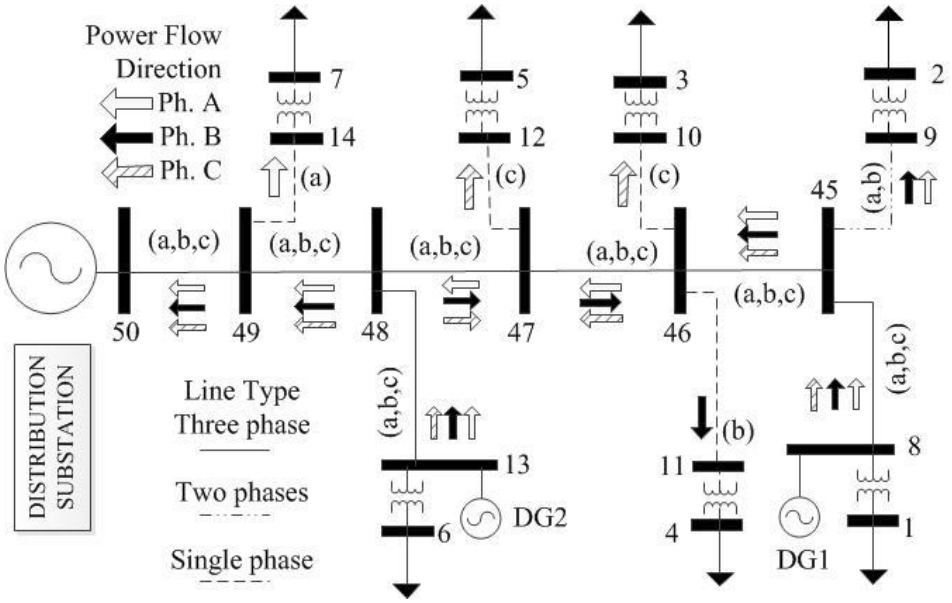

Loads / DG

Bus No.	Ph. A	Ph. B (MW)	Ph. C	Ph. A	Ph. B (MVAr)	Ph. C
1	0.09	0.10	0.10	0.03	0.03	0.02
2	0.15	0.16	0.00	0.04	0.04	0.00
3	0.00	0.00	0.10	0.00	0.00	0.04
4	0.00	0.09	0.00	0.00	0.04	0.00
5	0.00	0.00	0.12	0.00	0.00	0.03
6	0.12	0.13	0.11	0.04	0.04	0.03
7	0.10	0.00	0.00	0.03	0.00	0.00
DG1	0.33	0.33	0.33			
DG2	0.33	0.33	0.33			

Figure 6.5 One-line diagram, loads and injections for RBTS feeder F1 with DG at HE3 (Example DG1)

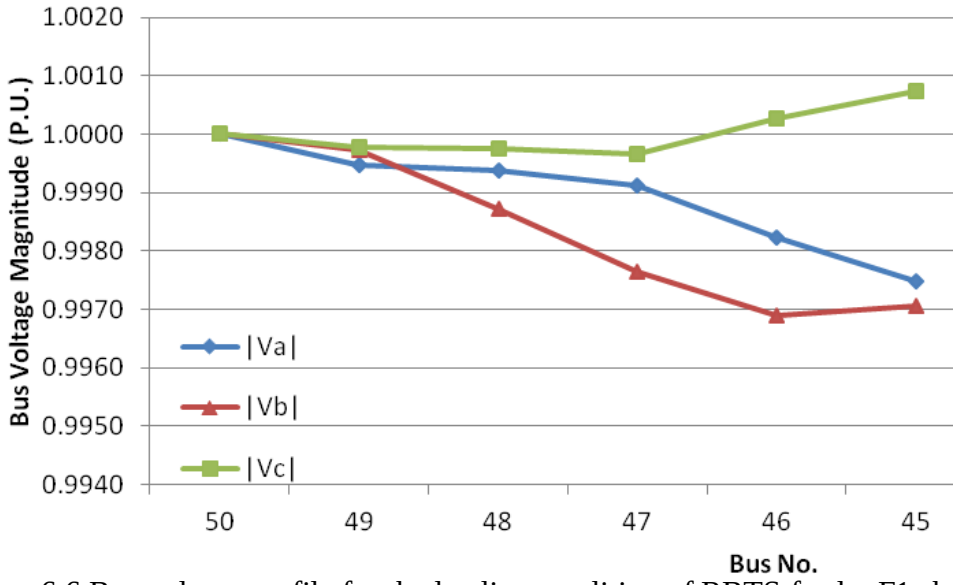

Figure 6.6 Bus voltage profile for the loading condition of RBTS feeder F1 shown in Figure 6.5 (Example DG1)

Voltage control using an estimator signal to alter DG power factor (Example DG2)

One possible application of the distribution state estimator for voltage control includes the provision of a signal to adjust distributed generator power factor to regulate local voltage. That is, estimator results may be interpreted near real-time; this information may be used as inputs to inverters (e.g., rooftop PV), or power factor control elements (e.g., capacitors) to absorb or inject reactive power as a means to counteract undesirable voltage levels. For example, the case of main feeder bus voltages shown in Figure 6.6 may favor a reactive power absorption by the DG to reduce voltage on phase *C*; although, given the bus voltage magnitudes shown they are within acceptable tolerances for both magnitude and unbalance.

For this illustration, the DG power factor is varied by changing the set-point of the unit to absorb VArs. The target value of bus 45 phase *C* voltage magnitude

is 1.0 p.u. To obtain this, reactive power is absorbed by the generator at 30 kVAr / phase and 40 kVAr / phase. The results have been plotted in Figure 6.7. Bus voltage on phase C is reduced to 1.0 p.u. when 40 kVAr / phase is absorbed by the distributed generator. This equates to a DG power factor of 0.993 leading.

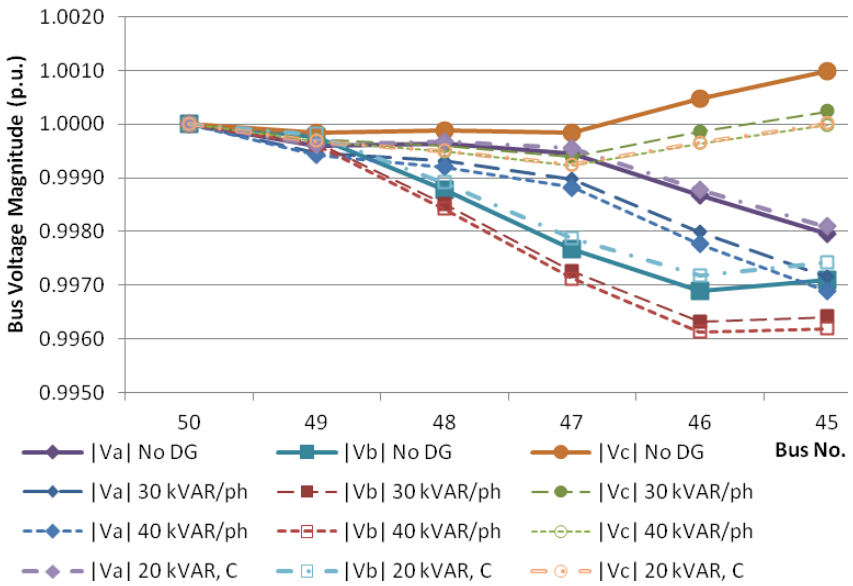

Figure 6.7 Bus voltage profile for the loading condition of RBTS feeder F1 shown in Figure 6.5 when DG power factor is changed to absorb reactive power, example DG2

Using energy storage and DG to reduce peak demand, example DG3

One possible alternative to controlling both bidirectional flows and voltage rises due to DG injections is the inclusion of energy storage elements such as flywheels, batteries or others. Energy storage elements may function as ipso facto loads on the distribution system. They typify controllable load elements since charging and discharging may be performed at desired time intervals.

Energy storage elements may be used to smooth variability due to intermittent generation, perform price arbitrage, supplement reliability efforts to keep loads

energized during short-duration outages or regulate voltages to some desired range [87], [92]-[95]. Scheduling and optimization of energy storage and DG elements is beyond the scope of the work presented here, but is elaborated in [72].

In an illustration presented here, feeder F1 of the RBTS shown in Figure 6.5 now has a 1.0 MW battery with 3 MWh of energy storage capacity (e.g., for an aggregated load). The excess DG injection is utilized to store energy locally (charging during time period 0:00 – 5:00). For this illustration, it is assumed that the battery cannot discharge below 40 %, energy storage efficiency is 85 %, and charging / discharging may occur in steps of 0.1 MW/phase. Figure 6.8 shows the load seen by the substation of RBTS feeder F1 for the base case (no DG or storage), DG only (Appendix G), and combined DG and storage.

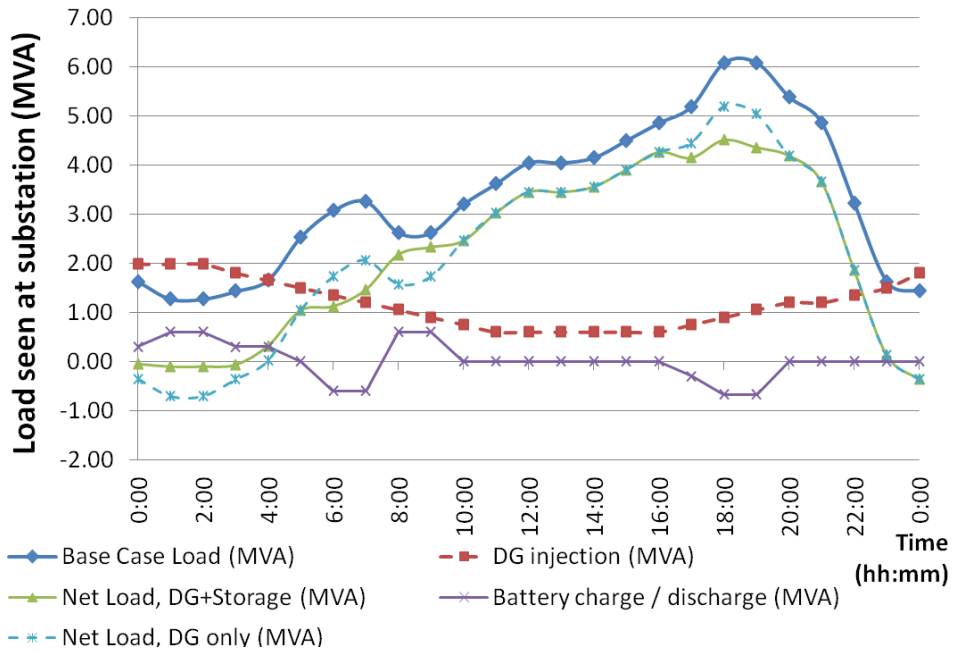

Figure 6.8 Energy storage and DG used to reduce peak load seen by the substation serving the RBTS feeder F1 (Example DG3)

Net peak load is reduced from 6.2 MW to 4.5 MW. The battery is charged in the early morning (low load), and after the morning peak. The battery discharges during morning peak and system peak. Note that voltage unbalance in these cases may be handled as indicated in section 6.2.

6.4 Large Scale Simulation System test bed (LSSS) illustration

The large scale simulation system (LSSS) test bed is described in subsection 4.4. Bus voltage magnitudes and angles for the solved power flow case for the transmission and networked subtransmission superstructure is shown in Figure 6.9. Illustrations consist of estimating all bus voltages magnitudes and angles for the entire LSSS test bed in three-phase detail.

Tables 6.3 – 6.6 present specified active and reactive power of loads installed at each load bus for the peak (HE18) load condition. Loads are presented in kW and kVAr. Missing phases are omitted from the tables. Note that data for feeder F1 are presented in previous chapters (also see Appendix F). Also note that data for the IEEE 34 bus test system are presented in [131]. Each feeder has unique characteristics and loading patterns for the purpose of analysis. Feeder F2 serves larger industrial loads at 11 kV, all three-phase, balanced. Feeder F3 has lightly loaded *B* phase. Feeder F4 has lightly loaded *A* phase. Feeder F6 has heavily loaded *A* phase and lightly loaded *C* phase.

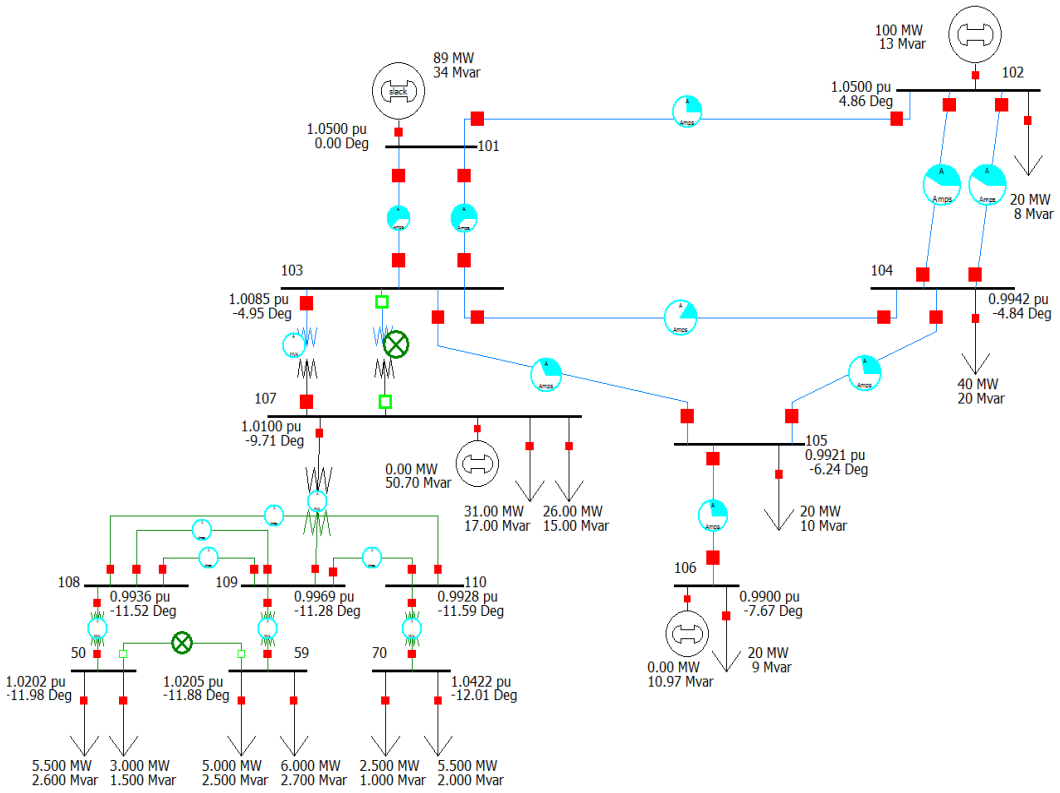

Figure 6.9 Transmission network and bus 3 distribution subtransmission network for the LSSS test bed where transmission buses are numbered from 101-107, and bus 103 is bus 3 at 138 kV as indicated in [38]

Table 6.4 Specified load on Each Phase for RBTS Feeder F2, Figure 4.3

Feeder F2	Specified load at each phase, P (kW), Q (kVAr)					
Bus No.	P_a	Q_a	P_b	Q_b	P_c	Q_c
8	345.68	175	335.51	165	335.51	160
9	335.51	160	335.51	160	345.68	165
10	335.51	165	345.68	165	335.51	170
Total	1016.70	500	1016.7	490	1016.7	495

Table 6.5 Specified load on Each Phase for RBTS Feeder F3, Figure 4.3

Feeder F3	Specified load at each phase, P (kW), Q (kVAr)					
Bus No.	P_a	Q_a	P_b	Q_b	P_c	Q_c
11	510	220	340	150		
12	510	200	255	115	85	40
13	255	115	170	80	425	225
14	277.50	125	370	175	277.50	105
15					775	350
16	182.77	100	161.88	70	177.55	90
17	174.07	93	174.07	85	174.07	90
Total	1909.34	853.00	1470.95	675.00	1914.12	900.00

Table 6.6 Specified load on Each Phase for RBTS Feeder F4, Figure 4.3

Feeder F4	Specified load at each phase, P (kW), Q (kVAr)					
Bus No.	P_a	Q_a	P_b	Q_b	P_c	Q_c
18	170	60	425	200	255	115
19	313.32	155	156.66	70	52.22	22
20					836.70	400
21			836.70	400		
22	83.67	40	251.01	115	502.02	205
23	292.85	110	259.38	110	284.48	110
24	284.48	110	276.11	100	276.11	120
Total	1144.31	475.00	2204.86	995.00	2206.53	972.00

Table 6.7 Specified load on Each Phase for RBTS Feeder F6, Figure 4.3

Feeder F6	Specified load at each phase, P (kW), Q (kVAr)					
Bus No.	P_a	Q_a	P_b	Q_b	P_c	Q_c
32	340	155	255	111	255	115
33	510	220	255	115	85	39
34	425	180	170	70	255	100
35	340	125	255	115	255	105
36	170	85	425	201	255	115
37	208.88	100	313.32	150		
38	208.88	100	313.32	150		
Total	2202.76	965.00	1986.64	912.00	1105.00	474.00

6.5 An application of distribution state estimation for demand response, energy and power management, example DR1

An application of the distribution state estimator is illustrated for demand response on the LSSS network. In DR applications, enabled loads are asked to curtail load during periods of high demand. Billinton in [38] identifies that 20 % of the RBTS loads are available for curtailment. In practice, it may be difficult to determine exact curtailment and response to commands. The utility must ensure that curtailing load does not exacerbate voltage unbalance or increase flows in heavily loaded branches.

Example DR1

The subsequent illustration presents the application of the estimator in a network with DR. Each load is assumed able to curtail up to 20 %. However, actual load curtailment may vary significantly. In the illustration, loads may curtail between 5.0 - 20.0 %. The exact value of load curtailment at non-measured buses is not known, but will be estimated. Demands at each load bus for the pre-DR case (base case) are presented in Table 6.4 - Table 6.7. The reduced load at each feeder is shown in Table 6.8 - Table 6.11. The estimator is used to calculate injections / loads and voltage profiles. Power flow at the substation is assumed to be measured; however, where substation flows are not measured, these flows may be calculated.

Table 6.8 Load Curtailed for RBTS Feeder F2, Figure 4.3, Example DR 1

Feeder F2	Percentage load remaining after curtailment at each phase (%), and substation load (MW) example DR1						Metered bus
Bus No.	P_a	P_b	P_c	Q_a	Q_b	Q_c	
8	80.87	91.58	80.63	80.87	91.58	80.63	Y
9	89.87	88.26	83.50	89.87	88.26	83.50	Y
10	88.97	92.42	85.01	88.97	92.42	85.01	Y
Substation	0.882	0.925	0.845	0.437	0.449	0.415	

Table 6.9 Load Curtailed for RBTS Feeder F3, Figure 4.3, Example DR 1

Feeder F3	Percentage load remaining after curtailment at each phase (%), and substation load (MW) example DR1						Metered bus
Bus No.	P_a	P_b	P_c	Q_a	Q_b	Q_c	
11	80.87	91.58		80.87	91.58		Y
12	89.87	88.26	83.50	89.87	88.26	83.50	N
13	88.97	92.42	85.01	88.97	92.42	85.01	N
14	90.39	80.47	93.04	90.39	80.47	93.04	N
15			89.66			89.66	Y
16	90.71	94.26	94.78	90.71	83.67	94.78	Y
17	89.09	83.67	90.68	89.09	83.67	90.68	Y
Substation	1.689	1.296	1.764	0.843	0.621	0.910	

Table 6.10 Load Curtailed for RBTS Feeder F4, Figure 4.3, Example DR 1

Feeder F4	Percentage load remaining after curtailment at each phase (%), and substation load (MW) example DR1						Metered bus
Bus No.	P_a	P_b	P_c	Q_a	Q_b	Q_c	
18	80.87	91.58	80.63	80.87	91.58	80.63	Y
19	89.87	88.26	83.50	89.87	88.26	83.50	Y
20			85.01			85.01	N
21			93.04			93.04	N
22	88.83	89.66	93.57	88.83	89.66	93.57	Y
23	90.71	94.26	94.78	90.71	94.26	94.78	Y
24	89.09	83.67	90.68	89.09	83.67	90.68	Y
Substation	1.017	1.950	1.943	0.433	0.951	0.972	

Table 6.11 Load Curtailed for RBTS Feeder F6, Figure 4.3, Example DR 1

Feeder F6	Percentage load remaining after curtailment at each phase (%), and substation load (MW) example DR1						Metered bus
Bus No.	P_a	P_b	P_c	Q_a	Q_b	Q_c	
32	80.87	91.58	80.63	80.87	91.58	80.63	Y
33	89.87	88.26	83.50	89.87	88.26	83.50	N
34	88.97	92.42	85.01	88.97	92.42	85.01	Y
35	90.39	80.47	93.04	90.39	80.47	93.04	N
36	88.83	89.66	93.57	88.83	89.66	93.57	N
37	90.71	94.26		90.71	94.26		Y
38	89.09	83.67		89.09	83.67		Y
Substation	1.982	1.756	0.972	0.947	0.862	0.428	

Example DR1 results

Voltage profiles for the main feeders F2, F3, F4 and F6 before and after DR loads are curtailed are presented in Figure 6.10 - Figure 6.13. Note that pre-DR loading is at HE18 (peak loading). Demand values for the unbalanced three-phase distribution feeders (represented as proxy buses) are shown in the LSSS in Figure 6.9. The unbalanced networks are solved using ladder-iterative techniques to obtain ideal theoretical solutions to each radial feeder. The estimator then provides estimates based on measurements. The source bus voltage for each radial

feeder is identified from Figure 6.9. Note that profiles for feeder F1 are presented in previous sections. Post curtailment ideal and estimated loads are presented in Table 6.12 - Table 6.15. The transmission network of the RBTS is re-solved after load curtailment. The reduced load at bus 3 causes a substation bus voltage rise.

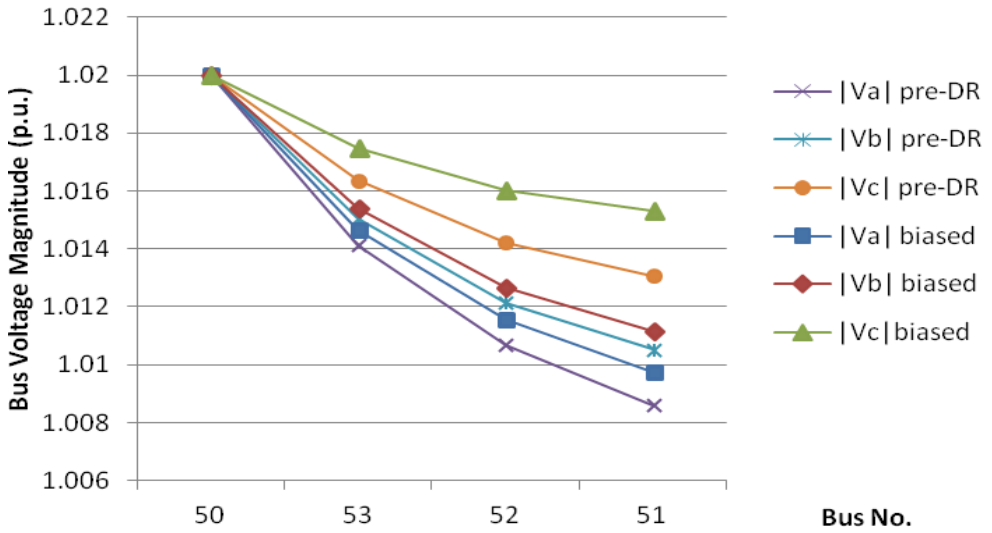

Figure 6.10 Bus voltage magnitudes before and after DR at HE18 on main feeder buses for RBTS feeder F2, example DR1

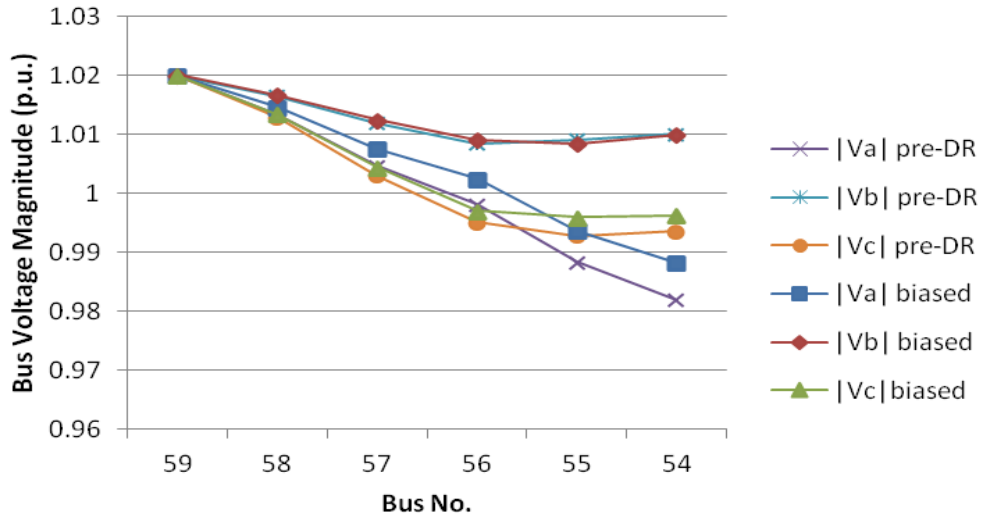

Figure 6.11 Bus voltage magnitudes before and after DR at HE18 on main feeder buses for RBTS feeder F3, example DR1

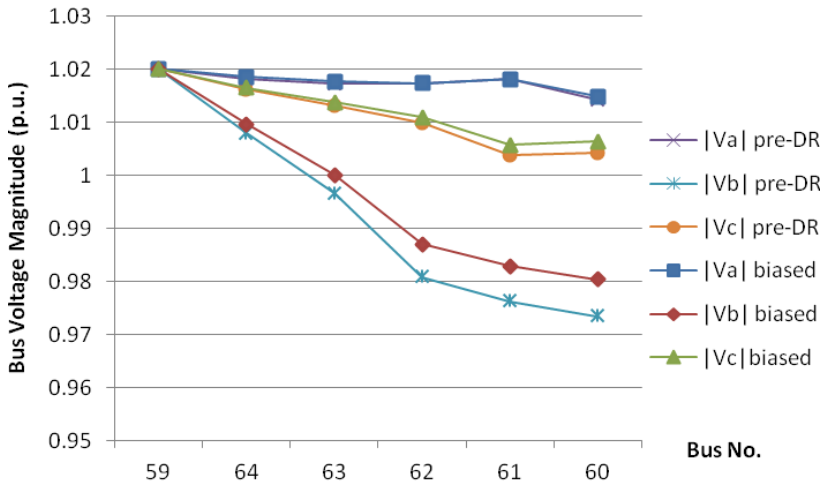

Figure 6.12 Bus voltage magnitudes before and after DR at HE18 on main feeder buses for RBTS feeder F4

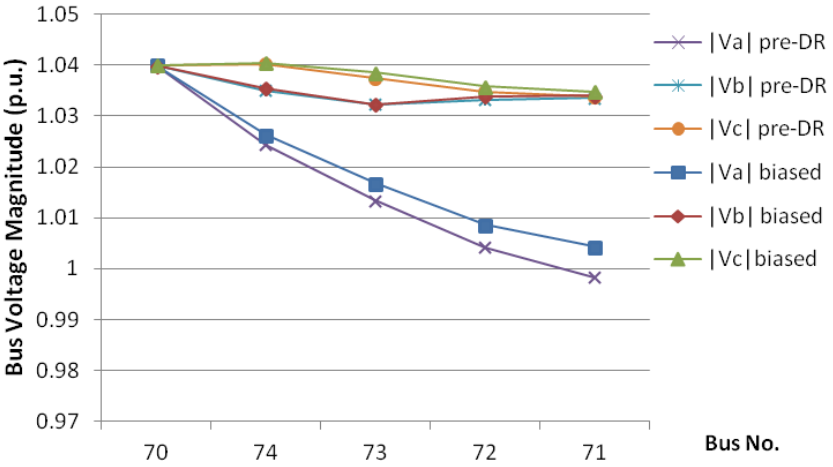

Figure 6.13 Bus voltage magnitudes before and after DR at HE18 on main feeder buses for RBTS feeder F6

Table 6.12 Ideal and Estimated Post-Curtailment Loads, Feeder F2, Example DR1

Bus	P_a	P_b	P_c	Q_a	Q_b	Q_c
	Post-curtailment loads, ideal (MW, MVAr)					
8	0.280	0.307	0.271	0.142	0.151	0.129
9	0.302	0.296	0.289	0.144	0.141	0.138
10	0.299	0.319	0.285	0.147	0.152	0.145
	Post-curtailment loads, estimated (MW, MVAr)					
8	0.281	0.309	0.271	0.146	0.155	0.132
9	0.303	0.298	0.289	0.147	0.144	0.141
10	0.300	0.321	0.285	0.149	0.155	0.147

Table 6.13 Ideal and Estimated Post-Curtailment Loads, Feeder F3, Example DR1

Bus	P_a	P_b	P_c	Q_a	Q_b	Q_c
	Post-curtailment loads, ideal (MW, MVAr)					
11	0.412	0.311		0.178	0.137	
12	0.458	0.225	0.071	0.180	0.101	0.033
13	0.227	0.157	0.361	0.102	0.074	0.191
14	0.251	0.298	0.258	0.113	0.141	0.098
15			0.725			0.327
16	0.166	0.153	0.168	0.091	0.066	0.085
17	0.155	0.146	0.158	0.083	0.071	0.082
	Post-curtailment loads, estimated (MW, MVAr)					
11	0.419	0.312		0.208	0.147	
12	0.466	0.226	0.072	0.214	0.108	0.036
13	0.229	0.158	0.366	0.115	0.077	0.210
14	0.252	0.301	0.262	0.124	0.148	0.108
15			0.736			0.379
16	0.166	0.154	0.170	0.096	0.068	0.090
17	0.155	0.146	0.158	0.085	0.072	0.084

Table 6.14 Ideal and Estimated Post-Curtailment Loads, Feeder F4, Example DR1

Bus	P_a	P_b	P_c	Q_a	Q_b	Q_c
	Post-curtailment loads, ideal (MW, MVAr)					
18	0.137	0.389	0.206	0.049	0.183	0.093
19	0.282	0.138	0.044	0.139	0.062	0.018
20			0.711			0.340
21		0.673			0.322	
22	0.074	0.225	0.470	0.036	0.103	0.192
23	0.266	0.244	0.270	0.100	0.104	0.104
24	0.253	0.231	0.250	0.098	0.084	0.109
	Post-curtailment loads, estimated (MW, MVAr)					
18	0.138	0.403	0.204	0.049	0.205	0.104
19	0.283	0.143	0.043	0.144	0.068	0.020
20			0.708			0.400
21		0.694			0.366	
22	0.075	0.232	0.468	0.036	0.112	0.219
23	0.266	0.249	0.269	0.103	0.110	0.113
24	0.254	0.234	0.250	0.101	0.088	0.114

Table 6.15 Ideal and Estimated Post-Curtailment Loads, Feeder F6, Example DR1

Bus	P_a	P_b	P_c	Q_a	Q_b	Q_c
	Post-curtailment loads, ideal (MW, MVAr)					
32	0.275	0.234	0.206	0.125	0.102	0.093
33	0.458	0.225	0.071	0.198	0.101	0.033
34	0.378	0.157	0.217	0.160	0.065	0.085
35	0.307	0.205	0.237	0.113	0.093	0.098
36	0.151	0.381	0.239	0.076	0.180	0.108
37	0.189	0.295		0.092	0.145	
38	0.186	0.262		0.089	0.126	
	Post-curtailment loads, estimated (MW, MVAr)					
32	0.281	0.232	0.207	0.142	0.109	0.095
33	0.469	0.224	0.071	0.229	0.109	0.033
34	0.386	0.157	0.218	0.182	0.069	0.088
35	0.312	0.205	0.238	0.125	0.098	0.101
36	0.153	0.381	0.239	0.081	0.194	0.111
37	0.192	0.295		0.095	0.149	
38	0.188	0.262		0.093	0.132	

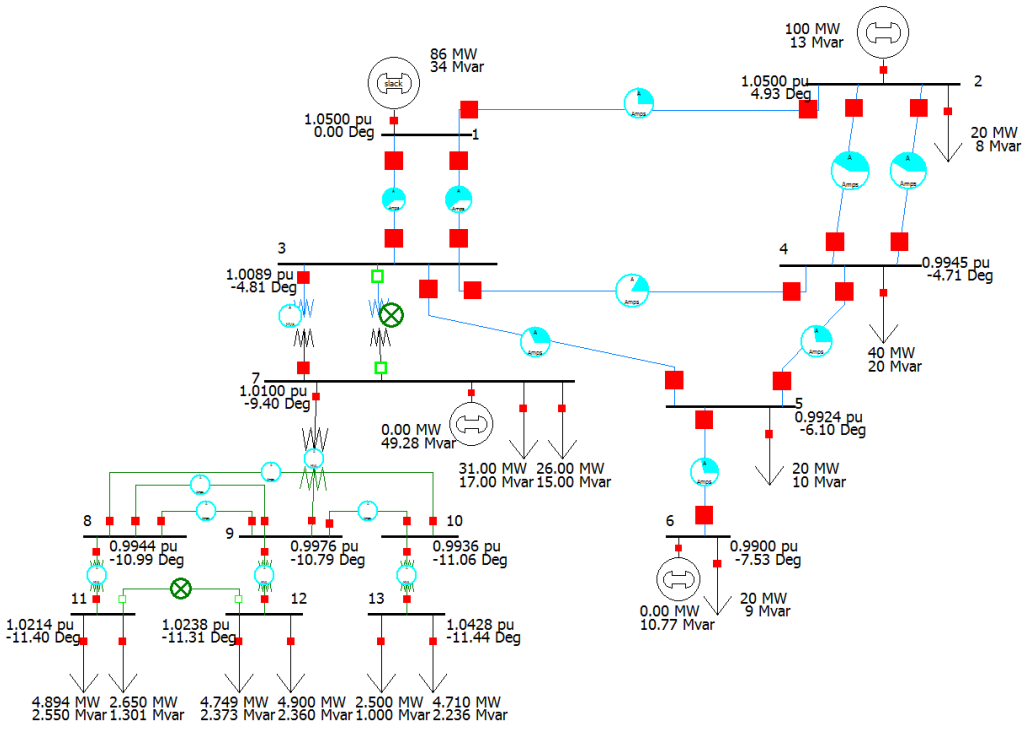

Figure 6.14 Solving the RBTS transmission network after DR load curtailment

6.6 Discussion of results

Discussion of voltage unbalance studies, examples VU1-VU6

An example was presented that studies the problem of voltage unbalance, and potential mitigation measures that may be required in a utility system. The combination of capacitor / reactor switching was used to control voltage magnitudes and reduce unbalance. The capacitor switching into the circuit reduces the need for reactive power from the source and concomitantly boosts bus voltage magnitude. However, results showed that conventional switching of three-phases of the cap bank would not help the under voltage issue, but would not combat unbalance. Single phase control of the capacitor bank in example *VU*3 provides the best overall impact on both reducing voltage unbalance and increasing magnitudes.

Examples shown are intended to illustrate new applications of static VAr systems in distribution systems. That is, mitigation measures to voltage unbalance issues using single-phase switching of shunt reactive elements may be required in smart distribution systems, examples of this are shown.

Discussion of DG and storage results, examples DG1-DG3

Smart distribution systems may benefit from higher penetration of DG, DER, storage technology or PHEV technologies. These technologies may provide ancillary voltage balancing as part of normal operations. Example DG1 illustrates the potential impacts of bidirectional flows in a distribution feeder. Power flow may be in different directions in each phase, and may flow towards the transmission system. This is a significant departure from conventional distribution system

operations. Implications for protection, coordination and energy management exist but are not elaborated here. The distribution system state estimator may be used as a tool to alert operators to these issues as they occur, and to capture operating state before / during events.

Example DG2 illustrates the use of DG in conjunction with estimator created signals to regulate feeder bus voltages. Illustration DG3 explores implications of energy storage, load balancing and peak shaving in the Smart Grid environment. The estimator may be utilized as a tool to assist operators in scheduling storage, energy management, and simultaneously maintaining adequate voltage profiles.

Discussion of LSSS illustration example DR1

The illustration of demand response load curtailment shows a potential application of the distribution state estimator. Loads are randomly reduced between 5.0 – 20.0 %. Note that not all loads are measured. The state estimator is then used to calculate bus voltage magnitudes on the feeder, and obtain estimates of individual loads, both measured and not measured. The estimator provides good estimates of loads after curtailment. The calculations and estimates are all done in three-phase detail.

Note the weakness in the analysis method used here: load curtailment in the distribution system produces changes in the transmission (LSSS) network voltage profile. However, in the foregoing analysis, the bus voltage magnitude at the substation is held constant. As shown in Figure 6.14, the bus voltage at the substation may change when loads are curtailed.

7. Conclusions, recommendations and future work

7.1 Contributions and concluding remarks

Distribution level focus areas of the Smart Grid initiative include: distribution automation (DA), DMS system integration; increased operator control, and expansion of customer owned DG. System integrity, reliability, fault tolerance and safety to consumers must be maintained. Future distribution systems may incorporate responsive loads, networking and more measurement devices – each of these items are illustrated in this dissertation. To maximize the use of existing assets and mitigate the need to expand large-generation portfolios, utilities and ISOs may continue to extend their reach into distribution circuits. Monitoring and estimation of system changes become an important function in this environment. DMS and distribution class state estimators may become a valuable tool in future distribution infrastructure.

The unique characteristics of the distribution system necessitate different tools for analysis when compared to transmission systems. Unique characteristics of distribution networks are discussed in Chapter 1. The Smart Grid initiative items discussed in the previous paragraph increase the complexity of distribution system modeling and analysis. Thus, enhanced tools for modeling, simulation and analysis are required. The distribution system state estimator is seen as one such tool to be used in near the real-time analysis applications.

This dissertation presents the formulation of a linear state estimation algorithm for distribution feeders. The estimator uses a weighted least squares formu-

lation and is developed in full three-phase detail. Reliance on measured data (i.e. widely deployed smart meters) allows a non-iterative solution procedure. Main and secondary contributions of this work are summarized in Table 7.1.

Table 7.1 Contributions of this research

Category	Contribution
Reliability and restoration enhancement	• Algorithms are developed and illustrated. • These algorithms present practical methods to study reliability in future distribution systems. • Networking and rapid restoration are known to improve reliability; methods such as the system status table and related algorithms present a framework around which these may be implemented
Distribution system state estimation	• The formulation of a linear, three-phase distribution system state estimator is presented. Practical considerations such as high *r/x* ratios, laterals and unbalanced loads are included. • Noting the measurement infrastructure likely in future distribution systems, the estimator utilizes available data to calculate system state – even where no measurement data is available. • Pseudo-measurement data, historical loads and conventional measurements and synchrophasors are utilized in the estimation formulation; these are all likely in practical systems of the future. • The estimator performance is illustrated, along with applications to voltage control, DG, and storage.
Implications of the Smart Grid initiative on the future distribution infrastructure	• While details of the future infrastructure remain uncertain, trends toward increased measurement availability are clear. The work in this dissertation supports an advanced metering infrastructure. • DG installations include a range of technologies not detailed here. The application and utilization of these technologies are enhanced by distribution state estimation. • Protection and coordination is identified as a major area of concern when operating principles change. Protection is likely to become more complex, but real-time monitoring of conditions may facilitate more complex networks.

7.2 General recommendations

Examples and illustrations presented in this dissertation are summarized here, and general recommendations are made subsequently. Chapter 4 illustrates various algorithms for distribution system reliability and restoration enhancement

through automation and switching. Chapter 5 illustrates the distribution system state estimation algorithm formulation and performance. Chapter 6 investigates voltage unbalance, mitigation options using shunt reactive elements, implications of DG in the distribution system, and a sample of a large scale test system. The illustrations presented throughout this report highlight various aspects of the estimator formulation, performance and applications. Illustrations include:

- Three-phase estimator formulation and performance
- Inclusion of the characteristics of distribution systems in modeling, analysis and distribution system state estimation (e.g., high *r/x* ratio, unbalance, single phase laterals)
- Estimator performance in the presence of noisy measurement data
- Biased estimation to improve accuracy for the examples presented
- Bad data detection on the system being studied
- Applications in voltage control and mitigation of voltage unbalance
- Applications in distributed generation including bidirectional flows
- DG and voltage regulation based on estimator inputs
- Applications for distributed resources, storage, energy management, and peak shaving
- Demand response and load curtailment in the LSSS network.

Table 7.2 Discussion and Observations of Illustrations Presented

Illustration topic	Details / results	Observations / conclusion
Reliability enhancement	• Switching automation demonstrated on RYG, RBTS test beds • RYG: adding 4 interrupting devices may reduce *E(U)* by 50% • RBTS: 14% reduction in *E(U)* • RBTS: 7% reduction in SAIDI	• Automation resulted in significant reliability improvements • Further improvements may be achieved via networking, adding DG or storage
Unbiased three-phase distribution system state estimation – Example SE3	• A state estimator algorithm for 3ϕ distribution was developed • The estimator is demonstrated on a radial 3ϕ RBTS feeder, F1, on transmission bus 3 • The algorithm runs in substation computer DMS for monitoring, control and to alert operators • Bus voltage magnitudes are well estimated with highly uncertain load data in examples shown	• Distribution circuit loading is highly uncertain • Measurement redundancy may significantly increase estimator accuracy • Bus voltage magnitudes and line currents are well estimated
Biased three-phase distribution system state estimation	• Examples SE2, SE3a are recreated with biased measurements • Resulting estimates are approximately 85% more accurate than unbiased estimates for examples shown here • Variance of calculated, linearized currents may be approximated	• Weighting measurements may provide better angle and line current estimates • Weights may be assigned in various ways • Heuristically, selecting the largest % uncertainty as a variance is appropriate
Voltage unbalance	• Voltage unbalance is observed for heavy load cases • Methods to mitigate voltage unbalance include single phase switching of shunt capacitor / reactor (VAr) devices • The preferred result is obtained by switching in 2 phases of a capacitor bank (VU3)	• Unbalanced loads / laterals, and mutual coupling of untransposed lines causes voltage unbalance • Estimator based control options are calculated • Single phase control of shunt devices may provide a finer detail of control
Distributed generation (DG) and storage	• Voltage rise and bidirectional flows are illustrated with DGs • Estimator created signals are used to adjust DG VAr output to regulate bus voltages • Storage/energy management are used to reduce peak load	• Near real-time monitoring allows greater control of available DG and storage resources as illustrated

7.3 Future work

The three-phase distribution estimator formulation presented here will accommodate networked feeders. Networked distribution primary feeders may become more prevalent in future distribution systems. In other applications, networked distribution *secondaries* may also be used. Effects of networking on loss reduction and voltage regulation may be explored further as future work. A potential application of the estimator may be selective networking to alter voltage profiles, control power flows or reduce losses. The protection and coordination of protective devices are an important consideration for the future distribution infrastructure, especially where selective networking and DG is concerned.

Perhaps the most significant future work involves the modeling and simulation of systems that incorporate both transmission and distribution networks. For example, analysis methods capable of solving transmission networks as positive sequence networks with distribution sub-systems as three-phase detailed networks may be of interest in the future power system infrastructure. This concept may have applications in networks with DG, storage or controllable elements, and where power-marketing concepts such as the LMP may be extended into the distribution system model.

As a final remark, an important element of future work surely includes actual implementation in a functioning distribution system.

REFERENCES

[1] 110th Congress of United States, "Smart Grid," Title XIII, Energy Independence and Security Act of 2007, Washington DC, December 2007.

[2] Office of Electric Transmission and Distribution, United States Department of Energy, "Grid 2030: A National Vision for Electricity's Second 100 Years," Washington DC, April 2003.

[3] Office of Electricity Delivery and Energy Reliability, United States Department of Energy, "The Smart Grid – An Introduction," Washington DC, 2008 [Available online]: http://www.oe.energy.gov/DocumentsandMedia/DOE_SG_Book_Single_Pages.pdf.

[4] Office of Electricity Delivery and Energy Reliability, United States Department of Energy, "What the Smart Grid Means to You (Utilities) and the People You Serve," Washington DC, 2009, [Available online]: http://www.oe.energy.gov/DocumentsandMedia/Utilities.pdf.

[5] Office of Electricity Delivery and Energy Reliability, United States Department of Energy, "What the Smart Grid Means To You (Technology Providers) And The People You Serve," Washington DC, 2009, [Available online]: http://www.oe.energy.gov/DocumentsandMedia/Technology Providers.pdf.

[6] United States Department of Energy, "Smart Grid System Report," Washington DC, July 2009 [Available online]: http://www.oe.energy.gov/DocumentsandMedia/SGSRMain_090707_lowres.pdf

[7] B. R. Sathyanarayanan, G. T. Heydt, M. Crow, F. Meng, "Test Bed Evaluation of Future Power Distribution Systems with Renewable Resources," North American Power Symposium (NAPS), Starkville, MS 2009, pp. 1-8.

[8] A. Q. Huang, M. L. Crow, G. T. Heydt, J. P. Zheng, S. J. Dale, "The Future Renewable Electric Energy Delivery and Management (FREEDM) system: the Energy Internet," Proceedings of the IEEE, v. 99, no. 1, January 2011, pp. 1-16.

[9] F. I. Denny, D. E. Dismukes, *Power System Operations and Electricity Markets*, CRC Press, New York, NY, 2002.

[10] M. Ilic, F. Galiana, L. Fink, *Power Systems Restructuring – Engineering and Economics*, Kluwer Academic Publishers, Massachusetts, 1998.

[11] Y. Song, X. Wang, *Operation of Market-oriented Power Systems*, Springer, New York, 2003.

[12] M. Kezunovic, G. T. Heydt, C. DeMarco, T. Mount, "Is Teamwork the Smart Solution?," IEEE Power and Energy Magazine, v. 7, No. 2, March, 2009 pp. 69 -78.

[13] Z. Alaywan, "Impact of Deregulation on System Operation in California," CIGRE/IEEE Power Engineering Society International Symposium, 2005, pp. 24-30.

[14] R. L. Chen, S. Sabir, "The Benefits of Implementing Distribution Automation and System Monitoring in the Open Electricity Market," Proceeding of the IEEE Canadian Conference on Electrical and Computer Engineering, v. 2, Toronto, 2001, pp. 825-830.

[15] V. Vittal, "Consequence and Impact of Electric Utility Industry Restructuring on Transient Stability and Small-Signal Stability Analysis," Proceedings IEEE, v. 88, no. 2, February 2000, pp. 196 – 207.

[16] American Wind Energy Association, "Renewable Portfolio Standards," [Available Online:] http://www.awea.org/policy/renewables_portfolio_standard.html.

[17] U.S. Department of Energy, Database of State Incentives for Renewables and Efficiency, [Available online]: www.dsireusa.org]

[18] U.S. Environmental Protection Agency, Renewable Portfolio Standards, [Available online]: http://www.epa.gov/chp/state-policy/renewable.html

[19] U.S. Energy Information Administration, *Annual Energy Review 2009*, August 19, 2010 [Available online]: http://www.eia.gov/electricity

[20] U.S. Energy Information Administration, *Annual Energy Outlook 2011*, April 26, 2011 [Available online]: http://www.eia.gov/electricity

[21] California State Senate Bills 1078, and 107, *California Renewables Portfolio Standard* [Available online]: http://www.cpuc.ca.gov/PUC/energy/Renewables

[22] "Solar statistics for the state of California," [Available online]: http://www.californiasolarstatistics.ca.gov/reports/agency_stats/

[23] A. Walsh, T. Fallon, "ESB Networks Smart Grid Demonstration Pilot," IEEE General Meeting, Detroit, MI, July 2011

[24] J. A. Momoh, Electric Power Distribution, Automation, Protection and Control, CRC Press, New York, NY, 2008.

[25] W. H. Kersting, Distribution System Modeling and Analysis, CRC Press, New York, NY, 2007.

[26] J. Burke, *Power Distribution Engineering – Fundamentals and Applications*, New York, NY: Marcel Dekker, 1994.

[27] H. L. Willis, *Power Distribution Planning Reference Book*, Marcel Dekker, New York, NY, 1997.

[28] J. D. Glover, M. S. Sarma, T. Overbye, *Power System Analysis* and Design, 4th ed., Thomson Learning, 2008.

[29] R. Allan, R. Billinton, *Reliability Evaluation of Power Systems*, 2nd ed., Springer, 1996.

[30] R. Billinton, R. Ringlee, A. Wood, *Power System Reliability Calculations*, MIT Press, Cambridge, MA, 1973.

[31] R. Brown, *Electric Power Distribution Reliability*, New York, NY: Marcel Dekker, 2002.

[32] R. P. Fanning, "Implementation of Networked Primary and Secondary Distribution Systems for U.S. Utilities," Proceedings IEEE Power Engineering Society General Meeting, July 2003, vol. 4, pp. 2425 – 2429.

[33] R. E. Brown, "Network Reconfiguration for Improving Reliability in Distribution Systems," in Proceedings 2003 IEEE PES General Meeting, Toronto, Canada, July 2003.

[34] W. Steeley, C. Perry, M. Vaziri, "Interconnection of Distributed Energy Resources in Secondary Distribution Network Systems," EPRI white paper 1012922, Technical Update, Palo Alto, CA, December 2005.

[35] G. Heydt, "Improving Distribution Reliability (the N9 problem) by the Addition of Primary Feeders," IEEE Transactions on Power Delivery, v. 19, No. 1, Jan. 2004, pp. 434-435.

[36] G. T. Heydt, *Electric Power Quality*, 2nd ed., Stars in a Circle Publications, Scottsdale, AZ, 1991.

[37] R. Billinton, S. Kumar, N. Chowdhury, K. Chu, K. Debnath, L. Goel, E. Khan, P. Kos, G. Nourbakhsh, J. Oteng-Odjei, "A Reliability Test System for Educational Purposes – Basic Data," IEEE Transactions on Power Systems, v. 4, No. 3, August 1989, pp. 1238 -1244.

[38] R. Billinton, S. Jonnavithalu, "A Test System for Teaching Overall Power System Reliability Assessment," IEEE Transactions on Power Delivery, v. 11, No. 4, November 1996, pp. 1670 – 1676.

[39] R. Billinton, *Reliability Assessment of Electrical Power Systems Using Monte Carlo Methods*, Plenum Publishers, New York, 1994.

[40] R. Billinton, W. Wangdee, "Delivery Point Reliability Indices of a Bulk Electric System Using Sequential Monte Carlo Simulation," IEEE Transactions on Power Delivery, vol. 21, no. 1, January, 2006, pp. 345-352.

[41] V. Werner, D. Hall, R. Robinson, C. Warren, "Collecting and Categorizing Information Related to Electric Power Distribution Interruption Events: Data Consistency and Categorization for Benchmarking Surveys," IEEE Transactions on Power Delivery, v. 21, No. 1, January 2006, pp. 480 – 483.

[42] A. J. Wood, B. F. Wollenberg, *Power Generation Operation and Control*, 2nd ed., John Wiley & Sons, 2007.

[43] B. Stott, "Fast Decoupled Load Flow," IEEE Transactions PAS, v. PAS 91, September-October, 1972, pp. 1955–1959.

[44] G. Heydt, *Computer Analysis Methods for Power Systems*, 2nd ed., Stars in a Circle Publications, Scottsdale, AZ, 1996.

[45] IEEE Standard 1547, *Standard for Interconnecting Distributed Resources with Electric Power Systems*, Piscataway, NJ, 2009.

[46] I. Roytelman, S. M. Shahidehpour, "State Estimation for Electric Power Distribution Systems in Quasi Real-Time Conditions," IEEE Transactions on Power Delivery, vol. 8, no. 4, October, 1993, pp. 2009-2015.

[47] M. E. Baran, A. W. Kelley, "State Estimation for Real-Time Monitoring of Distribution Systems," IEEE Transactions on Power Systems, v. 9, no. 3, August 1994, pp. 1601–1609.

[48] M. E. Baran, A. W. Kelley, "A Branch-Current Based State Estimation Method for Distribution Systems," IEEE Transactions on Power Systems, v. 10, no. 1, February 1995, pp. 483–491.

[49] C. N. Lu, J. H. Teng, W. E. Liu, "Distribution System State Estimation," IEEE Transactions on Power Systems, v. 10, no. 1, February 1995, pp. 229–240.

[50] A. P. S. Meliopoulos, F. Zhang, "Multiphase Power Flow and State Estimation for Power Distribution Systems," IEEE Transactions on Power Systems, v. 11, no. 2, May 1996, pp. 939–946.

[51] J. Wan, K. Miu, "Weighted Least Squares Method for Load Estimation in Distribution Networks," IEEE Transactions on Power Systems, v. 18, no. 4, November 2003, pp. 1338–1345.

[52] R. Singh, B. C. Pal, R. A. Jabr, "Choice of Estimator for Distribution System State Estimation," IET Generation, Transmission and Distribution, v. 3, no. 7, 2009, pp. 666–678.

[53] E. Manitsas, R. Singh, B. Pal, G. Strbac, "Modeling of Pseudo-Measurements for Distribution System State Estimation," Proceedings IET CIRED Smart Grids for Distribution, Frankfurt, 2008, pp. 1–4.

[54] R. Hoffman, "Practical State Estimation for Electric Distribution Networks," IEEE PES Power Systems Conference and Expositions, October, 2006, pp. 510-517.

[55] M. Powalko, K. Rudion, P. Komarnicki, J. Blumschein, "Observability of the Distribution System," CIRED International Conference on Electricity Distribution, June 2009, pp. 8-11.

[56] M. E. Baran, J. Jung, T. McDermott, "Topology Error Identification Using Branch Current State Estimation for Distribution Systems," Transmission and Distribution Conference and Exposition, Asia and Pacific, October, 2009, pp. 1-4.

[57] A. Abur, H. Singh, H. Liu, W. N. Klingensmith, "Three Phase Power Flow for Distribution Systems with Dispersed Generation," 14th PSCC, Sevilla, June 2002, Session 11, Paper 3, pp. 1-7.

[58] T. Gonen, Electric Power Distrbution System Engineering, 2nd ed., CRC Press, Boca Raton, FL, 2007.

[59] M. W. Davis, R Broadwater, J. Hambrick, "Modeling and Testing of Unbalanced Loading and Voltage Regulation," NREL report number NREL/SR-581-41805, July, 2007.

[60] P. Pillay, P. Hofmann, M. Manyage, "Derating of Induction Motors Operating With a Combination of Unbalanced Voltages and Over or

Undervoltages," IEEE Transactions of Energy Conversion, v. 17, no. 4, December 2002, pp. 485-491.

[61] P. Pillay, M. Manyage, "Definitions of Voltage Unbalance," IEEE Power Engineering Review, May 2001, pp. 50-51.

[62] Pacific Gas and Electric, "Voltage Unbalance and Motors," October, 2009.

[63] Motors and Generators, National Electrical Manufacturers Association (NEMA) Publication No. MG 1-1998.

[64] J. Eto, K. LaCommare, "Tracking the Reliability of the U.S. Electric Power System: An Assessment of Publicly Available Information Reported to State Public Utility Commissions," LBNL Report LBNL-1092E, October 2008. [Available online]: http://certs.lbl.gov/pdf/lbnl1092e-puc-reliability-data.pdf

[65] Consortium for Electric Reliability Technology Solutions, "Microgrid Concept," [Available online]: http://certs.lbl.gov/certs-der-micro.html

[66] S. Chowdhury, S. P. Chowdhury, P. Crossley, *Microgrids and Active Distribution Networks*, Institution of Engineering and Technology: Renewable Energy Series, 2009.

[67] M. Shahidehpour, "Role of Smart Microgrid in a Perfect Power system," IEEE PES General Meeting, Minneapolis, MN, July, 2010, pp. 1.

[68] J. Northcote-Green, R. G. Wilson, *Control and Automation of Electrical Power Distribution Systems*, CRC Press, Boca Raton, FL, 2006.

[69] Singh, N.; Kliokys, E.; Feldmann, H.; Kussel, R.; Chrustowski, R.; Joborowicz, C., "Power system modelling and analysis in a mixed energy management and distribution management system," IEEE Transactions on Power Systems, v. 13, no.3, Aug. 1998, pp. 1143-1149.

[70] Open Systems International (OSI), "Distribution Management Systems," [Available online]: http://www.osii.com/solutions/products/distribution-management.asp

[71] Operation Technology, Inc. (OTI) – Electrical Transient Analyzer Program (ETAP), "Real-Time Distribution Management System," [Available online]: etap.com.

[72] B. S. Sathyanarayana, "A Roadmap for Distribution Energy Management via Multiobjective Optimization," Proceedings IEEE General Meeting, July, 2010.

[73] S. Mak, "Smart Meters Serving As Synchro-Sensors For Smart Distribution Grid Applications," IEEE PES General Meeting, Detroit, MI, 2011.

[74] D. Wight, et al., "Assessment of Demand Response and Advanced Metering – Staff Report," U.S. Federal Energy Regulatory Commission, February 2011.

[75] K. Lindsey, "Practical Aspects of Using Line Sensors in the Field," Proceedings IEEE General Meeting, Minneapolis, MN, July 2010.

[76] K. Lindsey, "Practical Aspects of Using Line Sensors In the Field," Proceedings IEEE PES General Meeting, Detroit, MI, July, 2011.

[77] D. Carty, M. Atanacio, "PMUs and Their Potential Impact on Real-time Control Center Operations," Proceedings IEEE General Meeting, Minneapolis, MN, July 2010.

[78] G. T. Heydt, S. Bhatt, "Present and Future Trends and Needs in Electric Power Quality Sensors and Instrumentation," Journal of Electric Machines and Power Systems, v. 27, No. 7, July, 1999, pp. 691-700.

[79] T. J. Browne, J. W. Stahlhut, G. T. Heydt, W. T. Jewell, R. Bezawada, "Innovative and Massively Deployed Sensors in Electric Power Systems," IEEE PES General Meeting, July 2008, pp. 1-6.

[80] "Solar PV Interconnection Guidelines, Maps and Requirements," [Available online]: http://www.sce.com/EnergyProcurement/renewables/spvp-ipp/spvp-ipp.htm

[81] U.S. Department of Energy, et al. "20% Wind Energy by 2030 - Increasing Wind Energy's Contribution to U.S. Electricity Supply," report DOE/GO-102008-2567, July, 2008 [Available online]: www.nrel.gov/docs/fy08osti/41869.pdf

[82] A. Mills, R. Wiser, "Implications of Wide-Area Geographic Diversity for Short-Term Variability of Solar Power," Lawrence Berkeley National Laboratory Report 3884E Sept. 2010, [Available online]: http://eetd.lbl.gov/ea/EMS/reports/lbnl-3884e.pdf

[83] S. Venkataraman, U. Helman, et al., "Integration of Renewable Resources – Operational Requirements and Generation Fleet Capability at 20 % RPS," California Independent System Operator, August, 2010.

[84] B.K. Parsons, Y. Wan, B. Kirby, "Wind Farm Power Fluctuations, Ancillary Services, and System Operating Impact Analysis Activities in the United States," July 2001

[85] J. W. Smith, R. Dugan, W. Sunderman, "Distribution Modeling and Analysis of High Penetration PV," IEEE General Meeting, Detroit, MI, July 2011

[86] M. P. Wakefield, "Smart Distribution System Research in EPRI's Smart Grid Demonstration Initiative," IEEE General Meeting, Detroit, MI, July 2011

[87] J. Mickey, "Using Load Resources to Meet Ancillary Service Requirements in the ERCOT Market: A Case Study," Proceedings IEEE General Meeting, Minneapolis, MN, July 2010.

[88] X. Zhang, R. Fields, K. Abreu, "Financial Benefits of Implementing Demand Response in CAISO Market," Proceedings IEEE General Meeting, Minneapolis, MN, July 2010.

[89] L. B. Lave, K. Spees, "Demand Response and Electricity Market Efficiency," The Electricity Journal, vol. 20, no. 3, April, 2007, pp. 69-85.

[90] E. J. Paulson, "Demand response as ancillary services in the PJM RTO," Proc. IEEE PES General Meeting, June, 2005, San Francisco, CA, pp. 1575-1578.

[91] R. Mukerji, "Demand Response in the NYISO Markets," Proc. IEEE Power Systems Conference and Exposition, March, 2011, Phoenix, AZ, pp. 1-2.

[92] S. Windergren, H. Kirkham, "Smart Grid – Transforming Power System Operations," Proceedings IEEE General Meeting, Minneapolis, MN, July 2010.

[93] H. Johal, D. Manz, K. O'Brien, J. Kern, "Grid Integration of Energy Storage," Proc. IEEE PES General Meeting, Detroit, MI, July 2011, pp. 1-2.

[94] G. D. Rodriguez, "A Utility Perspective of the Role of Energy Storage in the Smart Grid," Proc. IEEE PES General Meeting, Minneapolis, MN, July 2010, pp. 1-2.

[95] D. Manz, N. Miller, H. Elahi, "Energy storage for the grid," A presentation to the New York Independent System Operator, 2011 [Available online]: www.nyiso.com/public/webdocs/committees/environmental_advisory_council/meeting_materials/2011-05-13/Energy_Storage_-GE_Energy_Consulting.pdf

[96] R. Dugan, M. McGranaghan, S. Santoso, H. Beaty, *Electrical Power Systems Quality*, 2nd ed., McGraw Hill, New York, 2002.

[97] Itron, *Smart Meter Specifications Data Sheets*, 2011 [Available online]: www.itron.com.

[98] E. Kyriakides, G. T. Heydt, "Synchronized Measurements in Power System Operation: International Practices and Research Issues," IEEE PES General Meeting, July 2009, pp. 1-3.

[99] IEEE Standard C37.118-2005, *Standard for Synchrophasors for Power Systems*, Piscataway, NJ, 2005.

[100] J. S. Thorpe, A. G. Phadke, K. J. Karimi, "Real-Time Voltage-Phasor Measurements for Static State Estimation," IEEE Trans. on Power Apparatus and Systems, v. PAS-104, no. 11, November 1985, pp. 3098 – 3 106.

[101] J. S. Thorpe, A. G. Phadke, S. H. Horowitz, M. M. Begovic, "Some Applications of Phasor Measurements to Adaptive Protection," IEEE Trans. on Power Systems, v. 3, no. 2, May 1988, pp. 791 – 798.

[102] A. G. Phadke, "Recent Advances in Monitoring, Protection, and Control of Power Systems," Proceedings, Joint International Power Conference, Athens Power Tech (APT), Athens, September, 1993, pp. 326 – 331.

[103] Damir Novosel, et al., Performance Requirements Task Team (PRTT), "Performance Requirements Part II - Targeted Applications: State Estimation," Eastern Interconnection Phasor Project (EIPP), North American Synchrophasor Initiative, July, 2006, pp. 1-33 [Available online]: http://www.naspi.org/resources/archive/archiveresources.stm.

[104] A. Abur, "Impact of Phasor Measurements on State Estimation," International Conference on Electrical and Electronics Engineering, November, 2009, pp. I3-I7.

[105] A. Abur, A. G. Exposito, *Power System State Estimation – Theory and Implementation*, New York, NY: Marcel Dekker, 2004.

[106] F. C. Schweppe, E. J. Handschin, "Static State Estimation in Electric Power Systems," Proceedings IEEE, vol. 62, no. 7, July 1974, pp. 972-982.

[107] A. Monticelli, *State Estimation in Electric Power Systems: A Generalized Approach*, Kluwer Academic Publishers, 1999.

[108] IEEE 1366, *Guide for Electric Power Distribution Reliability Indices*, Piscataway, NJ, 2003.

[109] M. M. Adibi, *Power System Restoration: Methodologies & Implementation Strategies*, IEEE Press, 2000.

[110] C. C. Lui, S. J. Lee, S. S. Venkata, "An Expert System Operational Aid for Restoration and Loss Reduction of Distribution Systems," IEEE Transactions on Power Systems, v. 3, no. 2, 1988, pp. 619 – 626.

[111] K. Matsumoto, T. Sakaguchi, R. J. Kafka, M. M. Adibi, "Knowledge Based Systems as Operational Aids in Power System Restoration," Proceedings of the IEEE, v. 80, no. 5, 1992, pp. 689-697.

[112] R. L. Wilde, "Effects of Cold Load Pickup at the Distribution Substation Transformer," IEEE Transactions on Power Apparatus and Systems, v. PAS-104, no. 3, 1985, pp. 704-710.

[113] E. Mondon, B. Heilbronn, Y. Harmand, O. Paillet, H. Fargier, "MARS: An Aid for Network Restoration After a Local Disturbance," Proceedings Power Industry Computer Application Conference, May 1991, pp. 344-349.

[114] Y. M. Park, K. H. Lee, "Application of an Expert System to Power System Restoration in Sub-Control Center," IEEE Trans. on Power Systems, v. 12, no. 2, May 1997, pp. 629-635.

[115] Q. Zhour, D. Shirmohammadi, W. H. E. Liu, "Distribution Feeder Reconfiguration for Service Restoration and Load Balancing," IEEE Transactions on Power Systems, v. 12, no. 2, May 1997, pp. 724-729.

[116] Tropos networks, "Outage Management: The Electric Utility's No. 1 Headache," A technology brief by TROPOS networks, July 2007, [Available Online]: http://www.tropos.com/pdf/technology_briefs/tropos_techbrief_outage_mgmt.pdf.

[117] D. A. Haughton, G. T. Heydt, "Smart Distribution System Design: Automatic Reconfiguration for Improved Reliability," Proceedings IEEE General Meeting, Minneapolis, MN, July, 2010.

[118] H. Brown, D. A. Haughton, G. T. Heydt, S. Suryanarayanan, "Some Elements of Design and Operation of a Smart Distribution System," Proceedings IEEE Power and Energy Society Transmission and Distribution Conference and Exposition, New Orleans, LA, April, 2010.

[119] G. Heydt, "The Next Generation of Power Distribution Systems," IEEE Transactions on Smart Grid, accepted for publication, 2010.

[120] M. Fiedler, *Special Matrices and their Applications in Numerical Mathematics*, Martinus Nijhoff Publishers (a member of Kluwer Academic Publishers Group), 1986.

[121] J.A. Bondy, U.S.R. Murty, *Graph Theory-Graduate Texts in Mathematics*, Springer, 2008.

[122] B. Liu, H. Lai, *Matrices in Combinatorics and Graph Theory*, Boston, MA: Kluwer Academic Publishers, 2000.

[123] IEEE Standard 1366-2003, *Guide for Electric Power Distribution Reliability Indices*, Piscataway, NJ, 2003.

[124] R.V. Patel, A. J. Laub, P. M Van Dooren, *Numerical Linear Algebra Techniques for Systems and Control*, IEEE Press, 1994.

[125] A.S. Householder, *The Theory of Matrices in Numerical Analysis*, Dover, NY, 1964.

[126] M. B Allen III, E. L Isaacson, *Numerical Analysis for Applied Science*, John Wiley and Sons, NY, 1998.

[127] A. S. Deif, *Advanced Matrix Theory for Scientists and Engineers*, Abacus Press, U.K. 1982.

[128] G. H. Golub, C. F. Van Loan, *Matrix Computations*, 3rd ed., John Hopkins University Press, MD, 1996.

[129] R. Ebrahimian, R. Baldick, "State Estimator Condition Number Analysis," IEEE Transactions on Power Systems, v. 16, no. 2, May, 2001, pp. 273-279.

[130] D. A. Haughton, G. T. Heydt, "A Linear State Estimation Formulation for Smart Distribution Systems," accepted for publication in IEEE Transactions on Power Systems, 2012.

[131] W. H. Kersting, et al., "Radial Distirubiton Test Feeders," IEEE Transactions on Power Systems, v. 6, no. 3, 1991, pp. 975-985.

[132] D. Montgomery, G. C. Runger, N. F. Hubele, *Engineering Statistics*, 3rd. ed., Wiley, 2004.

[133] Bharadwaj Ranganathan Sathyanarayana, "Sensitivity-based Pricing and Multiobjective Control for Energy Management in Power Distribution Systems," PhD Thesis, Arizona State University, Tempe AZ, July, 2012

[134] D. A. Haughton, G. T. Heydt, "Synchronous Measurements in Power Distribution Systems," chapter in "Control and Optimization Methods for Electric Smart Grids, A. Chakrabortty and M. Ilić editors, Springer, Publishers, New York, 2012, Part III, pp. 295 – 312.

APPENDIX A

POWER FLOW RESULTS OF DIFFERENT MODELING ASSUMPTIONS

Appendix A. Power flow results of different modeling assumptions

This appendix demonstrates the effect of using an approximate line impedance model versus the exact line impedance model. Note that results show slight differences, but these differences may be significant enough to impact control actions and alarms based on algorithms that detect voltage magnitude difference.

Table A.1 Base Case Comparison of Voltage Magnitudes from an Exact and Approximate Model

Case C1 – Base case									
Bus No.	Exact model (p.u.)			Approximate model (p.u.)			Difference† (%)		
	|Va|	|Vb|	|Vc|	|Va|	|Vb|	|Vc|			
1	0.9880	0.9893	1.0021	0.9905	0.9906	0.9979	-0.25	-0.14	0.42
2	0.9872	0.9901		0.9896	0.9914		-0.24	-0.13	0.00
3			1.0016			0.9980	0.00	0.00	0.36
4		0.9889			0.9901		0.00	-0.12	0.00
5			1.0000			0.9972	0.00	0.00	0.28
6	0.9944	0.9938	0.9997	0.9959	0.9946	0.9974	-0.15	-0.08	0.23
7	0.9971			0.9976			-0.05	0.00	0.00
8	0.9880	0.9893	1.0022	0.9905	0.9907	0.9979	-0.25	-0.14	0.43
9	0.9873	0.9902		0.9896	0.9914		-0.24	-0.13	0.00
10			1.0016			0.9980	0.00	0.00	0.36
11		0.9890			0.9902		0.00	-0.12	0.00
12			1.0000			0.9972	0.00	0.00	0.28
13	0.9944	0.9938	0.9998	0.9959	0.9947	0.9974	-0.15	-0.08	0.23
14	0.9971			0.9977			-0.05	0.00	0.00
45	0.9885	0.9898	1.0023	0.9909	0.9910	0.9983	-0.24	-0.13	0.40
46	0.9903	0.9898	1.0021	0.9925	0.9910	0.9985	-0.22	-0.12	0.36
47	0.9935	0.9916	1.0005	0.9953	0.9926	0.9978	-0.18	-0.10	0.27
48	0.9951	0.9945	1.0000	0.9964	0.9952	0.9979	-0.13	-0.07	0.20
49	0.9977	0.9984	0.9996	0.9982	0.9987	0.9987	-0.05	-0.03	0.09
50	1.0000	1.0000	1.0000	1.0000	1.0000	1.0000	0.00	0.00	0.00
† Difference calculated as $(V_{exact} - V_{approx}) / V_{exact}$									

Perhaps the most revealing visualization of the impact of different modeling methods is to observe the bus voltage magnitudes along the main three-phase feeder of the RBTS feeder F1, as shown in Figure 5.1. The following figures show voltage magnitude differences between modeling the exact detail based on line geometry, versus an approximate model for the main 11 kV feeder buses of the RBTS feeder F1.

Table A.2 Case C5 Comparison of Voltage Magnitudes from an Exact and Approximate Model

Case C5 – Heavy load 3									
Bus No.	Exact model (p.u.)			Approximate model (p.u.)			Difference† (%)		
	|*Va*|	|*Vb*|	|*Vc*|	|*Va*|	|*Vb*|	|*Vc*|			
1	0.9511	0.9610	1.0075	0.9543	0.9615	1.0010	-0.34	-0.06	0.65
2	0.9507	0.9610		0.9539	0.9615		-0.34	-0.06	0.00
3			0.9953			0.9897	0.00	0.00	0.56
4		0.9601			0.9607		0.00	-0.07	0.00
5			0.9903			0.9860	0.00	0.00	0.44
6	0.9704	0.9720	0.9916	0.9728	0.9726	0.9880	-0.24	-0.05	0.37
7	0.9821			0.9829			-0.08	0.00	0.00
8	0.9582	0.9679	1.0075	0.9613	0.9685	1.0010	-0.33	-0.05	0.65
9	0.9581	0.9679		0.9613	0.9685		-0.33	-0.06	0.00
10			1.0007			0.9951	0.00	0.00	0.56
11		0.9663			0.9670		0.00	-0.07	0.00
12			0.9971			0.9928	0.00	0.00	0.43
13	0.9790	0.9807	0.9984	0.9813	0.9812	0.9948	-0.24	-0.05	0.36
14	0.9889			0.9897			-0.08	0.00	0.00
45	0.9613	0.9685	1.0062	0.9645	0.9691	1.0000	-0.33	-0.06	0.62
46	0.9677	0.9697	1.0034	0.9708	0.9704	0.9978	-0.32	-0.07	0.56
47	0.9762	0.9764	0.9994	0.9788	0.9770	0.9951	-0.27	-0.06	0.43
48	0.9818	0.9834	0.9990	0.9838	0.9838	0.9959	-0.20	-0.04	0.32
49	0.9913	0.9944	0.9993	0.9921	0.9945	0.9979	-0.08	-0.02	0.13
50	1.0000	1.0000	1.0000	1.0000	1.0000	1.0000	0.00	0.00	0.00
† Difference calculated as $(V_{exact} - V_{approx}) / V_{exact}$									

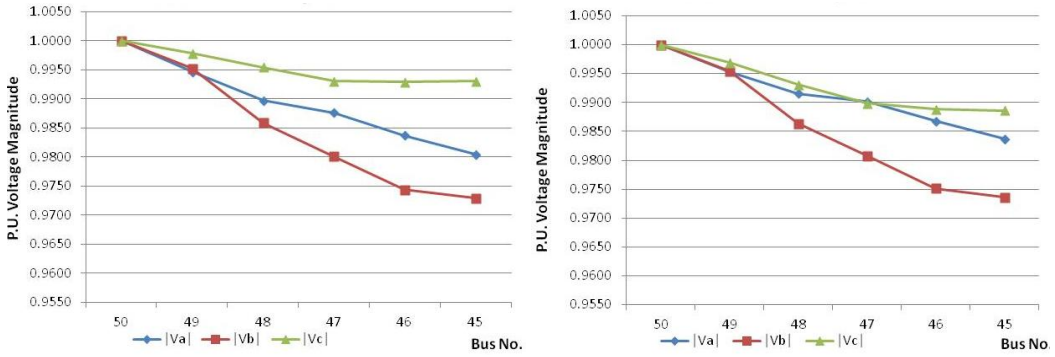

Figure A.1 Bus voltage magnitudes at main feeder buses for detailed and approximate model, Case C2: heavy load 1

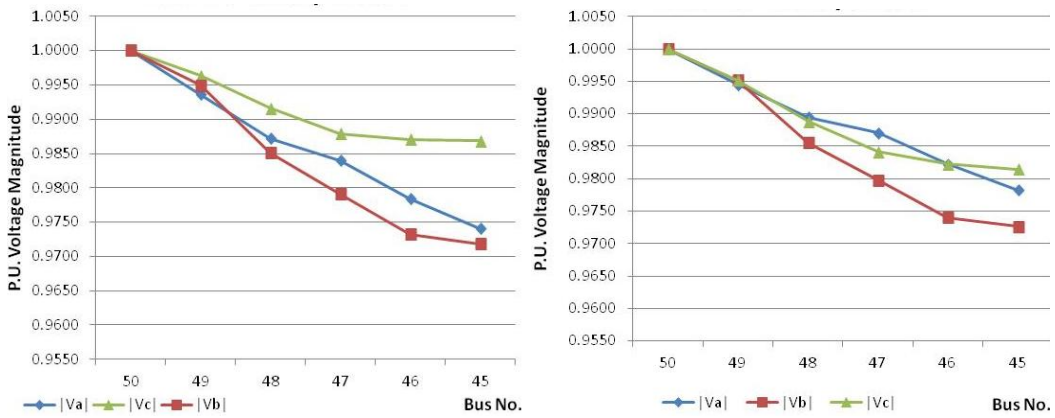

Figure A.2 Bus voltage magnitudes at main feeder buses for detailed and approximate model, Case C3: heavy load 2

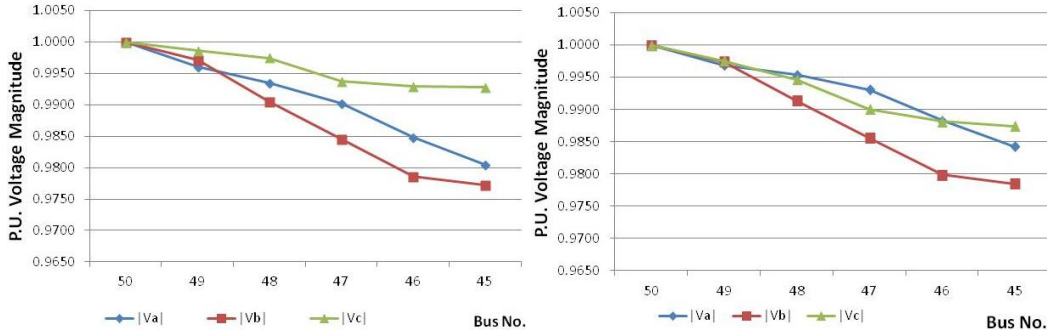

Figure A.3 Bus voltage magnitudes at main feeder buses for detailed and approximate model, Case C4: heavy load 2 with shunt capacitor at bus 48

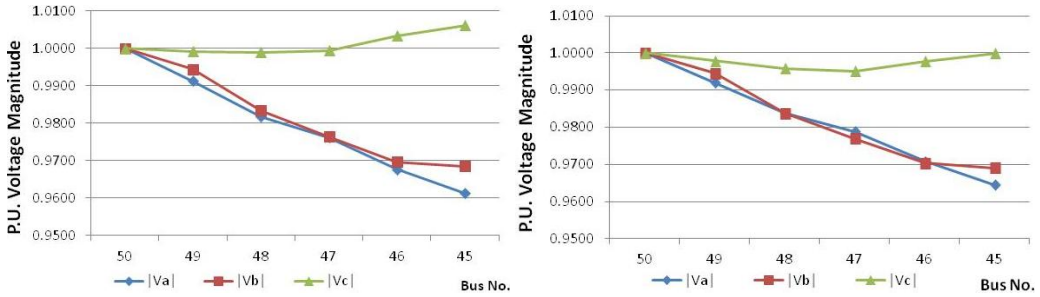

Figure A.4 Bus voltage magnitudes at main feeder buses for detailed and approximate model, Case C5: heavy load 3 (peak)

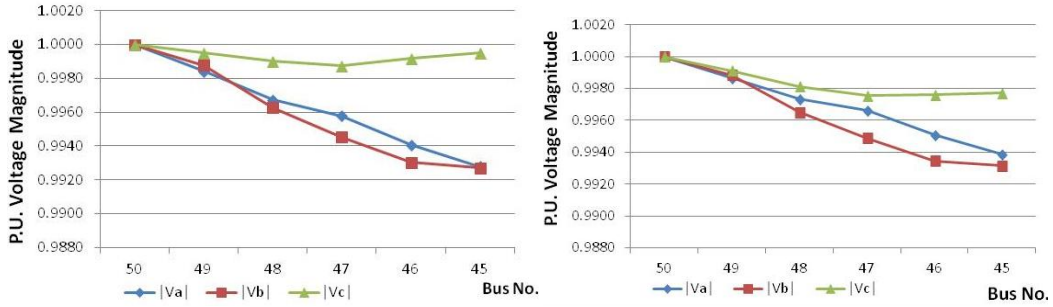

Figure A.5 Bus voltage magnitudes at main feeder buses for detailed and approximate model, Case C6: light load

APPENDIX B

FORWARD / BACKWARD LADDER ITERATIVE

POWER FLOW ALGORITHM

Appendix B. Forward / backward ladder iterative power flow algorithm

Figure B.1 and Figure B.2 outline basic steps in the forward sweep of the algorithm used to calculate the three-phase voltages on the radial distribution system. Note that the substation bus is taken as the slack bus/root node and all forward paths to end-nodes are traced for connectivity, voltage calculated at next upstream node until all nodes are processed.

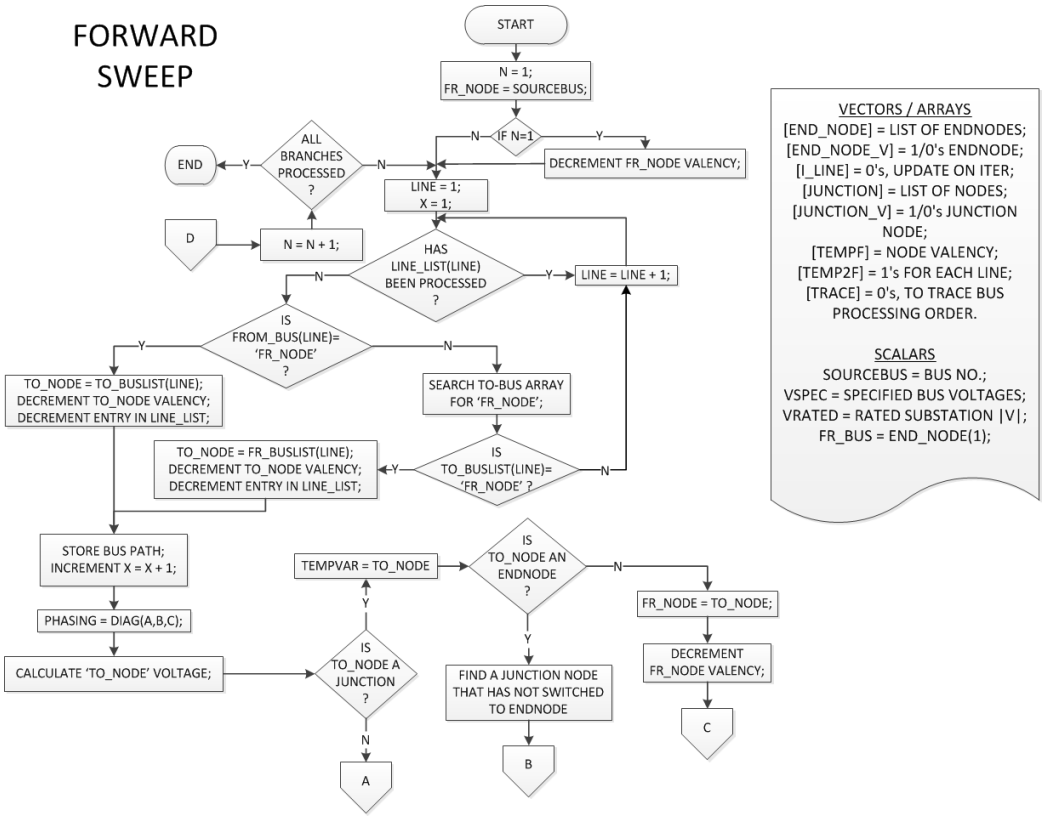

Figure B.1 Forward sweep algorithm overview 1 of 2

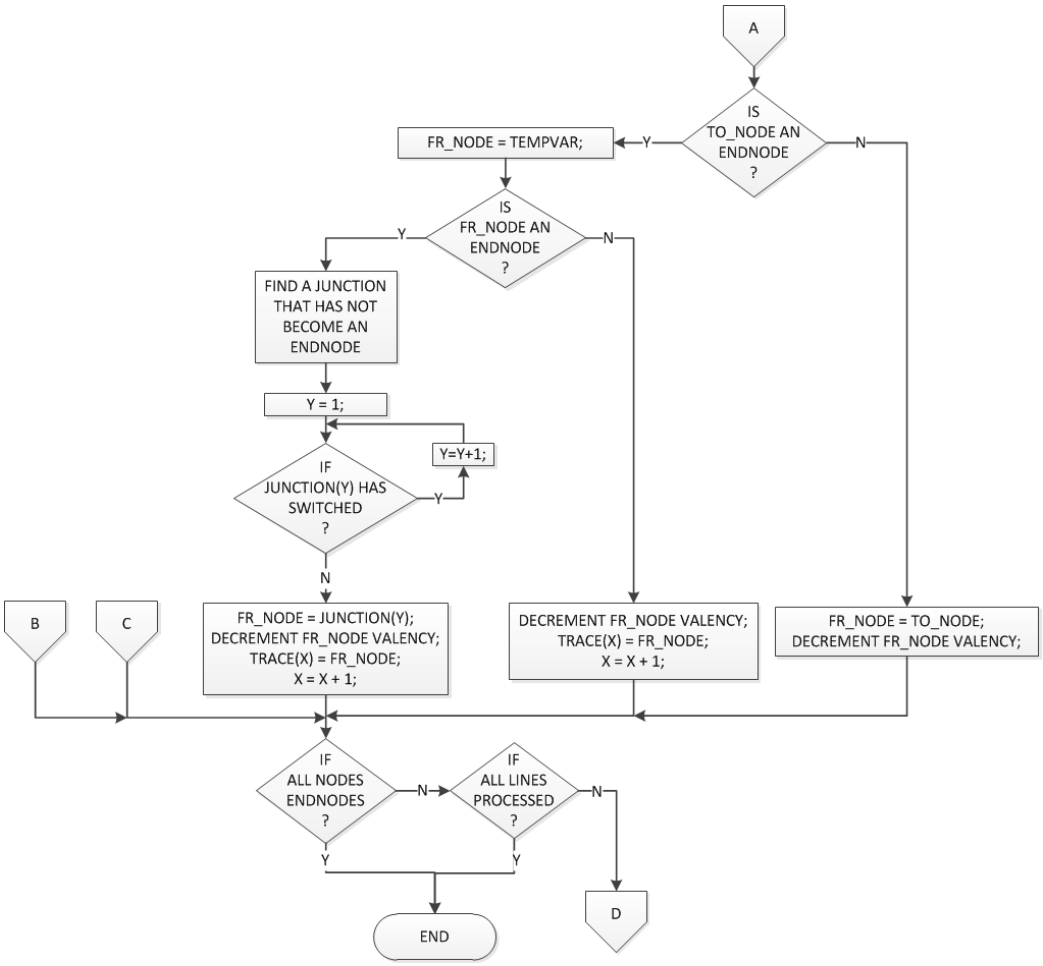

Figure B.2 Forward sweep algorithm overview 2 of 2

Figure B.3 and Figure B.4 present the steps of the backward sweep algorithm that is used to calculate bus voltages and line flows in the radial distribution system. The algorithm starts at an arbitrary end-node, and calculates back to each junction node until all nodes are analyzed. The program terminates when the source bus voltage has been calculated.

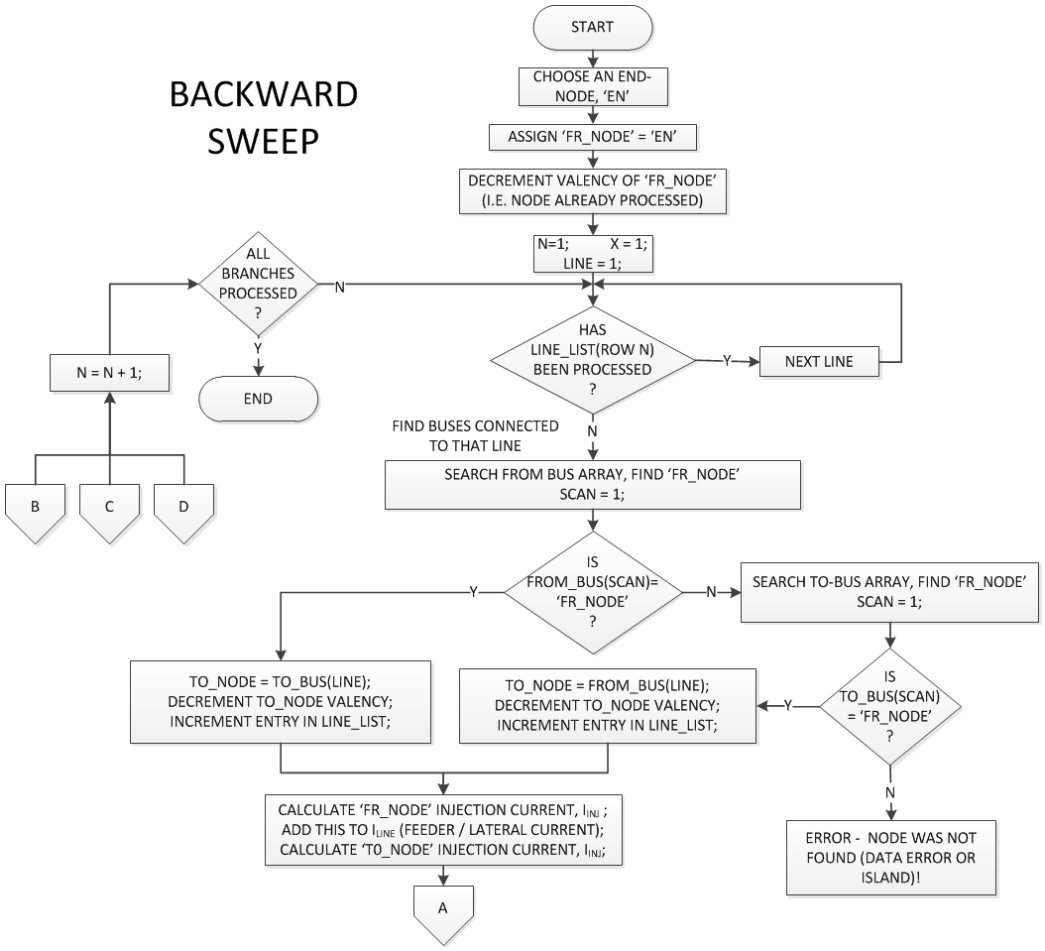

Figure B.3 Backward sweep algorithm overview 1 of 2

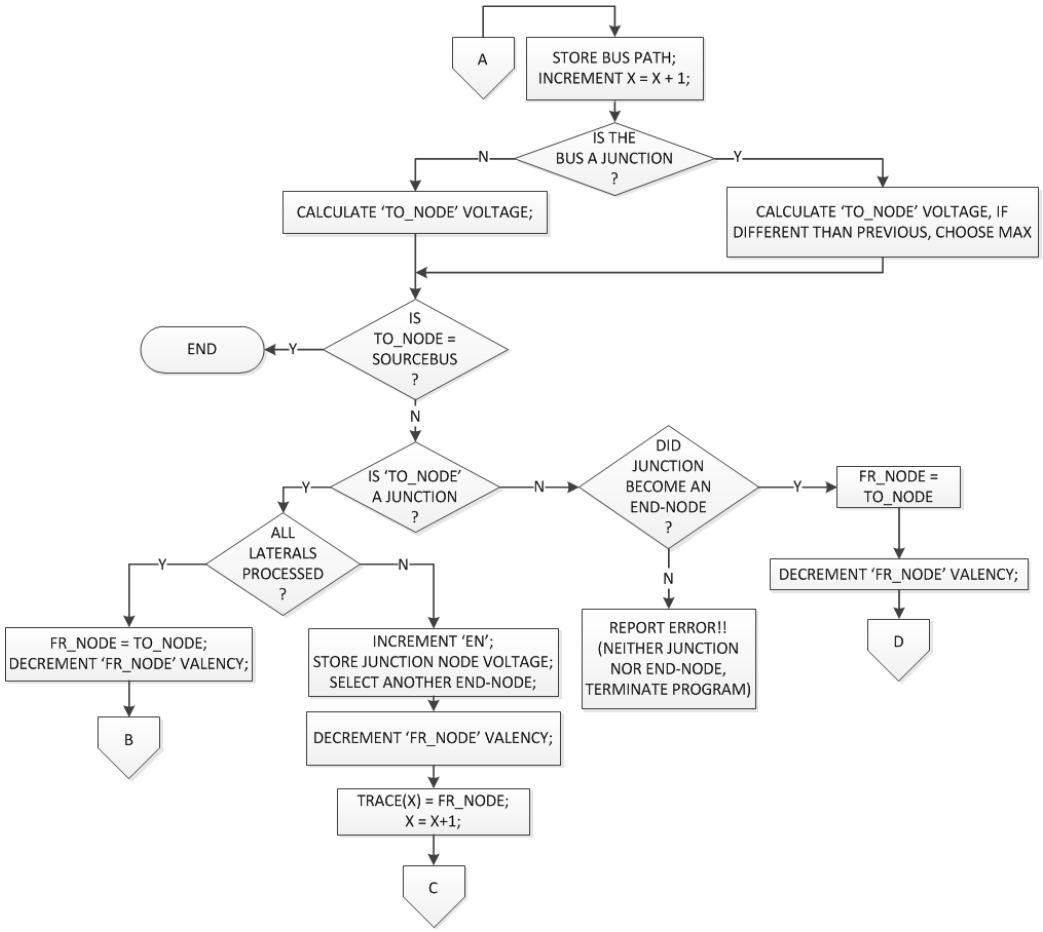

Figure B.4 Backward sweep algorithm overview 2 of 2

APPENDIX C

CONDITION NUMBER OF A MATRIX

Appendix C. Condition number of a matrix

References [124]-[128] provide detailed discussions concerning matrix theory and condition number. It is especially important to consider the conditioning of a matrix when a digital computer is used to solve the system of equations or compute solution estimates. A matrix is said to be *ill-conditioned* if small errors in the set of equations that describe the system, or small perturbations to the measurement vector, cause large errors in the calculation of the state vector (or estimates). Conversely, a well conditioned matrix is expected to produce less magnification of error terms in the final solutions; however, state vector errors when small perturbations in the measurement vector may still be present.

As discussed in Chapter 3, common sources of ill-conditioning related to the power system state estimation formulation include: a large proportion of injection current measurements, long and short lines connected to the same bus and large weighting factors applied to virtual measurements [105][129]. Using Equation 3.19, the condition number of the following matrices may be evaluated.

$$A = \begin{bmatrix} 1 & 0 \\ 0 & 1 \end{bmatrix} \qquad B = \begin{bmatrix} 1.001 & 0.999 \\ 0.999 & 1 \end{bmatrix}$$

The singular values (and eigenvalues in this case) of A are obviously [1, 1]. Therefore, the condition number of A is found to be unity,

$$\kappa(A) = 1.$$

Conversely, by observation, B appears to be close to singularity, the single value decomposition produces values of [1.995, 0.0015] (also eigenvalues of B), and the condition number of B is,

$$\kappa(B) = 1333.$$

Quite obviously, *A* is a much better conditioned matrix as compared to *B*.

Figure C.1 summarizes a discussion from [124]. The following discussion relates Figure C.1 to the state estimation problem. Given an exact data set, *d*, and a transformation (set of equations) given by the function, *f*, the true solution to this problem may be denoted as *f(d)*. For a well-conditioned system described by the function *f*, given an approximation (such as an estimate or sample) of the data set, *d**, the well conditioned system produces an *f(d*)* that is near *f(d)* (i.e. the true solution). However, for an ill-conditioned function / system, *f*, the estimated/ calculated solution, *f(d*)* may lie far away from the true solution, *f(d)*. Generally the more ill-conditioned the function *f*, the further the solution *f(d*)* may potentially be away from the true solution *f(d)*.

The same argument applies to an approximation of a function, *f**, that approximates the function, *f*. The approximation *f** must also be well-conditioned for the solution of *f*(d)* of the original data set, *d*, to lie near the true solution, *f(d)*. Implications in power system state estimation lie in the inherent ill-conditioned nature of the set of equations used to solve power system problems. For example, Newton Raphson is a first order Taylor series expansion that neglects higher order derivatives. Also, in the system described in Chapter 3, the linearization of the system of equations around an operating point creates the potential for inaccuracies in both the measurement function and measurement vector.

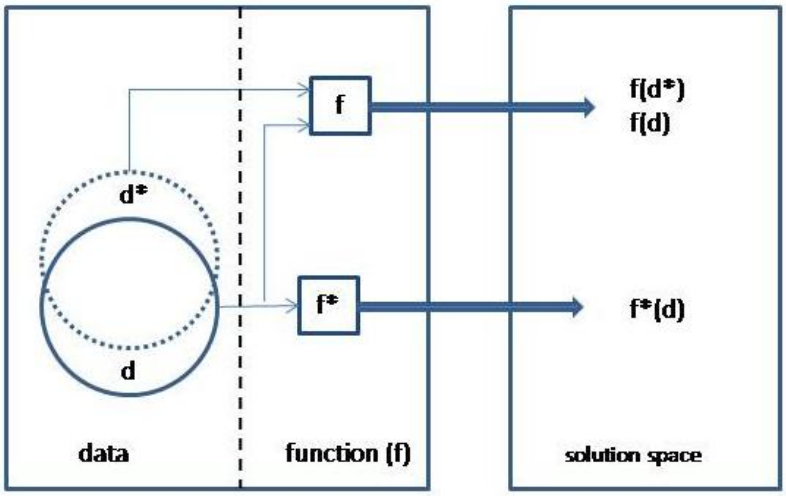

Figure C.1 Graphic representation of condition number, estimation and solution accuracy

State estimation involves taking a sample of the data, *d**, that is near d (i.e. state measurements), and estimating the system parameters utilizing the system model (i.e. *f* or *f**). Note that in power system state estimation, the system model is approximate (best model based on knowledge of the system and physical measurements). It is apparent that a reasonably accurate solution depends on the system model and how 'close' the measurements, *d**, and how accurate the system model, *f** are to their true values.

The vector and matrix norms introduced in Chapter 3 provide a measure of how close the true solution is to the estimated solution. A large norm of the residual vector indicates significant mismatch between measurement and estimate. Conversely, a small value for norm indicates accurate match between estimated and measured values. The state estimation formulation essentially tries to minimize the norm of the residual of measurements to calculated solution. Generally in the power operation center, a 'close enough' solution can give an operator

enough information to make decisions that continue to keep the grid in a stable operating region.

APPENDIX D

ASSIGNING WEIGHTS TO CALCULATED CURRENTS

Appendix D. Assigning weights to calculated currents

An illustrative example of the approximate of current variance is presented here. Note that given measurements M_k = {P, Q, V_m, δ}, and their variances Var_k =$\{\sigma_P^2, \sigma_Q^2, \sigma_{V_m}^2, \sigma_{\delta_v}^2\}$, the variance of the calculated current may be approximated. The generic expectation for all measurements is μ_k= M_k. The expected value of I, is a nonlinear function of M_k,

$$\mathrm{E}(I) = \mu_I \cong h(\mu_P, \mu_Q, \mu_V, \mu_\delta) \tag{D.1}$$

The variance may be approximated by

$$\mathrm{V}ar(I) = \sigma_I^2 \cong \sum_{\mathrm{k}=1}^{\mathrm{n}} \left(\frac{\partial h}{\partial M_k}\right)^2 \sigma_k^2 \tag{D.2}$$

Given expectation of the real part of current,

$$\mathrm{E}(I_{re}) = \mu_{I_{re}} \cong \frac{P\cos(\delta) + Q\sin(\delta)}{V_m} \tag{D.3}$$

and imaginary part of current,

$$\mathrm{E}(I_{im}) = \mu_{I_{im}} \cong \frac{P\sin(\delta) - Q\cos(\delta)}{V_m} \tag{D.4}$$

Variances are approximated by,

$$\mathrm{V}ar(I_{re}) = \sigma^2_{I_{re}} \cong \sum_{\mathrm{k=1}}^{\mathrm{n}} \left(\frac{\partial \mu_{I_{re}}}{\partial M_k} \right)^2 \sigma_k^2 \tag{D.5}$$

and

$$\mathrm{V}ar(I_{im}) = \sigma^2_{I_{im}} \cong \sum_{\mathrm{k=1}}^{\mathrm{n}} \left(\frac{\partial \mu_{I_{im}}}{\partial M_k} \right)^2 \sigma_k^2 \tag{D.6}$$

The Taylor series expansion is evaluated at each μ_k. The variance is then calculated according to Equation D.6. The expressions for real and imaginary parts of the Taylor series expansion of the current equations are given in Table D.1.

Table D.1 Real and Imaginary Expressions for Taylor Series Expansion of μ_{re}, μ_{im}

Real Quantities	Imaginary Quantities
$E(I_{re}) = \frac{P\cos(\delta) + Q\sin(\delta)}{V_m}$	$\mathrm{E}(I_{im}) = \frac{P\sin(\delta) - Q\cos(\delta)}{V_m}$
$\frac{\partial \mu_{I_{re}}}{\partial P} = \left[\frac{\cos(\delta)}{V_m} \right]$	$\frac{\partial \mu_{I_{im}}}{\partial P} = \left[\frac{\sin(\delta)}{V_m} \right]$
$\frac{\partial \mu_{I_{re}}}{\partial Q} = \left[\frac{\sin(\delta)}{V_m} \right]$	$\frac{\partial \mu_{I_{im}}}{\partial Q} = \left[\frac{\cos(\delta)}{V_m} \right]$
$\frac{\partial \mu_{I_{re}}}{\partial V_m} = -\left[\frac{P\cos(\delta) + Q\sin(\delta)}{V_m^2} \right]$	$\frac{\partial \mu_{I_{im}}}{\partial V_m} = -\left[\frac{P\sin(\delta) - Q\cos(\delta)}{V_m^2} \right]$
$\frac{\partial \mu_{I_{re}}}{\partial \delta} = \left[\frac{-P\sin(\delta) + \mathrm{Q}\cos(\delta)}{V_m} \right]$	$\frac{\partial \mu_{\mathrm{I_{im}}}}{\partial \delta} = \left[\frac{\mathrm{P}\cos(\delta) + \mathrm{Q}\sin(\delta)}{V_m} \right]$
$\sigma^2_{I_{re}} = \sum_{k=1}^{n} \left(\frac{\partial \mu_{I_{re}}}{\partial M_k} \right)^2 \sigma_k^2$	$\sigma^2_{I_{im}} = \sum_{i=1}^{n} \left(\frac{\partial \mu_{I_{im}}}{\partial M_k} \right)^2 \sigma_k^2$
$\sigma_{I_{re}} = \sqrt{\sigma^2_{I_{re}}}$	$\sigma_{I_{im}} = \sqrt{\sigma^2_{I_{im}}}$

The illustrative example proceeds to calculate the expected current and approximate variance for the set of measurements provided in Table D.2. Resulting

approximations are shown in Table D.3. Note that if the standard deviations in Table D.2 are changed, the resulting real and imaginary current standard deviations also change. The real portion of current is more sensitive to changes in V_m and P. Note also that the standard deviation of imaginary portion of current is more sensitive to changes in V_m and δ.

Table D.2 Measurement data used to illustrate approximation of variance

Quantity M_k	Measurement	Expectation $E(M_k) = \mu_k$	St. Dev Σ_k	Variance σ_k^2
P (p.u.)	1.0	$\mu_P = 1.0$	$\sigma_P = 0.01$	$\sigma_P^2 = 0.0001$
Q (p.u.)	0.4	$\mu_Q = 0.4$	$\sigma_Q = 0.03$	$\sigma_Q^2 = 0.0009$
V_m *(p.u.)*	1.0	$\mu_{Vm} = 1.0$	$\sigma_{Vm} = 0.05$	$\sigma_{Vm}^2 = 0.0025$
δ *(rad)*	0.0	$\mu_\delta = 0.00$	$\sigma_\delta = 0.000873$	$\sigma_\delta^2 = 7.62e^{-7}$

Table D.3 Results for approximate real and imaginary current variance

Real Quantities	Value	Imaginary Quantities	Value
$E(I_{re})=$	1.0	$E(I_{im})$	-0.04
$\frac{\partial \mu_{I_{re}}}{\partial P} =$	1.0	$\frac{\partial \mu_{I_{im}}}{\partial P} =$	0.0
$\frac{\partial \mu_{I_{re}}}{\partial Q} =$	0.0	$\frac{\partial \mu_{I_{im}}}{\partial Q} =$	1.0
$\frac{\partial \mu_{I_{re}}}{\partial V_m} =$	-1.0	$\frac{\partial \mu_{I_{im}}}{\partial V_m} =$	0.4
$\frac{\partial \mu_{I_{re}}}{\partial \delta} =$	0.4	$\frac{\partial \mu_{I_{im}}}{\partial \delta} =$	1.0
$\sigma_{I_{re}}^2 =$	0.003	$\sigma_{I_{im}}^2 =$	0.0038
$\sigma_{I_{re}} =$	0.05477	$\sigma_{I_{im}} =$	0.06164

APPENDIX E

RYG TEST BED DATA

Appendix E. RYG test bed data

Table E.1 Bus Load Data for the RYG Test System

Bus No.	P (MW)	Q (MVAr)	Circuit
1	Source	-	Red
2	0	-0.5	Red
3	2	1	Red
4	2	2	Red
5	1	0.4	Red
6	Source	-	Yellow
7	0.5	0	Yellow
8	0.5	0.5	Yellow
9	0	-0.5	Red
10	0.1	0.5	Red
11	0.5	0	Green
12	0.5	0.5	Yellow
13	0.5	0.5	Green
14	0.2	0	Red
15	0	-0.5	Green
16	0.2	0	Green
17	Source	-	Green
18	0	0	Green
19	1	0.5	Green
Total Demand	9	4.4	-

Table E.2 Line Data for the RYG Test System

Line No.	From Bus	To Bus	Length (km)
1	1	2	0.71
2	2	3	0.50
3	3	4	0.50
4	3	8	0.50
5	4	5	0.50
6	4	9	0.50
7	6	7	0.50
8	7	8	0.50
9	7	12	0.50
10	8	13	0.50
11	9	10	0.50
12	9	13	0.71
13	9	14	0.50
14	11	15	0.56
15	13	15	1.00
16	14	16	0.50
17	15	18	0.50
18	16	19	1.00
19	17	18	2.00
20	18	19	1.50

The following are for copper conductor at 60 Hz:

Red – 2/0; GMR, 0.01252 in.

Yellow – No. 2 AWG; GMR, 0.00883 in.

Green – No. 2 AWG; GMR, 0.0093 in.

APPENDIX F

RBTS TEST BED MODELING AND LOAD ASSUMPTIONS

Appendix F. RBTS test bed modeling and load assumptions

This appendix contains data pertaining to the RBTS test bed. RBTS stands for the Roy Billinton Test System after its creator. This data used in the state estimation algorithm for feeder F1. The RBTS originally published in [38] presents a realistic power system test bed. It contains generation, transmission and distribution networks. Line, load and bus data is given. Reliability analyses are shown.

The RBTS contains six buses in an HV transmission network. Five buses are load buses. There are 11 large generators, 9 transmission lines, a total of 240 MW of installed capacity, and 185 MW peak load. The system has 230 kV, 138 kV, 33 kV, 11 kV and 400 V voltages. The full RBTS system is small enough to be studied and but large enough to be considered non-trivial. The largest distribution sub-network in the RBTS is load bus 3 as depicted in Figure 4.2. Bus 3 has a peak load of 85 MW, average load of 52.63 MW, and has various load types.

Figure F.1 presents the load profile as seen at the distribution transformer of feeder F1. Load data used to create the load profile are provided in Table F.1 based on the average and peak provided in [38]; however, reasonable assumptions are made to obtain a 24 hour load profile curve representative of a mixed load-type feeder. Note that the data is provided by each phase, but loads are distributed along the feeder length according to Figure 4.2.

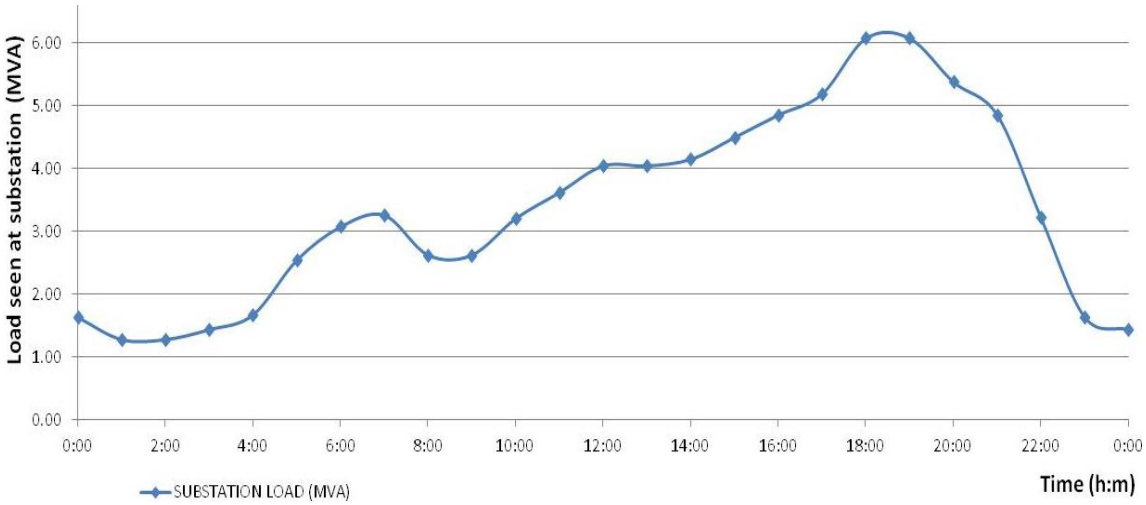

Figure F.1 Load profile seen at the distribution transformer of RBTS Bus 3 feeder F1

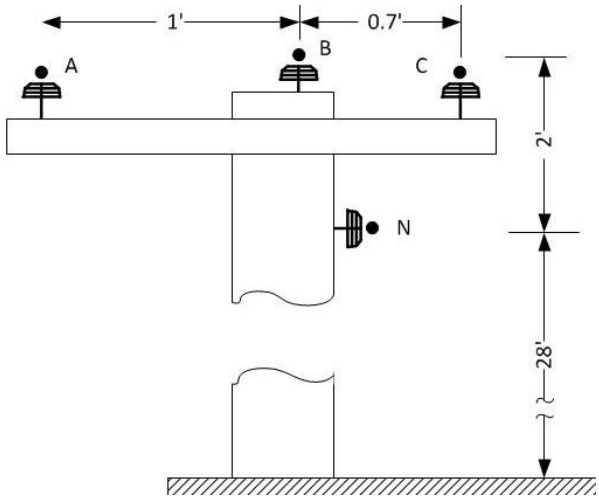

Figure F.2 Line geometry for RBTS feeder F1

Table F.1 Data for Feeder F1 Load Profile as Seen at the Substation Transformer

Case	Hour starting	MVA			MW total	MVAr total	Substation load (MVA)
		Phase A	Phase B	Phase C			
	0:00	0.56	0.56	0.52	1.60	0.30	1.63
LOW	1:00	0.42	0.43	0.42	1.21	0.39	1.27
	2:00	0.42	0.43	0.42	1.21	0.39	1.27
C6	3:00	0.48	0.50	0.45	1.38	0.39	1.43
	4:00	0.57	0.56	0.53	1.60	0.46	1.66
HE5	5:00	0.85	0.88	0.80	2.47	0.59	2.54
	6:00	1.02	1.02	1.03	3.01	0.60	3.07
C1	7:00	1.11	1.11	1.03	3.20	0.60	3.26
	8:00	0.88	0.91	0.83	2.47	0.89	2.62
	9:00	0.88	0.91	0.83	2.47	0.89	2.62
	10:00	1.08	1.11	1.01	3.01	1.08	3.20
	11:00	1.17	1.27	1.18	3.13	1.82	3.62
C2	12:00	1.32	1.47	1.26	3.59	1.86	4.04
	13:00	1.32	1.47	1.26	3.59	1.86	4.04
	14:00	1.40	1.44	1.31	3.74	1.79	4.15
	15:00	1.52	1.58	1.40	3.89	2.26	4.50
C3	16:00	1.66	1.64	1.55	4.27	2.32	4.85
	17:00	1.77	1.82	1.59	4.55	2.49	5.19
C5	18:00	2.05	2.11	1.91	5.48	2.63	6.08
C5	19:00	2.05	2.11	1.91	5.48	2.63	6.08
	20:00	1.84	1.90	1.64	4.84	2.36	5.38
C3	21:00	1.66	1.64	1.55	4.27	2.32	4.85
C1	22:00	1.10	1.10	1.02	3.20	0.60	3.26
	23:00	0.56	0.56	0.52	1.60	0.30	1.63
C6	0:00	0.48	0.50	0.45	1.38	0.39	1.43

Table F.2 is recast from the RBTS data provided in [38] identifying each load point, and indicating loads on the corresponding phase. The common power base for the RBTS system modeling is taken as 100 MVA, 3-phase. Voltage bases are assumed to be the respective nominal line-line voltage at that bus. Transformer power base is taken as the transformer rating. Line resistances and reactance are provided in Table F.3.

For simplicity, the same line geometry was assumed for all line segments. Figure F.2 shows this line model. The mutual coupling resulting from this phase configuration contributes to the mutual coupling between phases that may contribute to voltage rise in some phases. Also, the untransposed lines contribute to significant mutual coupling.

Table F.2 Feeder F1 Load Points, Customer Type, Load and Phase

Load point	Customer type	Peak (MW)	Average (MW)	No. customers	Phase
LP 1	residential	0.8367	0.4684	250	A,B,C
LP 2	residential	0.775	0.4339	190	A,B
LP 3	commercial	0.5222	0.2886	15	C
LP 4	residential	0.8367	0.4684	250	B
LP 5	residential	0.8367	0.4684	250	C
LP 6	residential	0.8367	0.4684	250	A,B,C
LP 7	residential	0.8367	0.4684	250	A
Total		5.4807	3.0645	1455	

Table F.3 Conductor impedance data for all voltage classes

Voltage (kV)	Max. feeder current (A)	Conductor name	Current carrying capacity (A)	*R* (Ω/mi)	*X* (Ω/mi) at 1' spacing	*r/x* ratio
11	292	Flamingo	800	0.1397	0.412	0.34
33	323	Lark	600	0.215	0.476	0.45
138	125	Drake	900	0.1288	0.557*	0.23

*Note: 138 kV impedance data are taken from [37]

Table F.4 Base Voltages, Impedance and Current

Voltage (kV_{LL})	Base voltage (kV_{LL})	Base impedance (Ω)	Base current (A)
138	$V_{B1} = 138$	190	418
33	$V_{B2} = 33$	11	1750
11	$V_{B3} = 11$	1.21	5248
0.415	$V_{B4} = 0.415$	0.0017	139120

APPENDIX G

RBTS FEEDER F1 WITH DISTRIBUTED GENERATION

Appendix G. RBTS feeder F1 with distributed generation

Distributed generation is assumed on feeder F1 for a variety of studies. Studies include obtaining bus voltage profiles in the presence of distributed generation. DG locations were varied. Also, DG characteristic injection profile for wind (night-peaking) and solar (day-peaking) was investigated. An approximate DG penetration level of approximately 30 % was used in both cases; note that penetration level in this case is measured by the installed DG capacity relative to load.

The 24 hour load profile as seen by the substation transformer, DG injections, and net load profile on RBTS feeder F1 are shown in Figure G.1 for solar DG injections and Figure G.2 for typical wind injection profile. The nominal load values (with no DG) are assumed to be identical to those in 0. Values for solar and wind injections for each hour of the 24 hour period are shown in Table G.1 (solar) and Table G.2 (wind). Note that installed solar capacity is 1.5 MW, while installed wind capacity is approximately 2.0 MW. This represents 24.8 and 32.6 installed capacities of solar and wind respectively.

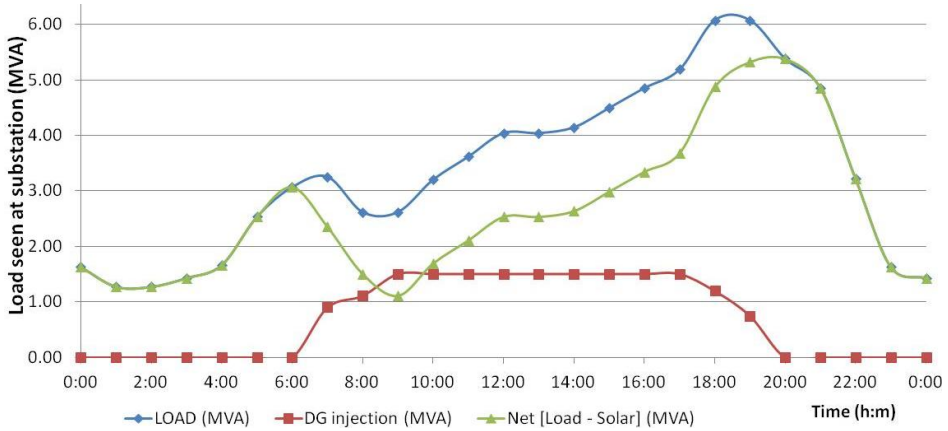

Figure G.1 Load, solar DG injection and net load profiles for a 24 hour peak day as seen by RBTS feeder F1

Table G.1 Solar Injection Values (MW) and Net Load for 24 Hour Profile on RBTS Feeder F1

	Hour starting	MW A	MW B	MW C	MW Total	DG injection (MVA)	Net (MVA) [Load-Solar]
	0:00	0.001	0.001	0.001	0.00	0.00	1.63
LOW	1:00	0.001	0.001	0.001	0.00	0.00	1.27
	2:00	0.001	0.001	0.001	0.00	0.00	1.27
C6	3:00	0.001	0.001	0.001	0.00	0.00	1.43
	4:00	0.001	0.001	0.001	0.00	0.00	1.66
	5:00	0.001	0.001	0.001	0.00	0.00	2.53
	6:00	0.001	0.001	0.001	0.00	0.00	3.07
C1	7:00	0.300	0.300	0.300	0.90	0.90	2.36
	8:00	0.370	0.370	0.370	1.11	1.11	1.51
	9:00	0.500	0.500	0.500	1.50	1.51	1.11
	10:00	0.500	0.500	0.500	1.50	1.51	1.70
	11:00	0.500	0.500	0.500	1.50	1.51	2.11
C2	12:00	0.500	0.500	0.500	1.50	1.51	2.54
	13:00	0.500	0.500	0.500	1.50	1.51	2.54
	14:00	0.500	0.500	0.500	1.50	1.51	2.64
	15:00	0.500	0.500	0.500	1.50	1.51	2.99
C3	16:00	0.500	0.500	0.500	1.50	1.51	3.35
	17:00	0.500	0.500	0.500	1.50	1.51	3.68
C5	18:00	0.400	0.400	0.400	1.20	1.20	4.88
C5	19:00	0.250	0.250	0.250	0.75	0.75	5.33
	20:00	0.000	0.000	0.000	0.00	0.00	5.38
C3	21:00	0.000	0.000	0.000	0.00	0.00	4.85
C1	22:00	0.000	0.000	0.000	0.00	0.00	3.21
	23:00	0.000	0.000	0.000	0.00	0.00	1.63
C6	0:00	0.000	0.000	0.000	0.00	0.00	1.43

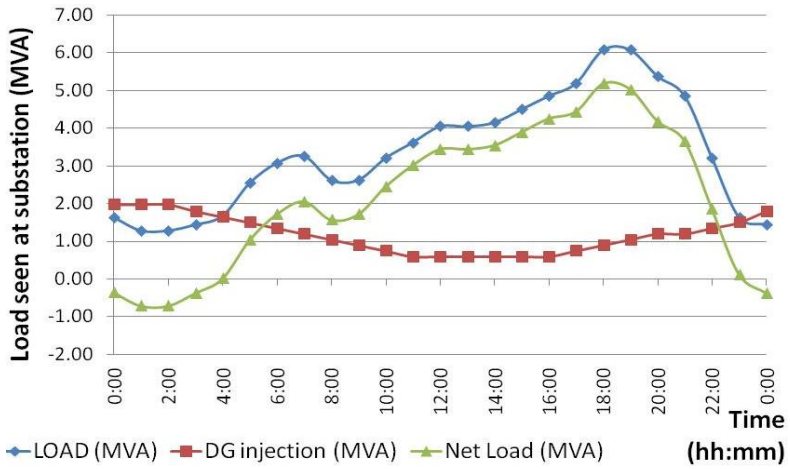

Figure G.2 Load, wind DG injection and net load profiles for a 24 hour peak day as seen by RBTS feeder F1

Table G.2 Wind Injection Values (MW) and Net Load for 24 Hour Profile on RBTS Feeder F1

	Hour starting	MW *A*	MW *B*	MW *C*	MW total	DG injection (MVA)	Net Load (Load-DG) (MVA)
	0:00	0.66	0.66	0.66	1.98	1.98	-0.35
LOW	1:00	0.66	0.66	0.66	1.98	1.98	-0.71
	2:00	0.66	0.66	0.66	1.98	1.98	-0.71
C6	3:00	0.60	0.60	0.60	1.80	1.80	-0.37
	4:00	0.55	0.55	0.55	1.65	1.65	0.01
	5:00	0.50	0.50	0.50	1.50	1.50	1.04
	6:00	0.45	0.45	0.45	1.35	1.35	1.72
C1	7:00	0.40	0.40	0.40	1.20	1.20	2.06
	8:00	0.35	0.35	0.35	1.05	1.05	1.57
	9:00	0.30	0.30	0.30	0.90	0.90	1.72
	10:00	0.25	0.25	0.25	0.75	0.75	2.45
	11:00	0.20	0.20	0.20	0.60	0.60	3.02
C2	12:00	0.20	0.20	0.20	0.60	0.60	3.44
	13:00	0.20	0.20	0.20	0.60	0.60	3.44
	14:00	0.20	0.20	0.20	0.60	0.60	3.55
	15:00	0.20	0.20	0.20	0.60	0.60	3.90
C3	16:00	0.20	0.20	0.20	0.60	0.60	4.25
	17:00	0.25	0.25	0.25	0.75	0.75	4.44
C5	18:00	0.30	0.30	0.30	0.90	0.90	5.18
C5	19:00	0.35	0.35	0.35	1.05	1.05	5.03
	20:00	0.40	0.40	0.40	1.20	1.20	4.18
C3	21:00	0.40	0.40	0.40	1.20	1.20	3.65
C1	22:00	0.45	0.45	0.45	1.35	1.35	1.86
	23:00	0.50	0.50	0.50	1.50	1.50	0.13
C6	0:00	0.60	0.60	0.60	1.80	1.80	-0.37

APPENDIX H

ILLUSTRATIVE EXAMPLES DESCRIBED

Appendix H. Illustrative Examples Described

Table H.1 summarizes illustrations presented throughout the dissertation.

Table H.1 Illustrative examples presented throughout this dissertation

Example name	Section	Test bed	Topic illustrated
RYG reliability / restoration	4.6	RYG	Interrupting device location
RYG reliability	4.7	RYG	Unserved energy vs. number of interrupting devices
RBTS reliability (7 cases)	4.8	RBTS	Automation
State estimation (SE1, SE2, SE3)	5.1	RBTS, Feeder F1	Unbiased estimation formulation. No noise, and estimating under various loading conditions
Biased state estimation (SE1, SE2, SE3)	5.2	RBTS, Feeder F1	Biased estimation formulation. No noise, and estimating under various loading conditions
Bad data detection	5.3	RBTS, Feeder F1	Detecting bad data when load on one phase is measured in error
Voltage unbalance and control (VU1 - VU6)	6.2	RBTS, Feeder F1	Voltage unbalance cases with various shunt reactive values
DG – bidirectional flows (DG1)	6.3	RBTS, Feeder F1	DG and bidirectional flows
DG – voltage control (DG2)	6.3	RBTS, Feeder F1	Estimator based voltage control using DG
DG – energy storage and peak shaving (DG3)	6.3	RBTS, Feeder F1	Energy management and peak shaving with storage and DG
LSSS – (DR1)	6.5	LSSS	Demand response in the LSSS

APPENDIX I

SAMPLE MATLAB CODE

Appendix I. Sample MATLAB code

Sample code for the main power-flow steering routine is presented.

```
% % DATE CREATED / MODIFIED:       12-07-2011
% % NAME:        pfMain_RBTS_3ph.m
% % DESCRIPTION:    Main steering routine for a forward / backward 3ph unbalanced  power
flow algorithm.  Build topology, convert bases, initialize data, display results, build Ybus (for SE),
plot feeder voltage profile, save data to an external (*.csv or *.xls) file.
% % ------- % ------- % ------- % ------- % ------- % ------- % -------

clear all; clc;

% % Enter conductor variables and line geometry
pfRBTS_linegeometry;

% % Enter system bus & line data (loads, branches)
% pfRBTS_busdata;     % % loads and buses
% pfRBTS_linedata;    % % topology

Sb_3ph = 100*10^6;   % VA
Sb_1ph = Sb_3ph/3;

Vsubstation = [1.02, 1.02, 1.02, 1.02, 1.04];

% % % READING DATA: Line Model, Load Model
Line_model_file = 'C:\Full RBTS Model\LSSSv3\HE 18\LSSS Line Model HE18_0.xlsx';
Load_model_file = 'C: Full RBTS Model\LSSSv3\HE 18\LSSS Load Models HE18_0.xlsx';
caseno_txt = 'HE 18';
% % % WRITING DATA: voltage, current, power
Current_file = 'C:\Full RBTS Model\LSSSv3\HE 18\HE18 Currents102T.xlsx';
Voltage_file = 'C:\Full RBTS Model\LSSSv3\HE 18\HE18 Voltages102T.xlsx';
Power_file = 'C:\Full RBTS Model\LSSSv3\HE 18\HE18 Power102T.xlsx';

% % Column headers:
VTextBlkR2 = {'Bus No.','|Va|','Ang A (deg)','|Vb|','Ang B (deg)','|Vc|','Ang C (deg)'};
VTextBlkR1 = {caseno_txt, 'Pa(MW)','Pb(MW)','Pc(MW)','Qa(MVAr)', 'Qb(MVAr)',
'Qc(MVAr)'};
ITextBlkR2 = {'Fr','To','|Ia|','Ang A (deg)','|Ib|','Ang B (deg)','|Ic|','Ang C (deg)'};
PTextBlkR1 = {'Fr','To','Pa','Pb','Pc','Qa','Qb','Qc'};

tic;
for feeder = 1:5
   disp('Reading in data...');
   switch feeder
      case 1     % Feeder F1
      % % Read in data file with busdata and linedata:
      [RawLineNum, RawLineTxt, RawLineRaw] = xlsread(Line_model_file,'F1');
      % % Read in data file with busdata and linedata:
      [RawLoadNum, RawLoadTxt, RawLoadRaw] = xlsread(Load_model_file,'F1');
      n_loadbus_meas = 3;
```

```
    case 2     % Feeder F2
    % % Read in data file with busdata and linedata:
    [RawLineNum, RawLineTxt, RawLineRaw] = xlsread(Line_model_file,'F2');
    % % Read in data file with busdata and linedata:
    [RawLoadNum, RawLoadTxt, RawLoadRaw] = xlsread(Load_model_file,'F2');
    n_loadbus_meas = 3;

    case 3     % Feeder F3
    % % Read in data file with busdata and linedata:
    [RawLineNum, RawLineTxt, RawLineRaw] = xlsread(Line_model_file,'F3');
    % % Read in data file with busdata and linedata:
    [RawLoadNum, RawLoadTxt, RawLoadRaw] = xlsread(Load_model_file,'F3');
    n_loadbus_meas = 4;

    case 4     % Feeder F4
    % % Read in data file with busdata and linedata:
    [RawLineNum, RawLineTxt, RawLineRaw] = xlsread(Line_model_file,'F4');
    % % Read in data file with busdata and linedata:
    [RawLoadNum, RawLoadTxt, RawLoadRaw] = xlsread(Load_model_file,'F4');
    n_loadbus_meas = 4;

    case 5     % Feeder F6
    % % Read in data file with busdata and linedata:
    [RawLineNum, RawLineTxt, RawLineRaw] = xlsread(Line_model_file,'F6');
    % % Read in data file with busdata and linedata:
    [RawLoadNum, RawLoadTxt, RawLoadRaw] = xlsread(Load_model_file,'F6');
    n_loadbus_meas = 4;

end;
disp('Done reading in data...');

% %  Create the array of linedata2 - fr, to, km, mi, config
Linedata2 = RawLineNum;     [m,n] = size(Linedata2);    % % Save array
n_lines = m;        % No. lines = No. rows
% %  Create the array of Busdata - bus, type, Pabc, Qabc, GenPabc, GenQabc, Gabc, Babc
[m,n] = size(RawLoadNum);          n_buses = m;        % n_buses = No. rows
Busdata = zeros(n_buses, 20);       % Create array in memory
Busdata(:,1:8) = RawLoadNum(:,1:8); % Add in 3 phase load values (kW)
Busdata(:,3:8) = Busdata(:,3:8)/1000;   % Convert loads to (MW)
Bus_ph_info = [RawLoadNum(:,1),RawLoadNum(:,9:11)]; % Track phasing of the bus
Bases = [RawLoadNum(:,1),RawLoadNum(:,12)]; % Vbase(LL)

% % Substation bus voltage
% % Future versions - value read from power flow output file
Vsub = Vsubstation(feeder);

% % Base voltages, per-unit Z, transformers, line impedance
pfRBTS_systemZ;
% % Renumber buses, find valency (ID endnodes & junctions)
pfRBTS_setup;

% % Set tolerance threshhold
e = 0.00001;
```

```
% % % % % % % % % % % % START: POWER FLOW% % % % % %
   tic;
      pfRBTS_solver;    % % Forward / backward sweep algorithm
   toc;
% % % % % % % % % % END: POWER FLOW % % % % % % % % % %

   % % Save results to new vectors so more power flows may be run
   V_pf = V;
   I_line_pf = I_line;

   % % % % % % % % % % START: PROCESS DATA FOR DISPLAY % % % % % % % % %
% %
   % % BUS VOLTAGES
   Vmag = abs(V_pf);        % % MAGNITUDE
   Vang = atan2(imag(V_pf),real(V_pf))*180/pi;        % % ANGLE

   % % DISPLAY AS:  [ BUS#, |Va#|, /Va#, |Vb#|, /Vb#, |Vc#|, /Vc# ...]
   row = Busdata(:,1)';
   Vdisp = [row;Vmag(1,:);Vang(1,:);Vmag(2,:);Vang(2,:);Vmag(3,:);Vang(3,:)]';
   Vdisp_pf = Vdisp;

   % % LINE CURRENTS
   Imag = abs(I_line_pf).*[I_bases';I_bases';I_bases'];        % % MAGNITUDE
   Iang = atan2(imag(I_line_pf),real(I_line_pf))*180/pi;       % % ANGLE

   % % DISPLAY AS: [ FBUS#, TBUS#, |Ia#|, /Ia#, |Ib#|, /Ib#, |Ic#|, /Ic# ...]
   Idisp=[Linedata2(:,1:2), [Imag(1,:);Iang(1,:);Imag(2,:);Iang(2,:);...
      Imag(3,:); Iang(3,:)]'];
%     pfIdisp = Idisp

   % % Calculate line power flows:
   pfRBTS_Sflows;

   % % Store LP values in 'pf for HE' for future use:
   pf_Busdata = Busdata_new;
   pf_S_flow = S_flow;
   pfSub_load_MW = Sub_load_MW;
   pfSub_load_MVAr= Sub_load_MVAr;

   Tot_load = sum(Busdata(:,3:8));
%     pf_Losses_approx = pf_S_flow(38,3:8) - Tot_load;

% % % % % % % % % % % % % % % % % % % % % % % % % % % % % % % % % % % %
% % ----- X ----- Write results to excel ----- X -----
   disp('Writing data...');
   switch feeder
      case 1     % Feeder F1
%        % Write data file with voltage / angle:
%        xlswrite(Voltage_file, VTextBlkR1,'F1','A1');
%        xlswrite(Voltage_file, [Sub_load_MW, Sub_load_MVAr],'F1','B2');
%        xlswrite(Voltage_file, VTextBlkR2,'F1','A3');
%        xlswrite(Voltage_file, Vdisp,'F1','A4');
```

```
%	% % Write data file with current / angle:%
%	xlswrite(Current_file, VTextBlkR1,'F1','A1');
%	xlswrite(Current_file, ITextBlkR2,'F1','A2');
%	xlswrite(Current_file, Idisp,'F1','A3');
%	% % Write data file with power flows:
%	xlswrite(Power_file, PTextBlkR1,'F1','A1');
%	xlswrite(Power_file, pf_S_flow,'F1','A2');
%
%	% % % % % % % % % % % % % % % % % % % % % % % % % % % % % % % % %
%
%	case 2	% Feeder F2
%	% Write data file with voltage / angle:
%	xlswrite(Voltage_file, VTextBlkR1,'F2','A1');
%	xlswrite(Voltage_file, [Sub_load_MW, Sub_load_MVAr],'F2','B2');
%	xlswrite(Voltage_file, VTextBlkR2,'F2','A3');
%	xlswrite(Voltage_file, Vdisp,'F2','A4');
%	% % Write data file with current / angle:
%	xlswrite(Current_file, VTextBlkR1,'F2','A1');
%	xlswrite(Current_file, ITextBlkR2,'F2','A2');
%	xlswrite(Current_file, Idisp,'F2','A3');
%	% % Write data file with power flows:
%	xlswrite(Power_file, PTextBlkR1,'F2','A1');
%	xlswrite(Power_file, pf_S_flow,'F2','A2');
%
%	% % % % % % % % % % % % %% % % % % % % %% % % % % % %% % % % %
%	case 3	% Feeder F3
%	% Write data file with busdata and linedata:
%	xlswrite(Voltage_file, VTextBlkR1,'F3','A1');
%	xlswrite(Voltage_file, [Sub_load_MW, Sub_load_MVAr],'F3','B2');
%	xlswrite(Voltage_file, VTextBlkR2,'F3','A3');
%	xlswrite(Voltage_file, Vdisp,'F3','A4');
%	% % Write data file with busdata and linedata:
%	xlswrite(Current_file, VTextBlkR1,'F3','A1');
%	xlswrite(Current_file, ITextBlkR2,'F3','A2');
%	xlswrite(Current_file, Idisp,'F3','A3');
%	% % Write data file with power flows:
%	xlswrite(Power_file, PTextBlkR1,'F3','A1');
%	xlswrite(Power_file, pf_S_flow,'F3','A2');
%
%	% % % % % % % % % % % % %% % % % % % % %% % % % % % %% % % % %
%	case 4	% Feeder F4
%	% Write data file with busdata and linedata:
%	xlswrite(Voltage_file, VTextBlkR1,'F4','A1');
%	xlswrite(Voltage_file, [Sub_load_MW, Sub_load_MVAr],'F4','B2');
%	xlswrite(Voltage_file, VTextBlkR2,'F4','A3');
%	xlswrite(Voltage_file, Vdisp,'F4','A4');
%	% % Write data file with busdata and linedata:
%	xlswrite(Current_file, VTextBlkR1,'F4','A1');
%	xlswrite(Current_file, ITextBlkR2,'F4','A2');
%	xlswrite(Current_file, Idisp,'F4','A3');
%	% % Write data file with power flows:
%	xlswrite(Power_file, PTextBlkR1,'F4','A1');
%	xlswrite(Power_file, pf_S_flow,'F4','A2');
```

```
%
%       % % % % % % % % % % % %% % % % % % % %% % % % % % %% % % % %
%       case 5     % Feeder F6
%       % Write data file with busdata and linedata:
%       xlswrite(Voltage_file, VTextBlkR1,'F6','A1');
%       xlswrite(Voltage_file, [Sub_load_MW, Sub_load_MVAr],'F6','B2');
%       xlswrite(Voltage_file, VTextBlkR2,'F6','A3');
%       xlswrite(Voltage_file, Vdisp,'F6','A4');
%       % % Write data file with busdata and linedata:
%       xlswrite(Current_file, VTextBlkR1,'F6','A1');
%       xlswrite(Current_file, ITextBlkR2,'F6','A2');
%       xlswrite(Current_file, Idisp,'F6','A3');
%       % % Write data file with power flows:
%       xlswrite(Power_file, PTextBlkR1,'F6','A1');
%       xlswrite(Power_file, pf_S_flow,'F6','A2');
   end
   disp('Done writing data...');


% % ======== -+- ======== -+- ======== -+- ======== -+- ======== % %
% % % % % % % % % % % STATE ESTIMATION ALGORITHM % % % % % % % % %
% % Build the 3-phase YBUS:
YBUS_3ph;

% % % Test the 3-phase YBUS, YV = I
RBTS_I_calc;

% xlswrite('C:\Users\Haughton\Desktop\Icalc',[real(I_calc),imag(I_calc)],'Icalc6cap3ph');
% xlswrite('C:\Users\Haughton\Desktop\Timeseries_sim',[Vdisp],'V6cap3ph');
% xlswrite('C:\Users\Haughton\Desktop\Timeseries_sim',[Idisp],'I6cap3ph');

pf_tstore_I_calc = I_calc;

disp('Entering the estimation algorithm ... ')

SEMain_RBTS_3ph_DR;
end;

toc;
```

The main steering routine for the state estimation portion of the algorithm is presented subsequently:

```
% % DATE CREATED / MODIFIED:         JULY. 29nd, 2012
% % NAME:        SEMain_RBTS_3ph.m
% % DESCRIPTION:     Main steering routine for a 3ph unbalanced state estimation algorithm.
Takes Ybus, estimated voltages at SOME NODES, substation power flows, and calculates loads at
unmeasured buses, then estimates bus voltage magnitudes and angles.  Calculates flows then dis-
play/saves data to an external (*.csv or *.xls) file.

% % Mod on Dec 22, 2011:
% % Remove hard-coded Isource, Sum MVA and meas MVA. Replace these values
% % with (a) read_timeloads, (b) pf_radial_solver, then calculate I_calc
% % using (c) pf_I_calc to obtain the new Isource values.
% % ------- % ------- % ------- % ------- % ------- % ------- % -------
clear V_mSE I_line_mSE Vmag_mSE Vang_mSE Vdisp_mSE Imag_mSE Iang_mSE...
    Idisp_mSE S_flow S_flow_SE Vm_mSE Isource SE_Busdata SE_S_flow...
    SESub_load_MW SESub_load_MVAr

%%%%%%%%%%%%%%%%%%%%%%%%%%%%%
Vaccuracy_data = 'C:\Full RBTS Model\LSSSv3\HE 18\Measurement Accuracy.xlsx';
Iaccuracy_data = 'C:\Full RBTS Model\LSSSv3\HE 18\Load Accuracy.xlsx';

[usethis, Volt_meas_var, Load_meas_var] =
Read_meas_data(Vaccuracy_data,Iaccuracy_data,busnos,newbusnos,n_buses,feeder);

% % Demand Response - reduce loads between 5-10(pct).
disp('Demand response - requesting 20% load curtailment');
SE_Demand_Response;

% % Perform power flow with new/modified loads (HE):
pfRBTS_solver;
% % Vector of measurements for SE= XX_mSE:
V_mSE = V;
I_line_mSE = I_line;

% % % % % % % % % START: PROCESS DATA FOR DISPLAY % % % % % % % % %
% % BUS VOLTAGES
Vmag_mSE = abs(V_mSE);       % % MAGNITUDE
Vang_mSE = atan2(imag(V_mSE),real(V_mSE))*180/pi;       % % ANGLE

% % DISPLAY AS:  [ BUS#, |Va#|, /Va#, |Vb#|, /Vb#, |Vc#|, /Vc# ...]
row = Busdata(:,1)';
Vdisp_mSE =[row;Vmag_mSE(1,:);Vang_mSE(1,:);Vmag_mSE(2,:);Vang_mSE(2,:);...
    Vmag_mSE(3,:);Vang_mSE(3,:)]';

% % LINE CURRENTS
Imag_mSE = abs(I_line_mSE).*[I_bases';I_bases';I_bases'];    % % MAGNITUDE
Iang_mSE = atan2(imag(I_line_mSE),real(I_line_mSE))*180/pi;  % % ANGLE

% % DISPLAY AS: [ FBUS#, TBUS#, |Ia#|, /Ia#, |Ib#|, /Ib#, |Ic#|, /Ic# ...]
Idisp_mSE=[Linedata2(:,1:2), [Imag_mSE(1,:);Iang_mSE(1,:);Imag_mSE(2,:);...
    Iang_mSE(2,:);Imag_mSE(3,:); Iang_mSE(3,:)]'];
```

```
% disp('I_disp_mSE'); Idisp_mSE;

% % % % % % % % % END: PROCESS DATA FOR DISPLAY % % % % % % % % %
% % Calculate line power flows:
pfRBTS_Sflows;
% % Display line power flows
S_flow_SE = S_flow;

% % Create a vector, [n_buses*3, 1] by interleaving a, b, c
Vm_mSE(1:3:n_buses*3,1) = V_mSE(1,:);
Vm_mSE(2:3:n_buses*3,1) = V_mSE(2,:);
Vm_mSE(3:3:n_buses*3,1) = V_mSE(3,:);

% % Calculate current injected into source bus:
Isource = Ybus(source_bus*3-2:source_bus*3,:) * Vm_mSE;

% % Store LP values in 'pf for HE' for future use:
SE_Busdata = Busdata_new;
SE_S_flow = S_flow;
SESub_load_MW = Sub_load_MW;
SESub_load_MVAr= Sub_load_MVAr;

%%%%%%%%%%%%%%%%%%%%%%%%%%%
% % Compare source current to threshhold (1MW here), If dI < I_TH, we
% % will adjust the I_calc vector... ie, Source = Load
SE_Sub_Load_Change;

% % Call the function V_measurements_3ph: Bus voltage measurements are
% % stored in arrays as:  V_MEAS_SET# = [BUSno(3x1) ; VOLTAGE(a+jb) ].
% % Note that the BUSno is a 3x1, 3 phases
SE_V_meas_3ph;

%%%%%%%%%%%%%%%%%%%%%%%%%%%%%%%%%%%%%%%%%%%%%%%%%%%%%%%%
% % Call the function Inj_measurements: % % bus injection currents are
% % stored in arrays as:  INJ_MEAS_SET# = [BUS ; CURRENT (a+jb) ]
SE_Inj_meas_3ph;

%%%%%%%%%%%%%%%%%%%%%%%%%%%%%%%%%%%%%%%%%%%%%%%%%%%%%%%% %
Call the function line_currents:  Measurements are provided as
% % I_LINE_MEAS = [FROM BUS; TO BUS ; CURRENT (a+jb) ]
SE_line_currents_3ph;

%%%%%%%%%%%%%%%%%%%%%%%%%%%%%%%%%%%%%%%%%%%%%%%%%%%%%%%% %
Call the function SE_Algorithm: This builds the x_hat = pinv(H)*z state estimation
tic;          % Start recording time
   SE_Algorithm_3ph;
toc;          % Report run-time

residual = [ (z_s - H_s * x_hat_s), ((z_s - H_s * x_hat_s2).*diag(W))];
J_x = [norm(residual(:,1)); norm(residual(:,2))];
deg_freedom = (n_buses - length(usethis) + n_loadbus_meas)*3 ;
bad_data_limit_99 = chi2inv(0.99,deg_freedom);
bad_data_limit_95 = chi2inv(0.95,deg_freedom);
```

```
bad_data_lim = [bad_data_limit_99; bad_data_limit_95];

% % Calculate power flows:
clear V
for nn = 1:n_buses
   V(1:3,nn) = x_hat_s(n_buses*3-2:n_buses*3);
end;
pfRBTS_Sflows;
SE_S_flow_result = S_flow;

disp('Writing state estimation results to file'); Voltage_file;
switch feeder
     %    case 1    % Feeder F1
     %    % Write data file with voltage / angle:
     %    xlswrite(Voltage_file, ['J';'J'],'F1_SE','A1');
     %    xlswrite(Voltage_file, [J_x,bad_data_lim],'F1_SE','B1');
     %    xlswrite(Voltage_file, VTextBlkR2,'F1_SE','A3');
     %    xlswrite(Voltage_file, SEVdisp_result,'F1_SE','A4');
     %    xlswrite(Voltage_file, VTextBlkR2,'F1_SE','I3');
     %    xlswrite(Voltage_file, WSEVdisp_result,'F1_SE','I4');

     case 1    % Feeder F1
          xlswrite(Power_file, PTextBlkR1,'F1_SE','A1');
          xlswrite(Power_file, SE_S_flow,'F1_SE','A2');
          xlswrite(Power_file, PTextBlkR1,'F1_SE','J1');
          xlswrite(Power_file, SE_S_flow_result,'F1_SE','J2');
end;
```